A Novel Approach for Traveling Wave-Based Fault Location Methods Using Low Sampling Rate Data

EDUARDO PASSOS AQUINO RIBEIRO

DOCTORAL THESIS
IN ELECTRICAL ENGINEERING

DEPARTMENT OF ELECTRICAL ENGINEERING

TECHNOLOGY COLLEGE

UNIVERSITY OF BRASÍLIA

University of Brasilia
Technology College
Department of Electrical Engineering

A NOVEL APPROACH FOR TRAVELING WAVE-BASED FAULT LOCATION METHODS USING LOW SAMPLING RATE DATA

EDUARDO PASSOS AQUINO RIBEIRO

ADVISOR: KLEBER MELO E SILVA

CO-ADVISOR: FELIPE VIGOLVINO LOPES

DOCTORAL THESIS IN ELECTRIC ENGINEERING

PUBLICATION: PPGEE 212/25

BRASÍLIA/DF: DECEMBER - 2024

CATALOGRAPHIC SHEET

PASSOS AQUINO RIBEIRO, EDUARDO

A Novel Approach for Traveling Wave-Based Fault Location Methods Using Low Sampling Rate Data. [Brasília/DF] 2024.

xii, 81p., 210 x 297 mm (ENE/FT/UnB, Doctor, Tese de Doutorado, 2024).

Universidade de Brasília, Faculdade de Tecnologia, Departamento de Engenharia Elétrica.

Departamento de Engenharia Elétrica

1. ATP
2. Fault location
3. Transmission line
4. Traveling wave
5. Interpolation
6. DS filter
7. Sampling rate
8. Subsynchronous oscilation

I. ENE/FT/UnB

BIBLIOGRAPHIC REFERENCE

PASSOS AQUINO RIBEIRO, EDUARDO (2024). A Novel Approach for Traveling Wave-Based Fault Location Methods Using Low Sampling Rate Data. Tese de Doutorado, Publicação PPGEE.212/25, Departamento de Engenharia Elétrica, Universidade de Brasília, Brasília, DF, 81p.

ASSIGNMENT OF RIGHTS

AUTHOR: Eduardo Passos Aquino Ribeiro

TITLE: A Novel Approach for Traveling Wave-Based Fault Location Methods Using Low Sampling Rate Data.

DEGREE: Doctor Year: 2024

Eduardo Passos Aquino Ribeiro

University of Brasília (UnB)

Darcy Ribeiro Campus

Technology College - FT

Departamento de Engenharia Elétrica(ENE)

Brasília - DF CEP 70919-970

I dedicate this work to my mother, wife, and family for guiding me, giving meaning to life, and supporting me.

ACKNOWLEDGEMENTS

Without her, this achievement would not have been possible. I dedicate the first thanks to my mother, who for twenty-nine years has dedicated herself to making me a happy and successful man. Thank you for beating cancer and continuing to be my safe haven, and I thank you every day for being my mother. I thank my family, my brother Leonardo Passos Aquino Ribeiro and my uncles Juarez and Railda, for their support, motivation, and affection. For me, you are the true meaning of the word Angel. I would like to thank Valéria Amancio dos Santos for her patience and companionship. Thanks to my steel tricolor friends, Dario, Marcelo, and Rodolfo. Our partnership is eternal! I would like to thank the friends I had the pleasure of meeting in Brasilia, Pedro, Marayanne, Tiago, João, Vitor, Gustavo, Letícia, and everyone present in the daily life of LAPSE. Giants who offered me the shoulder to reach higher. I thank my great friends from Paraíba, Prof. Doctor Felipe Vigolvino Lopes and Prof. Doctor Kleber Melo Silva, for accepting to guide me on this journey. Thanks to the LAPSE family for their friendship and motivating environment. A laboratory that, in addition to making a difference in the world scenario of protection of electrical power systems, makes a difference in the lives of its members. I would like to thank CAPES and UnB for their financial support, professional environment, and knowledge. I would like to thank the National Electrical System Operator (ONS) for the support and support of my co-workers. I would like to thank the entire IATI, Evoltz, and Cepel teams who provided technical and financial support for the development of this research.

ABSTRACT

A Novel Approach for Traveling Wave-Based Fault Location Methods Using Low Sampling Rate Data

This doctoral thesis presents an interpolation-based solution that allows the application of the traveling wave (TW)-based double-ended fault location algorithm even using sampling rates lower than those typically considered as a requirement for classical approaches. Two phasor (PH)-based and one TW-based fault location methods are compared with the proposed technique and applied through Alternative Transients Program (ATP) fault simulations in a 500 kV/60 Hz Brazilian double circuit series-compensated transmission lines with high-voltage direct current transmission lines (HVDCs) and static var compensators (SVCs) in the vicinity. The results show that the proposed interpolation-based technique is reliable and suitable for TW-based fault location using data records with sampling rates lower than those used in commercially available equipment. Moreover, its accuracy is comparable to classical TW-based fault location solutions, revealing its usefulness for practical application when only traditional digital fault recorders (DFRs) are available.

Keywords: Traveling waves, fault location, interpolation, power systems, transmission line, sampling rate.

RESUMO

Uma Nova Abordagem para Métodos de Localização de Faltas Baseados em Ondas Viajantes Utilizando Registros de Baixa Taxa de Amostragem

Esta tese de doutorado apresenta uma solução baseada em interpolação que permite a aplicação do algoritmo de localização de faltas de dois terminais baseado em ondas viajantes (OVs) mesmo usando taxas de amostragem menores do que aquelas tipicamente consideradas como um requisito para abordagens clássicas. Dois métodos de localização de faltas baseados em fasores e um baseado em OVs são comparados com a técnica proposta e aplicados por meio de simulações de faltas, utilizando o *software Alternative Transients Program* (ATP), em linhas de transmissão brasileiras de 500 kV/60 Hz de circuito duplo compensadas em série com vizinhança composta por linhas de transmissão de corrente contínua de alta tensão (do inglês, HVDCs) e compensadores estáticos de var. Os resultados mostram que a técnica proposta, baseada no uso de interpolação, é confiável e adequada para localização de faltas baseada em OVs usando registros oscilográficos com taxas de amostragem menores do que aquelas usadas em equipamentos disponíveis comercialmente. Além disso, sua precisão é comparável às soluções clássicas de localização de faltas baseadas em OVs, revelando sua utilidade para aplicação prática quando apenas registradores digitais de perturbações (RDPs) tradicionais estão disponíveis.

Palavras-chave: Ondas viajantes, localização de faltas, interpolação, sistemas de energia, linha de transmissão, taxa de amostragem.

TABLE OF CONTENTS

LIST OF FIGURES

LIST OF TABLES

LIST OF SYMBOLS

$Buffer[n]$	Most recent stored samples window for traveling-waves calculation.
$C\Delta x$	Shunt capacitance per unit of the length
$DS[n]$	Differentiator-smoother filter coefficient window
F	Fault location inception point
fc	Cutoff frequency
f_i	Frequency of interest in the frequency spectrum
F_s	Sampling frequency
G	Filter gain
$G\Delta x$	Shunt conductance per unit of the length
H	Random measuring point on a transmission line
h	Random measuring point distance on a transmission line
i_A	Phase A current
i_B	Phase B current
i_C	Phase C current
i_{DS}	Current in the output of the differentiator-smoother filter
$i_{DS}\alpha$	Alpha mode current in the output of the differentiator-smoother filter
$i_{DS}\beta$	Beta mode current in the output of the differentiator-smoother filter
$i_{DS}0$	Zero mode current in the output of the differentiator-smoother filter
$IF[n]$	Interpolation filter coefficient window
$\hat{I}_{F1}$	Positive-sequence current at fault point origin

$\hat{I}_{F2}$	Negative-sequence current at fault point origin
$\hat{I}_{R1}$	Positive-sequence current at remote terminal
$\hat{I}_{R2}$	Negative-sequence current at remote terminal
$\hat{I}_{S1}$	Positive-sequence current at local terminal
$\hat{I}_{S2}$	Negative-sequence current at local terminal
i_{TW}	Current traveling wave
LL	Line length
L	Interpolation factor
$L\Delta x$	Series inductance per unit of the length
m	Fault location estimation
N_{DS}	Number of coefficients of the differentiator-smoother filter
NL	First traveling-wave arrival time index in the local terminal of the monitored transmission line
NR	First traveling-wave arrival time index in the remote terminal of the monitored transmission line
R_f	Fault resistance
$R\Delta x$	Series resistance per unit of the length
T_{DS}	DS filter time window length
v_f	Instantaneous voltage at m
$\hat{V}_{F1}$	Positive-sequence voltage at fault point origin
$\hat{V}_{F2}$	Negative-sequence voltage at fault point origin
v_p	Transmission line propagation velocity
$\hat{V}_{R1}$	Positive-sequence voltage at remote terminal
$\hat{V}_{R2}$	Negative-sequence voltage at remote terminal
$\hat{V}_{S1}$	Positive-sequence voltage at local terminal

$\hat{V}_{S2}$	Negative-sequence voltage at local terminal
v_{TW}	Voltage traveling wave
Z_{LT_2}	Negative-sequence transmission line impedance
Z_{S1}	Positive-sequence Thévenin impedance at local terminal
Z_{R1}	Positive-sequence Thévenin impedance at remote terminal
Z_S	Surge impedance
α	Aerial alpha-mode
β	Aerial Beta-mode
$\delta[n]$	Unitary impulse.
γ	Line propagation constant
τ	Traveling-wave propagation time
θ	Fault incidence angle

GLOSSARY

AG	Phase-A-to-ground fault
BC	Phase-B-to-phase-C fault
CA	Phase-C-to-phase-A fault
DS	Differentiator-smoother filter
DWT	Discrete Wavelet transform
EPSR	Electric Power Systems Research
FFT	Fast Fourier transform
FSC	Fixed series capacitor
GAIN	Generative adversarial interpolation network
HVDC	High-voltage direct current transmission lines
ICEEMDAN	Improved complete ensemble empirical mode decomposition with adaptive noise
IED	Intelligent electronic device
IEEE	Institute of Electrical and Electronics Engineers
IFFT	Inverse fast Fourier transform
IFFR	Interpolator filter frequency response
IF	Interpolation filter
IIR	Infinite impulse response
NDS	Numbers of differentiator-smoother filter coefficients
ONS	Brazilian Transmission Electric System Operator

PHFL	Phasor based fault location
SNR	Sigal-to-noise Ratio
SVC	Static var compensator
TW	Traveling-wave
TWFL	Traveling-wave based fault location

CHAPTER 1

INTRODUCTION

Generation, transmission, and distribution utilities are constantly expanding, aiming to supply the growing electrical demand. It has guided studies and technological developments to keep the electric power system in balance with generating units in synchronism during the steady-state regime of the electrical network, as well as promoting its return to operation under normal conditions when a disturbance occurs (ANDERSON; FOUAD, 2008; GRAINGER *et al.*, 2003). As depicted in Figure 1.1, Brazil is a continent-sized country in which its electric matrix is mainly composed of decentralized hydroelectric power plants, which implies a complex transmission system with 216 thousand kilometers of transmission lines operating in several voltage rates (ONS, 2023b).

According to the Brazilian Transmission Power System Operator (ONS), historically transmission lines are equipment with the highest number of forced switching-offs, as detailed in Table 1.1. In this context, it is important that the fault location algorithms facilitate operation and maintenance work to make the equipment available to return to operation as quickly as possible.

Table 1.1: Equipment switching-off history in the Brazilian national interconnected system.

Equipment	Number of forced switching-offs
Busbar	2,170
Series capacitor	7,960
Shunt capacitor	1,817
Static var compensator	2,673
Synchronous var compensator	1,361
AC transmission lines	42,291
DC transmission lines	807
Shunt reactor	2,844
Two winding transformer	3,376
Three winding transformer	11,619

Source: (ONS, 2023a).

Figure 1.1: Brazilian interconnected power system.

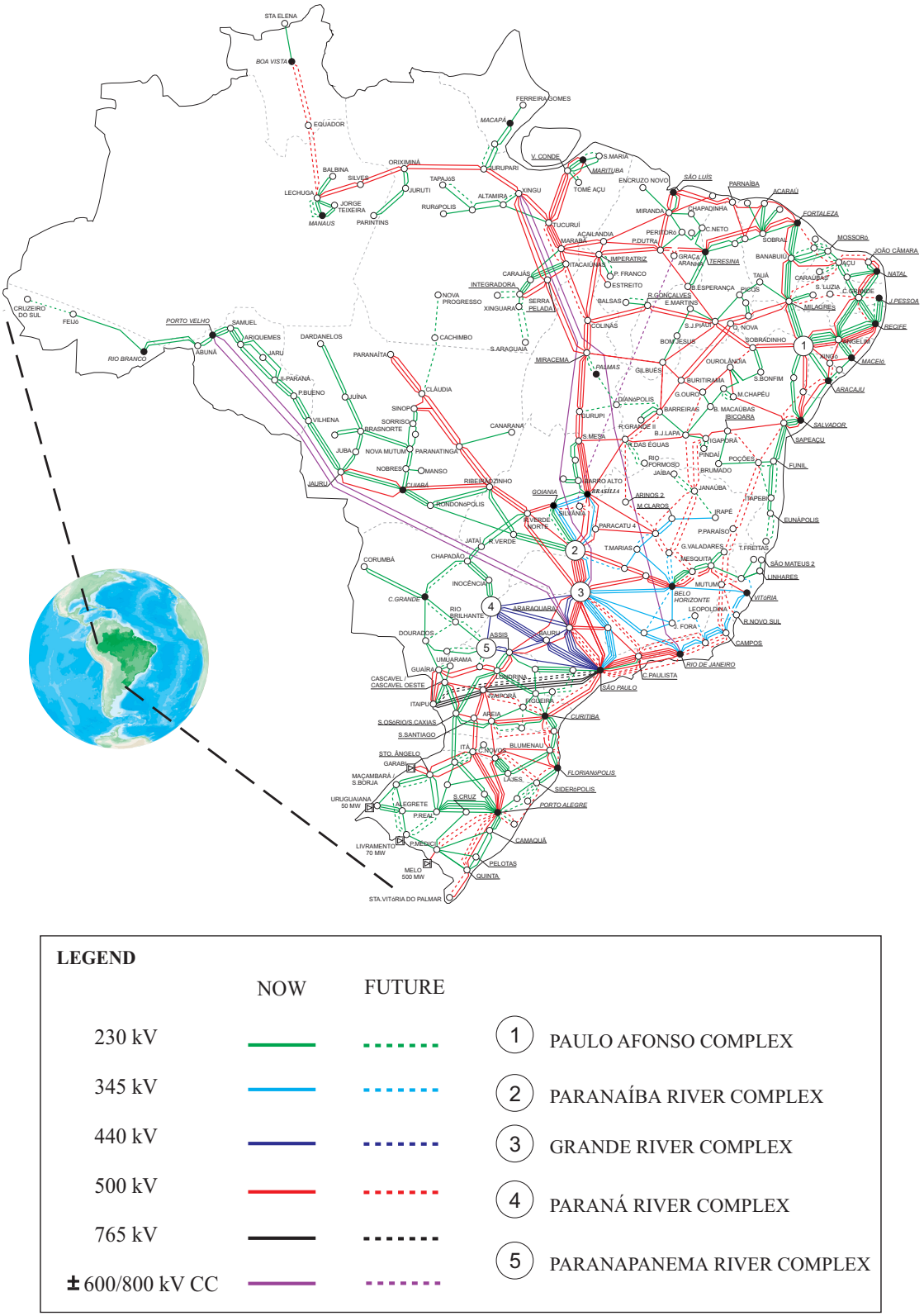

LEGEND

	NOW	FUTURE
230 kV		
345 kV		
440 kV		
500 kV		
765 kV		
± 600/800 kV CC		

1. PAULO AFONSO COMPLEX
2. PARANAÍBA RIVER COMPLEX
3. GRANDE RIVER COMPLEX
4. PARANÁ RIVER COMPLEX
5. PARANAPANEMA RIVER COMPLEX

Source: Adapted from (ELETROBRAS, 2018).

In the context of this work, it is essential to understand the particularities of fault location methods. Stand out among them: technique used, type of input signal, and sampling rate are fundamental topics (LOPES *et al.*, 2021). Several techniques are reported in the literature and can be divided into methods that use data monitored in one, two, or more terminals of the evaluated transmission line (SAHA *et al.*, 2010).

Traditionally, fault location algorithms are based on phasors (PH-based) (SAHA *et al.*, 2010). Still, with technological advances in signal processing and increased sampling rates used in intelligent electronic devices (IEDs), fault location algorithms based on traveling waves (TW-based) gained notoriety, presenting high reliability and precision (DONG, 2022). In contrast to the benefits of TW-based techniques, the cost of IEDs that support these functions is higher due to the need for robust hardware capable of performing sampling at high rates (RIBEIRO *et al.*, 2023).

1.1 THESIS MOTIVATION

Technological advances in the area of signal processing allowed the development of IEDs with more robust algorithms and higher sampling rates, making it possible to analyze a greater range of the frequency spectrum of signals generated by electrical disturbances in electrical power systems. According to Abboud & Dolezilek (2017), the launch of TW-based fault location functions broke paradigms in the field of power systems by presenting benefits when compared to traditional PH-based functions, such as:

- Immunity to saturation of current transformers (CTs);
- Greater robustness against subsynchronous oscillations;
- Average accuracy of one to two tower spans (*i.e.*, 0 m $\leq$ error $\leq$ 800 m);
- Reliability against high impedance faults; and
- Predictive fault location through indications of the fault point even before the fault occurs.

In contrast to its benefits, the cost of fault location IEDs that use TW-based algorithms is high due to the need for robust hardware that allows the sampling of signals in the order of

hundreds of kHz (RIBEIRO *et al.*, 2023). Therefore, in this thesis, the differentiator-smoother (DS) filter, an algorithm used to perform TW extraction over records containing transient data, is adapted and used together with an interpolation technique, being then proposed to enable the application of TW-based fault location methods on low sampling rate data. As a result, it is possible to maintain the fault location average precision between two tower spans, which is reasonable and presents a good solution for challenging power system configurations over fault location reliability and accuracy.

1.2 GOALS

The main goal of this thesis is to explain the development and application of the signal processing technique to allow the use of TW-based fault location algorithms on reduced sampling rates. Therefore, the following specific objectives are defined:

- Present the necessary theoretical foundation to support the combination of the adapted DS filter with the interpolation method that can be used on low sampling rate records in the order of 1024 samples/cycle, 512 samples/cycle, and 256 samples/cycle.
- Validate the methodology developed through performance comparisons with TW-based and PH-based fault location methods proposed in the literature over simulated and actual cases.

1.3 CONTRIBUTIONS AND PUBLICATIONS

As the main contribution of this work, we highlight the proposed adaptations over the DS filter along with an interpolation method to enable the use of TW-based fault location methods in low sampling rate records.

1.3.1 Publication Directly Related to the Thesis

The main publication regarding this thesis was published in the Electric Power Systems Research (EPSR) journal. Also, an important paper was published in a conference of the

Institute of Electrical and Electronics Engineers (IEEE). Both publications are listed below:

- **Ribeiro, E. P. A.**, Lopes, F. V., Silva, K. M., Martins-Britto, A. G., Reis, R. L., Moraes, C. M., Agostinho, R. L., & Rodrigues, M. A. (2023). An interpolation-based solution to use low sampling rate records in traveling wave-based fault location methods. Electric Power Systems Research, 224, 109605.

- **Ribeiro, E. P. A.**, Lopes, F. V., Ribeiro, J. P. G., & Leite, E. J. (2018, November). Atp/models differentiator-smoother filter model validated using actual time-domain relay. In 2018 Workshop on Communication Networks and Power Systems (WCNPS) (pp. 1-4). IEEE.

1.3.2 Other Publications

In addition, studies in the area of protection of electrical power systems also stand out:

- Analysis of the latency impacts of communication channels in time-domain protections tripping times; and

- Analysis of the impacts of commutation failures on converter transformers of line-commuted converters LCC-HVDC systems on time-domain protections applied to transmission lines in the neighborhood.

The aforementioned studies were published at international conferences but without relation to the thesis proposal:

- **Ribeiro, E. P.**, Lopes, F. V., Silva, K. M., & Martins-Britto, A. G. (2023). Assessment of communication channel effects on time-domain protection functions tripping times. Electric Power Systems Research, v. 223, p. 109589.

- Lopes, F. V., **Ribeiro, E. P.**, Reis, R. L., Silva, K. M., Britto, A. M., Moraes, C. M., Agostinho, R. L., & Rodrigues, M. A. (2023). Three-parameter ATP/ATPDraw transmission line high impedance fault model. Electric Power Systems Research, 223, 109577.

- Reis, R. L. A., Lopes, F. V., **Ribeiro, E. P.**, Moraes, C. M., Silva, K. M., Britto, A. M., Agostinho, R. L., & Rodrigues, M. A. M. (2023). Traveling wave-based fault locators: performance analysis in series-compensated transmission lines. Electric Power Systems Research, 223, 109567.

- Moraes, C. M., Martins-Britto, A. G., Lopes, F. V., Silva, K. M., Ribeiro, E. P., & Rodrigues, M. A. (2021, November). On the Effects of EMI and the Soil Structure on Transmission Line Parameters - Part I: Theoretical Model. In 2021 Workshop on Communication Networks and Power Systems (WCNPS) (pp. 1-6). IEEE.

- Moraes, C. M., Martins-Britto, A. G., Lopes, F. V., Silva, K. M., Ribeiro, E. P., & Rodrigues, M. A. (2021, November). On the Effects of EMI and the Soil Structure on Transmission Line Parameters - Part II: Impacts on Fault Locators. In 2021 Workshop on Communication Networks and Power Systems (WCNPS) (pp. 1-6). IEEE.

- **Ribeiro, E. P. A.**, e Silva, K. M., Lopes, F. V., & Martins-Britto, A. (2021, November). Time-Domain-Based Relay Model to Assess Line Protection Nearby HVDC Systems. In 2021 Workshop on Communication Networks and Power Systems (WCNPS) (pp. 1-6). IEEE.

- Vásquez, F. A. M., **Ribeiro, E. P.**, Silva, K. M., & Lopes, F. V. (2021). A new time domain-based busbar protection algorithm. Electric Power Systems Research, 196, 107282.

- Lopes, F. V., Reis, R. L., Silva, K. M., Martins-Britto, A., **Ribeiro, E. P.**, Moraes, C. M., & Rodrigues, M. A. M. (2021, November). Past, Present, and Future Trends of Traveling Wave-Based Fault Location Solutions. In 2021 Workshop on Communication Networks and Power Systems (WCNPS) (pp. 1-6). IEEE.

- Ribeiro, L. M. A., Cunha, G. A., Martins-Britto, A. G., **Ribeiro, E. P. A.**, & Lopes, F. V. (2021). Impact of transmission line modeling aspects on TW-Based fault location studies. Electric Power Systems Research, 196, 107204.

- Ribeiro, L. M., Cunha, G. A., **Ribeiro, E. P.**, Britto, A. G., & Lopes, F. V. (2020, November). Analysis of traveling waves propagation characteristics considering different

transmission line emtp models. In 2020 Workshop on Communication Networks and Power Systems (WCNPS) (pp. 1-6). IEEE.

Finally, two papers were presented at a Brazilian national event: XVII Technical Seminar on Protection and Control (STPC). The first paper is directly related to the thesis, and the second is related to protection of electrical systems, namely:

- Methodology for applying the classical two-terminal fault location method based on traveling waves in 15,360 Hz oscillograph records; and
- Computational model in ATP for studies and analysis of protections based on quantities in the time domain.

1.4 TEXT ORGANIZATION

This work is organized as described below:

- In Chapter 2, a brief bibliographic review regarding references reported in the literature on TW-based algorithms used on low sampling rate records is reported. Thus, the review is organized in chronological order, emphasizing positive and negative points;
- In Chapter 3, TW propagation on transmission lines basic concepts, the basic structure of the DS filter and the interpolation method is explained as well as the fault location methods studied in this thesis;
- In Chapter 4, the proposed combination of the DS filter and the interpolation method is presented along with the test power system and simulations performed to enable the evaluation of the proposed technique;
- In Chapter 5, the results obtained by applying TW-based fault location algorithms using low sampling rate, in the order of 1024 samples/cycle, 512 samples/cycle, and 256 samples/cycle, in ATP/ATPDraw simulations records through the proposed technique are presented, along with comparisons made with three traditional fault location methods reported in the literature, one TW-based and two PH-based, and with clarifications on

the resilience over noisy signals and comparisons between TW extraction strategies and interpolation methods;

- In Chapter 6, results obtained from applying the proposed algorithm over actual oscillograph data recorded in traditional DFRs installed in the 500 kV double-circuit transmission line Silves / Oriximiná using the sampling rate of 256 samples/cycle (*i.e.*, 15.360 kHz) are demonstrated and compared with PHFL algorithms studied in this thesis.

- In Chapter 7, the conclusions of the work are presented.

CHAPTER 2

LITERATURE SURVEY

This chapter presents a brief literature survey of papers that report the use of interpolation in miscellaneous science areas and papers that report the use of fault location approaches regarding the use of different frequency spectrum components from fault-generated signals. Fault location techniques that look forward to using the different components present in a fault-generated signal spectrum date back to the 1940s (GALE *et al.*, 1993; SAHA *et al.*, 2010; REPORT, 1955; MARIHART; HAAGENSON, 1972). Lopes *et al.* (2021) explain that, nowadays, new developments regarding making algorithms simpler or through filtering techniques that allow the reduction of production costs of IEDs capable of emulating the proposed techniques are classified as potential trends.

2.1 USE OF INTERPOLATION IN DIFFERENT AREAS OF SCIENCE

Currently, interpolation is considered a common method for handling abnormal data or missing values in miscellaneous science areas, such as computational processing complexity, image processing, biomedicine, mathematics, power systems, etc.

Tan *et al.* (2011) analyze linear interpolation and sinc interpolation (interpolation kernel) applied for waveform reconstruction in beacon transmitter detector. The beacon transmitter detector is designed to measure and display the carrier signal of the non-directional beacon and marker beacon. A characteristic of beacon detectors is that the carrier signals are uniformly sampled and stored in digital form, in which the waveform displayed on the screen is the reconstruction of the sampling points after extraction or interpolation. Thus, the authors propose a combination of these techniques to overcome the high computational complexity of sinc interpolation and the high distortion of linear interpolation. As result, the combined interpolation method has the advantages of satisfactory waveform reconstruction performance

and relatively low computational complexity.

Dai *et al.* (2014) present a novel directionally adaptive cubic-spline kernel interpolation method that applies to mobile zoom systems. The proposed technique involves a directionally adaptive interpolation using the optimal interpolation kernel according to the edge orientation to solve blurring and jagging artifacts in the digitally zoomed image.

Luo *et al.* (2020) study three interpolation techniques: right triangular, equilateral triangular, and rectangular. In this work, the errors obtained in each type of interpolation are demonstrated as a function of the interpolation order. In this way, the results show which interpolation technique to use and what order to use for the objectives of precision and efficiency.

Zhao *et al.* (2023) propose the use of an improved complete ensemble empirical mode decomposition with adaptive noise (ICEEMDAN) method with a generative adversarial interpolation network (GAIN) to preprocess wind power generation and interpolate missing wind power generation sub-components. In this work, the application of interpolation solves problems in a wind power plant that affect the operation of a power system, such as abnormal data in wind power generation, guaranteeing reductions in the impacts of the error caused by wind power generation sequence fluctuations.

Na *et al.* (2023) present an interpolation applied with the backward Euler's method that enhances the switching simulations accuracy in an electromagnetic transient simulation with a fixed time-step. It is widely known that a fixed time-step simulation presents critical issues when modeling semiconductor switches such as thyristors, gate turn-off thyristors, insulated gate bipolar transistors, etc, which, if not applied alongside another technique, could result in numerical oscillation, voltage spikes, etc. In counterpart, reducing the simulation time-step to improve accuracy directly proportionally increases the simulation time. Thus, to solve this problem, the authors propose using interpolation with the backward Euler's method by combining the half-time step Backward Euler with additional interpolation and extrapolation steps to return to the original time grid.

Bucelli *et al.* (2023) combine rescaled localized Radial Basis Function interpolation with Singular Value Decomposition to preserve the positivity of the determinant of the deformation gradient tensor. As an advantage, the authors affirm that the proposed combination overcomes limitations of existing interpolation methods, including nested intergrid interpolation and Ra-

dial Basis Function interpolation of the displacement field, that may lead to the loss of physical meaningfulness of the mathematical formulation and then to solver failures at the algebraic level, due to negative determinant values. As a result, cardiac electromechanical simulations are enhanced in flexibility and accuracy.

2.2 WORKS REGARDING HIGH FREQUENCY FAULT LOCATION ALGORITHMS AND SAMPLING RATE

Gale *et al.* (1993) categorize four TW-based fault location methods into A, B, C, and D groups, which are assessed and suggested as a solution to overcome the well-known deficiencies of impedance and/or reactance methods, such as high fault resistance values, infeed effect, series compensation, among others. The type A method uses one-terminal data (*i.e.*, it is single-ended) and it assumes that the reflection coefficient at the fault point approximates +1, since the fault arc remains ionized for an extended period, presenting a very low fault resistance. Hence, the method depends on the detection of the first incident TW and first fault-reflected TW to estimate the fault location. On the other hand, the type D method is double-ended and it relies on detecting the first incident TWs at both monitored line terminals. Finally, methods of types B and C consist in active techniques, which require a pulse generator circuit, being the type B-method double-ended and the type C-method single-ended. For both B and C methods, the injected pulses are provided by reclosing maneuvers of the faulty circuit at one terminal of the line, and by pulse-generating units, respectively.

Abur & Magnago (2000) replace the correlation method by the discrete Wavelet transform (DWT), whose main advantage is automatically adjust its data window relative to the desired frequency resolution, for locating faults using one terminal data. The authors main contribution lies on using a time delay between modal components of the same signal for computing the fault location, *i.e.*, different frequencies from the aerial-mode and ground-mode, which relies in different propagation speeds.

Lin *et al.* (2012) explain that fault generated TWs are wideband signals which cover the entire frequency range. In the frequency domain, the magnitude of the individual signal components decreases and the travelling velocity increases as the frequency increases. From another

point of view, in the time domain, different frequency components have different arrival times. The first TW that will reach the monitored terminal first is the one with the highest frequency, and the components of other frequencies will be delayed to arrive at the measuring point. So, this phenomena describes that the TW detected at the locator is not an ideal step signal, but is spread out by rise time or fall time. Still, the authors explain that the frequency range that can be evaluated is limited to the sampling frequency. So, the arrival time of the first TW is that of the highest frequency component detected. Also, by propagation means, the component of the TW with higher frequency decays faster and also possesses a smaller reflection coefficient and refraction coefficient. This means that although the first incidence presents a more significant influence of the highest possible frequency component to be measured, in the second incidence, lower frequency components may have a more substantial influence, depending on the fault inception point. Based on the concepts mentioned above, the authors propose a fault location algorithm based on the TW of a terminal using Wavelet to calculate different propagation speeds for the first and second TWs measured at the monitored transmission line terminal and then apply the obtained results in equations for faults originating in the first or second section of the transmission line. The method identifies the transmission line section according to the polarity of the first waves measured at the monitored terminal.

Jia (2017), as well as in Lin *et al.* (2012), details that when a fault occurs, many frequency components are generated, each with different propagation velocity, which implies a complex task to correctly determine the arrival time and velocity when using TW fault location (TWFL) algorithms. Thus, a correction method for the dispersion effect of TWs is proposed to shorten the wavefront's fall or rise time and enhance the singularity of TW. The author presents that the TWs singularity decreases (*i.e.*, larger fall times) as a function of the distance they propagate from the fault point to the transmission line monitored terminal. To achieve what the author calls "the perfect TW", a correction factor is proposed, which multiplies the receiving TW at the measuring point in the frequency domain. To do so, firstly, an approximate fault distance is obtained using α-mode of the Wavelet transform. Then, the mother Wavelet function is calculated using the fast Fourier transform (FFT) over the measured TWs in both transmission line monitored terminals as a second step. As a third step, the inverted fast Fourier transform (IFFT) is applied to result in the decomposed Wavelet transform. As a fourth step, the propagation function is calculated by using R, L, and C parameters obtained from

Carson formulation, and, using the propagation function, the correction function is calculated. Finally, the corrected decomposition result for Wavelet transform (enhancement of singularity) is obtained by applying the IFFT. As a result, fault location errors were reduced through performance analysis of different fault inception angles, fault resistance values, fault types, noise levels, and transmission line tower geometries.

Schweitzer *et al.* (2019) summarize the benefits of high-quality data acquisition are depicted through transient modeling, Bewley diagrams, and spectral analysis. Firstly, a description of breaker health monitoring is shown, highlighting details provided in megahertz sampling: pole sequencing, pre-insertion resistor health, reignitions, and restrikes. Also, an important insight is settled down: the pre-fault high-frequency records contain high-frequency content, indicating that the fault will occur before it happens.

Costa *et al.* (2020) provide an explanation of the sampling frequency effects in the classical two-terminal TWFL-based method. Furthermore, an additional error component to the classical fault location equation is proposed and represented by time-space lozenges, which support a probabilistic analysis to take advantage of sampling frequency effects. In practice, it is proposed that the real TW arrival time indexes, considering a continuous time, are located between two discrete samples. The related difference from discrete to continuous time implies a TW arrival time error associated with the sampling frequency. Finally, a probabilistic analysis is carried out so that faults can be found with 100% certainty regarding the sampling frequency effects.

Mitra *et al.* (2021) propose a passive method for an offline-fault location in multi-terminal direct current networks using the natural attenuation of the transmission line current. The FFT is used for fault location, and linear regression is used to calculate the attenuation constant. Thus, after a fault occurs and the breakers open isolating the monitored transmission line, the stored energy in the transmission line capacitance discharges into the fault. Therefore, the transmission line capacitance discharges the stored energy over the series resistance and inductance. This discharge has a resonating behavior of an RLC oscillating circuit, and the presence of resistances implies a decaying over time. Finally, the author proposes the fault location by analyzing the discharging transmission line current. Still, it's worth registering that the DC system control does not affect this method since the transmission line is already isolated. In the context of sampling frequency, three sampling frequencies are tested, namely:

10 kHz, 50 kHz, and 100 kHz. Results present fault location errors in the order of 0.05%.

Lopes *et al.* (2022) investigate an assessment of the anti-aliasing filter influence on the classical double-ended TWFL method described in (GALE *et al.*, 1993). As a result, it is identified that the frequency spectrum energy of line fault-induced transients is mainly concentrated at the lower band of the spectrum. Moreover, tests of disturbance detection were performed using the differentiator-smoother (DS) filter, also considering different numbers of DS coefficients (NDS). Thus, it was noticed that, if low anti-aliasing cutoff frequencies (fc) are used, *i.e.*, if the lower part of the spectrum is considered, DS filters with large number of NDS can improve the TW amplitude estimation, also improving the TW detection.

2.3 CHAPTER SUMMARY

This chapter presents a wide range of fault location methods and applications with regard to sampling rate, highlighting their main characteristics. It is observed that, although in the literature there are algorithms applying the superior band of the frequency spectrum of transients launched by faults, algorithms using the inferior band of the frequency spectrum of transients launched by faults, which brings benefits regarding to investment in the hardware necessary to emulate the algorithms, are still scarce. Furthermore, although Mitra *et al.* (2021) present an algorithm with good results in fault location through the use of the inferior band of the frequency spectrum, its application is recommended for HVDC systems.

Therefore, in the next chapter, a proposal for using the traditional linear interpolation technique will be presented together with a technique adapted from a TW extraction filter incorporated into a commercially available IED. This proposal fits into the need for developments in the field of fault location that enable the cost reduction of these IEDs, described by Lopes *et al.* (2021). As illustrated in Table 2.1, the method proposed in this thesis and published in Ribeiro *et al.* (2023) overcomes the difficulty of applying TW-based algorithms in the inferior band of the frequency spectrum.

Table 2.1: Summary of the literature review regarding the sampling rate for fault location based on transients generated for faults in transmission lines.

Reference	ACTL	DCTL	HSF	LSF
Gale *et al.* (1993)	✓	✓	✓	
Abur & Magnago (2000)	✓		✓	
Lin *et al.* (2012)	✓		✓	
Jia (2017)	✓		✓	
Schweitzer *et al.* (2019)	✓		✓	
Costa *et al.* (2020)	✓		✓	
Mitra *et al.* (2021)		✓	✓	✓
Lopes *et al.* (2022)	✓		✓	
Ribeiro *et al.* (2023)	✓		✓	✓

Legend:
ACTL = Alternating Current Transmission Line
DCTL = Direct Current Transmission Line
HSF = High Sampling Frequency, *i.e.*, $\geq$ 100 kHz
LSF = Low Sampling Frequency, *i.e.*, $\leq$ 100 kHz

Source: Own authorship.

CHAPTER 3

BASICS

In this chapter, concepts related to transmission lines faults and TW propagation are presented. The proposal uses the traditional linear interpolation technique in data, moving from a low sampling frequency to a higher one in the order of 1 MHz. The feasibility of applying the TW-based two-terminal fault location technique on the signals extracted from the proposed method is evaluated. Finally, PH-based fault location methods and the TW-based method mentioned beforehand, which will be used to evaluate the proposed method, are described.

3.1 TRANSIENT PROPAGATION ON TRANSMISSION LINES

This section is dedicated to explaining the fundamentals of modeling transmission lines with distributed parameters and the TW phenomenon.

3.1.1 Distributed Parameter Line Mode

To correctly represent the phenomena studied in this thesis, it is necessary to substantiate the propagation of electromagnetic waves throughout an electrical system. In this way, the electrical quantities of voltage and current at the monitored terminals are a function of time and space – $y(x,t)$ – that is, they depend on the distance from the point for which they are being calculated (SAHA *et al.*, 2010).

A transmission line of length LL modeled with distributed parameters comprises the following elements:

- Series resistance per unit length($R\Delta x$);
- Series inductance per unit length($L\Delta x$);

- Shunt capacitance per unit length($C\Delta x$); and
- Shunt conductance per unit length($G\Delta x$).

In Figure 3.1, a transmission line modeled with distributed parameters is illustrated, in which it is necessary to know the quantities at the measuring point H. The point H is located at a distance h from terminal S, where a voltage $v(x,t)$ and a current $i(x,t)$ are verified. It is important to highlight that the soil is ideal, that is, it has zero resistivity, and the parameters are considered constants in frequency. Thus, for a single incremental element of the transmission line, $v(x,t)$ and $i(x,t)$ can be related to the transmission line parameters using the following expressions (NAIDU, 1985):

Figure 3.1: transmission line modeled using distributed parameters.

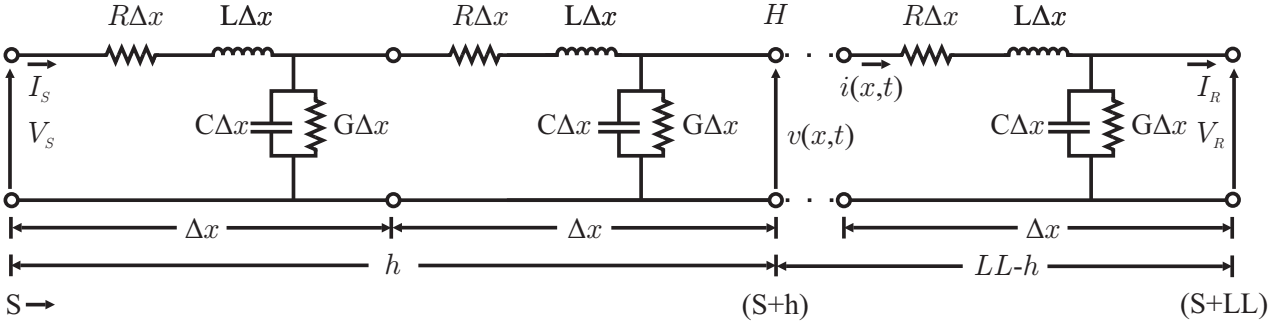

Source: Adapted from (LOPES, 2014).

$$-\frac{\partial v\,(x,t)}{\partial x} = R \cdot i\,(x,t) + L \cdot \frac{\partial i\,(x,t)}{\partial t}\ , \tag{3.1a}$$

$$-\frac{\partial i\,(x,t)}{\partial x} = G \cdot v\,(x,t) + C \cdot \frac{\partial v\,(x,t)}{\partial t}\ . \tag{3.1b}$$

Taking the Laplace transform of Equations (3.1),

$$-\frac{\partial V\,(x,s)}{\partial x} = R \cdot I\,(x,s) + s \cdot L \cdot I\,(x,s)\ , \tag{3.2a}$$

$$-\frac{\partial I\,(x,s)}{\partial x} = G \cdot V\,(x,s) + s \cdot C \cdot V\,(x,s)\ . \tag{3.2b}$$

in which zero initial conditions are assumed. $V(x,s)$ and $I(x,s)$ are the Laplace transforms of $v(x,t)$ and $i(x,t)$, respectively. Also, ordinary rather than partial derivatives are used since

the derivatives are now related to only one variable, x (GLOVER *et al.*, 2012). Thus, Equations (3.3) can be written from differentiating Equations (3.2) with respect to x:

$$-\frac{\partial^2 V(x,s)}{\partial^2 x} = R \cdot \frac{\partial I(x,s)}{\partial x} + s \cdot L \cdot \frac{\partial I(x,s)}{\partial x} \ , \tag{3.3a}$$

$$-\frac{\partial^2 I(x,s)}{\partial^2 x} = G \cdot \frac{\partial V(x,s)}{\partial x} + s \cdot C \cdot \frac{\partial V(x,s)}{\partial x} \ . \tag{3.3b}$$

Using Equations (3.2) in order to eliminate $V(x,s)$ and $I(x,s)$ from Equations (3.3), Equations (3.4), known as telegraphic equations, can be obtained as follow:

$$\frac{\partial^2 V(x,s)}{\partial^2 x} = R \cdot G \cdot V(x,s) + s \cdot (R \cdot C + L \cdot G) \cdot V(x,s) + s^2 \cdot (L \cdot C) \cdot V(x,s) \ , \tag{3.4a}$$

$$\frac{\partial^2 I(x,s)}{\partial^2 x} = R \cdot G \cdot I(x,s) + s \cdot (R \cdot C + L \cdot G) \cdot I(x,s) + s^2 \cdot (L \cdot C) \cdot I(x,s) \ . \tag{3.4b}$$

Simplifying Equations (3.4), one can obtain that

$$\frac{\partial^2 V(x,s)}{\partial^2 x} = V(x,s) \cdot \Big[R \cdot G + s \cdot (R \cdot C + L \cdot G) + s^2 \cdot (L \cdot C)\Big] \ , \tag{3.5a}$$

$$\frac{\partial^2 I(x,s)}{\partial^2 x} = I(x,s) \cdot \Big[R \cdot G + s \cdot (R \cdot C + L \cdot G) + s^2 \cdot (L \cdot C) \cdot I(x,s)\Big] \ . \tag{3.5b}$$

For the sake of simplicity, losses can be neglected, that is, $R = G = 0$. This is possible since, for high-frequencies analysis, reactances $\omega \cdot L$ and $\omega \cdot C$ reach much higher values than r and G, that is, $\omega \cdot L \gg r$ and $\omega \cdot C \gg G$, in which ω is the angular frequency of the electrical system (GLOVER *et al.*, 2012). According to the aforementioned, Equations (3.4) can be rewritten as:

$$\frac{\partial^2 V(x,s)}{\partial^2 x} = s^2 \cdot (L \cdot C) \cdot V(x,s) \ , \tag{3.6a}$$

$$\frac{\partial^2 I(x,s)}{\partial^2 x} = s^2 \cdot (L \cdot C) \cdot I(x,s) \ , \tag{3.6b}$$

or

$$\frac{\partial^2 V(x,s)}{\partial^2 x} - s^2 \cdot (L \cdot C) \cdot V(x,s) = 0 \ , \tag{3.7a}$$

$$\frac{\partial^2 I(x,s)}{\partial^2 x} - s^2 \cdot (L \cdot C) \cdot I(x,s) = 0 \ , \tag{3.7b}$$

Equations (3.6) are linear, second-order homogeneous differential equations. By inspection, one can obtain that them solutions are:

$$V(x,s) = V^+(s) \cdot e^{-s \cdot x/v} + V^-(s) \cdot e^{+s \cdot x/v} \ , \tag{3.8a}$$

$$I\left(x,s\right) = I^{+}\left(s\right) \cdot e^{-s \cdot x/v} + I^{-}\left(s\right) \cdot e^{+s \cdot x/v} \ . \tag{3.8b}$$

The "constants" $V^{+}\left(s\right)$, $V^{-}\left(s\right)$, $I^{+}\left(s\right)$, and $I^{-}\left(s\right)$, which in general are functions of s but are independent of x, can be evaluated from the boundary conditions at the sending and receiving ends of the line (GLOVER *et al.*, 2012). The superscripts + and − refer to waves traveling in the positive and negative x directions.

So, now evaluating the terms $I^{+}\left(s\right)$ and $I^{-}\left(s\right)$, Equations (3.8) can be used in Equation (3.2b) for a lossless line according as follow:

$$\overbrace{\frac{s}{v} \cdot \left[I^{+}\left(s\right) \cdot e^{-s \cdot x/v} - I^{-}\left(s\right) \cdot e^{+s \cdot x/v}\right]}^{-\frac{\partial I(x,s)}{\partial x}} = \overbrace{s \cdot C \cdot \left[V^{+}\left(s\right) \cdot e^{-s \cdot x/v} + V^{-}\left(s\right) \cdot e^{+s \cdot x/v}\right]}^{s \cdot C \cdot V(x,s)} \ . \tag{3.9}$$

Rearranging the term $\frac{s}{v}$ to the left side of the Equation (3.9), the term s is canceled, resulting in $\frac{v}{C}$, *i.e.*, $\sqrt{\frac{L}{C}} = Z_S$,

$$I^{+}\left(s\right) \cdot e^{-s \cdot x/v} - I^{-}\left(s\right) \cdot e^{+s \cdot x/v} = \frac{1}{Z_S} \cdot \left[V^{+}\left(s\right) \cdot e^{-s \cdot x/v} + V^{-}\left(s\right) \cdot e^{+s \cdot x/v}\right] \ . \tag{3.10}$$

Now, by inspection, the relationship between the "constants" $V^{+}\left(s\right)$, $V^{-}\left(s\right)$, $I^{+}\left(s\right)$, and $I^{-}\left(s\right)$ is obtained,

$$I^{+}\left(s\right) = \frac{1}{Z_S} \cdot V^{+}\left(s\right) \ , \tag{3.11a}$$

$$I^{-}\left(s\right) = \frac{1}{Z_S} \cdot \left[-V^{-}\left(s\right)\right] \ . \tag{3.11b}$$

Thus, Equation (3.8b) can be rewritten as

$$I\left(x,s\right) = \frac{1}{Z_S} \cdot \left[V^{+}\left(s\right) \cdot e^{-s \cdot x/v} - V^{-}\left(s\right) \cdot e^{+s \cdot x/v}\right] \ . \tag{3.12}$$

Taking the inverse Laplace transform of Equations (3.8a) and (3.12), and recalling the time shift properly, $\mathscr{L} = \left[f\left(t-\pi\right)\right] = F\left(s\right) \cdot e^{-s \cdot \pi}$, results in

$$v\left(x,t\right) = v^{+} \cdot \left(t - \frac{x}{v_p}\right) + v^{-} \cdot \left(t - \frac{x}{v_p}\right) \ , \tag{3.13a}$$

$$i\left(x,t\right) = \frac{1}{Z_S} \cdot \left[v^{+} \cdot \left(t - \frac{x}{v_p}\right) - v^{-} \cdot \left(t - \frac{x}{v_p}\right)\right] \ . \tag{3.13b}$$

where:

- Z_S is the no losses transmission line surge impedance;

- v_p is the transmission line propagation velocity for lossless transmission lines, calculated by $\sqrt{\frac{1}{L \cdot C}}$; and
- the functions v^+ and v^- can be evaluated from the boundary conditions.

The knowledge presented in this section regarding transmission line modeling using distributed parameters is of utmost importance for studies related to electromagnetic transients in transmission line. Thereby, it is possible to estimate the quantities $v\,(x,t)$ and $i\,(x,t)$ at point H of a transmission line with known parameters. This finding is made by analyzing each line propagation mode for polyphase transmission lines, considering that it is perfectly transposed (WEDEPOHL; WILCOX, 1973; CLARKE, 1943).

3.1.2 TW Phenomenon on Transmission Lines

The occurrence of events such as short circuits in a transmission line, switching maneuvers, lightning strokes, and so on are characterized by an abrupt variation in voltage at the location of the event, modifying the original configuration of the electrical power system (GREENWOOD, 1991). Therefore, this abrupt voltage variation propagates in the form of electromagnetic waves toward the transmission line terminals at speeds close to that of light (for aerial transmission lines) (RIBEIRO *et al.*, 2021; LOPES *et al.*, 2019; RIBEIRO *et al.*, 2018; COSTA *et al.*, 2010).

Figure 3.2 illustrates the pure fault circuit of a transmission line, used to explain the TW phenomenon, in which v_f represents the voltage at the location and moment of the fault, v_{TW} and i_{TW} represent, respectively, the amplitudes of the voltage and current TWs released in the transmission line; and R_f represents the fault resistance.

Figure 3.2: Pure of fault circuit.

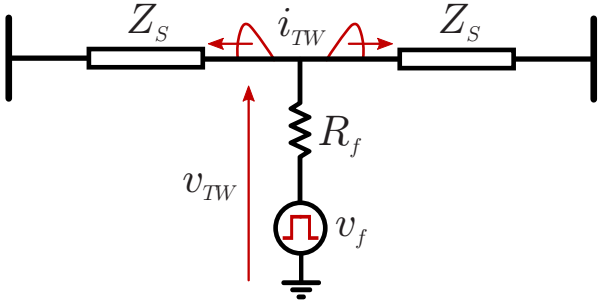

Source: Adapted from (LOPES *et al.*, 2019).

With v_f being an instantaneous value of the power system voltage $V_{Sys} \cdot \sin(\theta)$, where θ is the fault inception angle, v_{TW} is calculated in Equation 3.14a by applying Kirchhoff voltage law in the pure fault circuit. Finally, according to Phadke & Thorp (2009), i_{TW} is calculated using Equation (3.14b) for single-phase faults, in which Z_{S0} and Z_{S1} are, respectively, the positive and zero sequence surge impedances of the transmission line.

$$v_{TW} = -V_{Sys} \cdot \sin(\theta) - 2 \cdot R_f \cdot i_{TW} = -v_f - 2 \cdot R_f \cdot i_{TW} \ , \tag{3.14a}$$

$$i_{TW} = \frac{-3}{Z_{S0} + 2 \cdot Z_{S1} + 6 \cdot R_f} \cdot v_f \ . \tag{3.14b}$$

3.1.3 Traveling Wave Extraction

TWs propagation phenomenon in transmission lines has transient behavior. So, to analyze fault-induced wave fronts, the use of reliable signal filtering is needed to eliminate low frequency components, in order to obtain TW information at the monitored line (COSTA *et al.*, 2010). To make possible measure TWs incident amplitude and time propagation on monitored transmission lines, a number of technologies have been reported, whose principles vary from one to another. Well-known TWs detection and analysis techniques have been reported, such as: discrete wavelet transform and maximal overlapped discrete wavelet transform (COSTA, 2014), Park's transform (LOPES *et al.*, 2013), FIR digital filters (SAHA *et al.*, 2010), and DS filter (SCHWEITZER *et al.*, 2014; SCHWEITZER *et al.*, 2016; LOPES *et al.*, 2019).

Among the aforementioned TWs filtering techniques, the DS filter is a modern and promising filtering solution that stood out for being embedded in a protection relay with functions applied in the time domain (SCHWEITZER *et al.*, 2014; SCHWEITZER *et al.*, 2016). One of the most significant DS filter features is that it creates standard output signals, with unit gain, which is crucial to TW-based protection applications (SCHWEITZER *et al.*, 2016). In addition, its prominence over other techniques for extracting TWs only became possible due to technological advances in signal processing carried out by IEDs which may employ sampling rate in the order of millions of samples per second. According to the papers available in the literature, the DS filter works with a sampling frequency of 1 MHz (f_s) and 21 coefficients (N_{DS}), which means that the filter has a time window length (T_{DS}) equal to 21 μs, making it possible to analyze signals up to a frequency of 500 kHz according to the Nyquist criterion (SCHWEITZER *et al.*,

2015; GUZMÁN *et al.*, 2017; SHARMA; MYNAM, 2018; METZGER *et al.*, 2018; RIBEIRO *et al.*, 2018; LOPES *et al.*, 2019).

According to Equation (3.15), the output of the DS filter is the result of the inner product between the window of filter coefficients ($DS[n]$) and the windowing of the input signal understood as N_{DS} current samples ($Buffer[n]$), in which $[n]$ represents the nth sample, characterized by presenting triangular waveform on its output in response to step changes on its input. Thus, to obtain the unitary gain, using Equation (3.16), observe that $DS[n]$ is composed of $\frac{N_{DS}-1}{2}$ adjusted coefficients with value G, a central coefficient with zero value and $\frac{N_{DS}-1}{2}$ with value -G, where δ is the unit impulse and $G = \frac{2}{N_{DS}-1}$ (LOPES *et al.*, 2019).

$$i_{DS}[n] = \sum_{m=0}^{N_{DS}-1} Buffer[m] \cdot DS[n-m] \ , \tag{3.15}$$

being

$$DS[n] = G \cdot \left\{ \sum_{k=0}^{\frac{N_{DS}}{2}-1} \delta[n-k] - \sum_{k=\frac{N_{DS}}{2}}^{N_{DS}-1} \delta[n-k] \right\} \ . \tag{3.16}$$

Figure 3.3 illustrates the DS filter filtering process, which can be divided into three stages, taking the monitored signal as a reference, namely: Step I) before the detection of a TW; Stage II) upon a TW incidence; and Step III) after a TW detection. In Step I, while the filter only receives signals at the nominal frequency as input, its output has an approximately null value, represented in Equation (3.17); in Step II, when the filter is centered on the step variation, its output has a maximum value, according to Equation (3.18); in Step III, when the filter is inside the step, its output has a value of approximately zero, according to Equation (3.19).

$$i_{DS} = \frac{N_{DS}-1}{2} \cdot G \cdot 0 + \frac{N_{DS}-1}{2} \cdot (-G) \cdot 0 = 0, \tag{3.17}$$

$$i_{DS} = \frac{N_{DS}-1}{2} \cdot G \cdot A + \frac{N_{DS}-1}{2} \cdot (-G) \cdot 0 = A, \tag{3.18}$$

$$i_{DS} = \frac{N_{DS}-1}{2} \cdot G \cdot A + \frac{N_{DS}-1}{2} \cdot (-G) \cdot A = 0. \tag{3.19}$$

To perform the analysis of the phenomena, the Clarke's transform is used to decouple the original signals into modal waves called air modes (α and β) and ground mode (0 or zero). This procedure can be observed in Equation (3.20), where $i_{DS}\alpha$, $i_{DS}\beta$ and $i_{DS}0$ are the decoupled modal currents referenced to phase A. Thus, it is possible to analyze the effect of the TWs

Figure 3.3: DS filter filtering process.

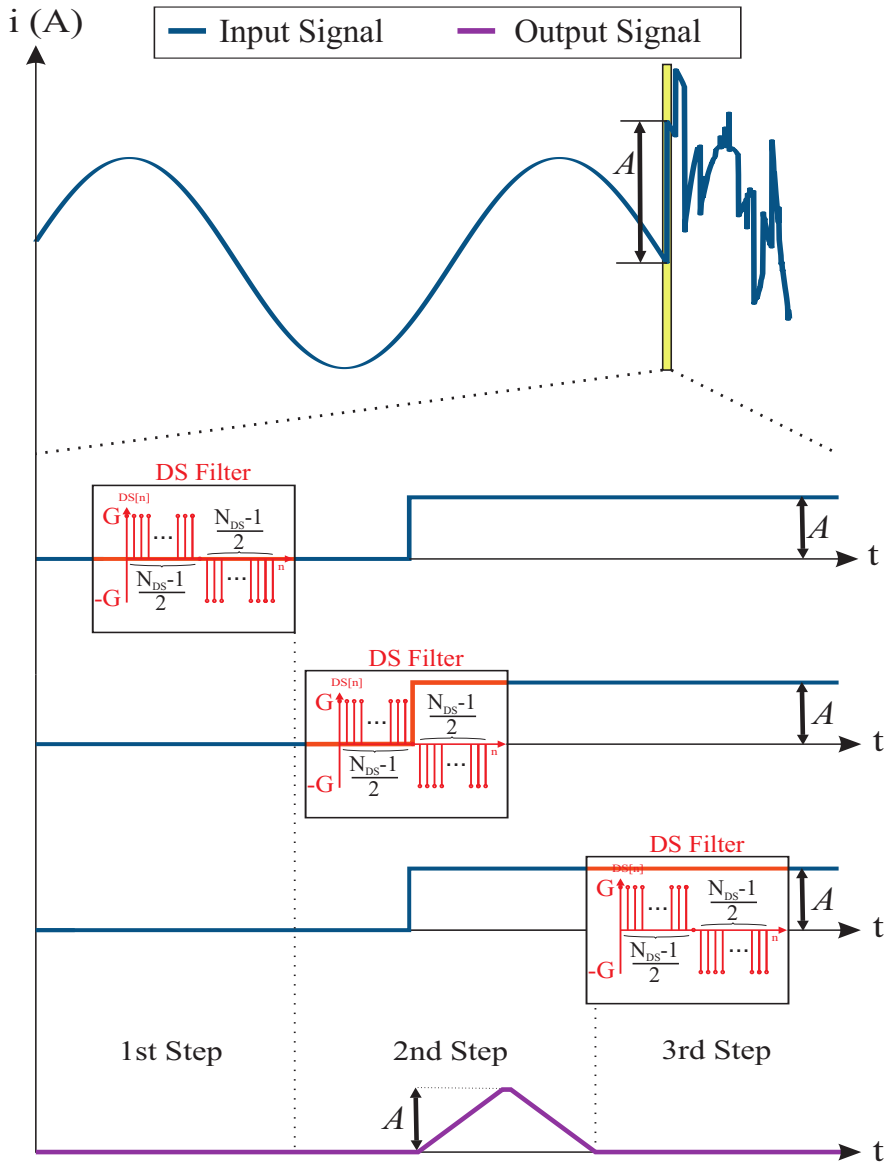

Source: Own authorship.

separately by mode, identifying the differences when using different models of transmission line (SCHWEITZER *et al.*, 2014).

$$\begin{bmatrix} i_{DS}\alpha \\ i_{DS}\beta \\ i_{DS}0 \end{bmatrix} = \frac{1}{3} \cdot \begin{bmatrix} 2 & -1 & -1 \\ 0 & \sqrt{3} & -\sqrt{3} \\ 1 & 1 & 1 \end{bmatrix} \cdot \begin{bmatrix} i_A \\ i_B \\ i_C \end{bmatrix}. \tag{3.20}$$

3.1.4 Analyzed TW Filter

The analyzed TW filter is proposed in (SCHWEITZER *et al.*, 2014) for TW applications on transmission lines. It has been successfully used in fault location methods, such that it

Figure 3.4: DS filter frequency response validation.

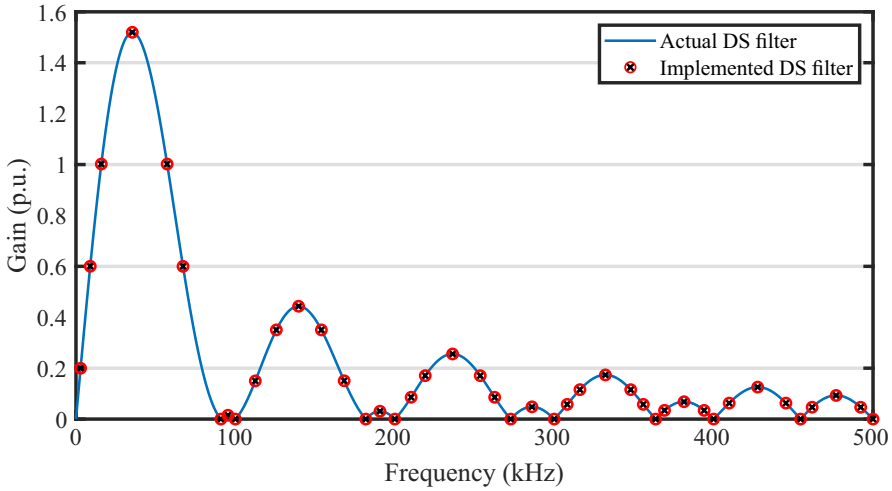

Source: (SCHWEITZER *et al.*, 2015; GUZMÁN *et al.*, 2017; SHARMA; MYNAM, 2018).

is adopted here to be applied in conjunction with the proposed interpolation-based solution. In this work, the DS filter implementation is in accordance to (RIBEIRO *et al.*, 2018), whose frequency response is depicted in Figure 3.4, where the DS filter model is validated through comparisons with the original one built into a commercial available time-domain-based relay. Moreover, besides the proposed scheme, the DS filter is also used to implement the classical TW1-method, but without applying interpolation procedures to simulated data.

3.2 DESCRIPTION OF FAULT LOCATION METHODS

This section describes the theoretical background of the fault location methods analyzed in this thesis. Phasor-based and TW-based fault location (PHFL and TWFL, respectively) techniques are explained, and, for the sake of simplicity, they will be called hereafter PH1, PH2, and TW1 methods.

In this thesis, the PHFL algorithms are used as references to compare the results with those obtained from the TWFL algorithm. Additionally, the traditional double-ended TWFL technique was chosen because this technique only uses the first arrival time of TWs in both transmission line ends, being the most reliable TWFL technique (GALE *et al.*, 1993) and, therefore, more suitable to assess the proposed method.

3.2.1 PH1-Method

The PH1-method is the one reported in (JOHNS; JAMALI, 1990). It assumes that, when a fault occurs on a transmission line, as depicted in Figure 3.5, a relationship between the positive sequence voltage at the fault inception point (F), $\hat{V}_{F1}$, can be expressed in terms of positive sequence voltages and currents measured at local terminal ($\hat{V}_{S1}$ and $\hat{I}_{S1}$) as follows:

$$\hat{V}_{F1} = \cosh(\gamma \cdot m) \cdot \hat{V}_{S1} - Z_S \cdot \sinh(\gamma \cdot m) \cdot \hat{I}_{S1} \ , \tag{3.21}$$

or using the remote terminal data ($\hat{V}_{R1}$ and $\hat{I}_{R1}$):

$$\hat{V}_{F1} = \cosh[\gamma \cdot (LL - m)] \cdot \hat{V}_{R1} - Z_S \cdot \sinh[\gamma \cdot (LL - m)] \cdot \hat{I}_{R1} \ , \tag{3.22}$$

in which γ is the line propagation constant (JOHNS; JAMALI, 1990).

Figure 3.5: Single-phase network.

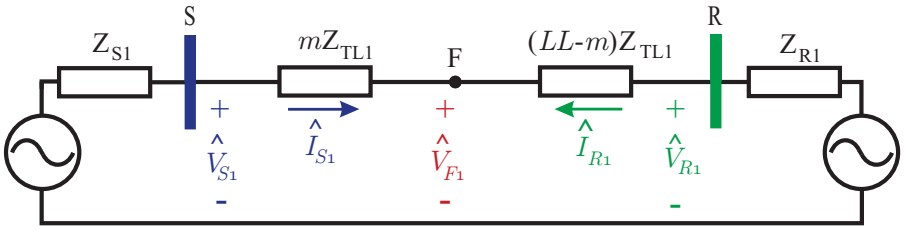

Source: Own authorship.

Rearranging Equations (3.21) and (3.22), the fault location estimation (m) can be estimated by:

$$m = \mathrm{Re}\left[\frac{\tanh^{-1}\left(-\frac{B}{A}\right)}{\gamma}\right] \ , \tag{3.23}$$

being:

$$A = Z_S \cdot \cosh(\gamma \cdot LL) \cdot \hat{I}_{R1} - \sinh(\gamma \cdot LL) \cdot \hat{V}_{R1} + Z_S \cdot \hat{I}_{S1} \ , \tag{3.24}$$

$$B = \cosh(\gamma \cdot LL) \cdot \hat{V}_{R1} - Z_S \cdot \sinh(\gamma \cdot LL) \cdot \hat{I}_{R1} - \hat{V}_{S1} \ . \tag{3.25}$$

3.2.2 PH2-Method

The double-ended PH2-method is reported in (TZIOUVARAS *et al.*, 2001; COMMITTEE *et al.*, 2005; SHRESTHA; MUTHA, 2023). It works based on the analysis of negative-sequence voltage profiles along the line for both symmetrical and asymmetrical faults, respectively. From

the negative-sequence network, as depicted in Figure 3.6, the negative-sequence voltage at F ($\hat{V}_{F2}$) can be calculated considering measurements taken from both local and remote line terminals as:

$$\hat{V}_{F2} = \hat{V}_{S2} - \frac{m}{LL} \cdot Z_{LT_2} \cdot \hat{I}_{S2} \ , \tag{3.26}$$

$$\hat{V}_{F2} = \hat{V}_{R2} - \frac{LL - m}{LL} \cdot Z_{LT_2} \cdot \hat{I}_{R2} \ . \tag{3.27}$$

Rearranging Equations (3.26) and (3.27), m can be obtained by:

$$m = LL \cdot \text{Re}\left[\frac{\left(\hat{V}_{S2} - \hat{V}_{R2}\right) + Z_2 \cdot \hat{I}_{R2}}{Z_{LT_2} \cdot \left(\hat{I}_{S2} - \hat{I}_{R2}\right)}\right] \ . \tag{3.28}$$

Figure 3.6: Negative-sequence network.

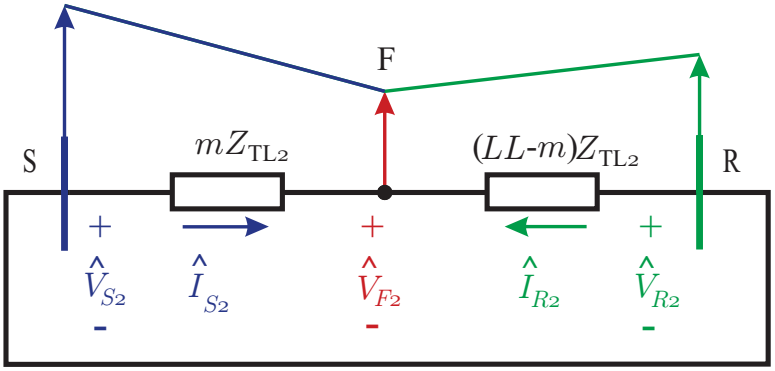

Source: Own authorship.

3.2.3 TW1-Method

The traditional double-ended TWFL technique is called here TW1-method. It is reported in (GALE *et al.*, 1993) and, according to the authors, this technique depends on using sampling frequencies in the order of hundreds of kHz to guarantee accurate fault distance estimations (LOPES *et al.*, 2019).

Indeed, high sampling rates ensure high time resolutions, which in turn improve the accuracy of TW detectors (SCHWEITZER *et al.*, 2014). In internal fault cases, as depicted in Figure 3.7, current TWs are launched toward both terminals, such that the fault location estimation (m) can be calculated by Equation (3.29), considering the τ and the arrival time indexes of the first

current TWs at both terminals (NS and NR for local and remote line ends, respectively) (GALE *et al.*, 1993).

$$m = \frac{LL}{2} \cdot \left[1 + \left(\frac{NS - NR}{\tau}\right)\right] . \tag{3.29}$$

Figure 3.7: TWs internal faults pattern.

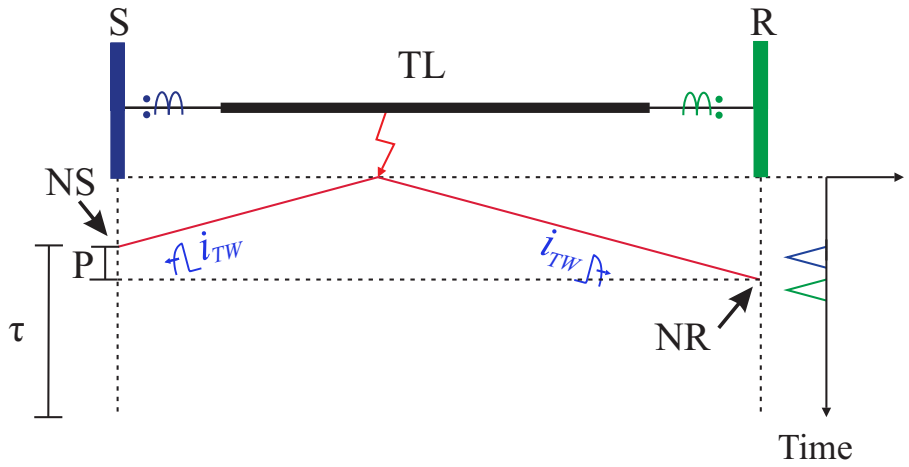

Source: Adapted from (SCHWEITZER *et al.*, 2014).

3.3 LINEAR INTERPOLATION: CONCEPT REVIEW

The sophistication of systems designed to do signal expression processing is directly influenced by the incorporation of fundamental signal processing concepts, theorems, and properties. As an example, environments that incorporate the relationship between sampling rate and aliasing can make effective use of decimation and interpolation strategies for filtering implementation (OPPENHEIM, 1999). Notwithstanding, the interpolation procedure to increase the number of samples in a given record is called here upsampling (OPPENHEIM, 1999; CROCHIERE; RABINER, 1983). To explain such a procedure, consider a signal $x[n]$, whose number of samples will be increased by an integer factor L, called here as interpolation factor. Thus, analogously to a discrete-to-continuous conversion, if a continuous-time signal $x_c(t)$ is taken into account, the main objective of the interpolation is to obtain samples $x_i[n] = x_c(nTi)$, where $Ti = T/L$, from the sequence of samples $x[n] = x_c(nT)$, being T the time period of the analyzed signal. Therefore, one may observe that:

$$x_i[n] = x[n/L] = x_c(n \cdot T/L), \; n = 0, \pm L, \pm 2 \cdot L, \ldots , \tag{3.30}$$

where $x_i[n]$ can be obtained from $x[n]$ using discrete-time processing. Ideally the ideal interpolation procedure occurs in two steps, as described in Figure 3.8, where a sampling rate expander is computed via Equation (3.31), being followed by an ideal low-pass discrete-time filter with cutoff frequency π/L, gain L, and impulse response as represented in Equation (3.32) (OPPENHEIM, 1999).

Figure 3.8: Upsampling system.

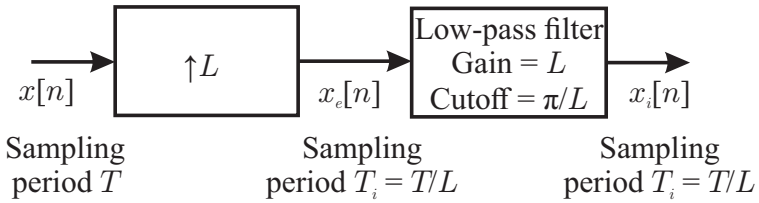

Source: (OPPENHEIM, 1999).

$$x_e[n] = \sum_{k=-\infty}^{\infty} x[k] \cdot \delta[n - k \cdot L] \ . \tag{3.31}$$

$$h_i[n] = \frac{\sin(\pi \cdot n/L)}{\pi \cdot n/L} \ . \tag{3.32}$$

According to (OPPENHEIM, 1999), although an ideal lowpass filter $h_i[n]$ cannot be implemented exactly for interpolation, approximations can be designed. Therefore, a simpler procedure to perform the linear interpolation uses two original samples to calculate a new sample, which takes place on a straight line connecting the initial samples. The impulse and frequency response of the interpolator filter (IF) are depicted in Figure 3.9a and 3.9b, respectively.

One may observe that the IF impulse response ($IF[n]$) is triangular shaped, and the interpolator filter frequency response (IFFR) is similar to those of low-pass filters, limited to the factor L. Thus, the IF coefficients are defined in Equation (3.33), being composed by $2 \cdot L + 1$ coefficients.

$$IF[n] = \begin{cases} 1 - |n|/L, & |n| \leq L \\ 0, \text{otherwise} \end{cases} \ . \tag{3.33}$$

3.4 FREQUENCY RESPONSES DETAILED STUDY FOR USING BUTTERWORTH, DS, AND IF FILTERS

This section presents the behavior of the frequency responses of the DS filter, the IF filter, and with the Butterworth filter. In this way, it is possible to strategically identify the best

Figure 3.9: Interpolator filter: (a) Impulse response; (b) Frequency response.

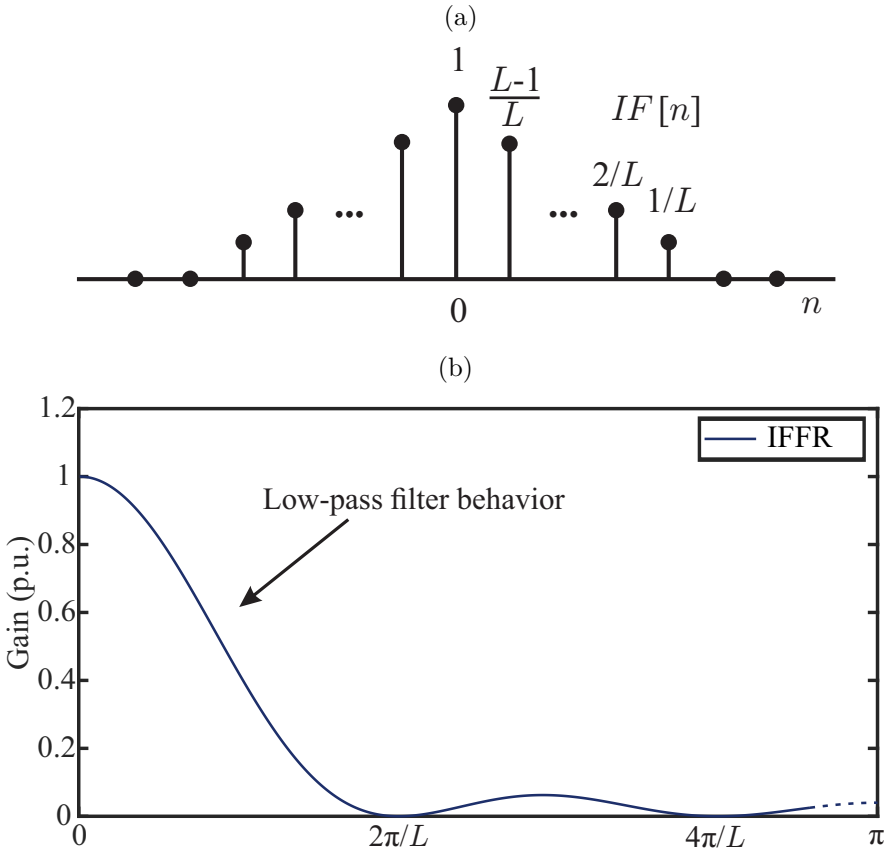

Source: Own authorship.

choice of the number of coefficients used in each filter for the desired sampling frequency. The Butterworth filter response is presented in all results because it guarantees compliance with Nyquist criteria.

3.4.1 On Combining DS and Butterworth Filters Frequency Responses

Figures 3.10, 3.11, and 3.12 depicts the behavior of a range of possible choices for NDS, when different fs are considered. The number of NDS coefficients studied are {10, 21, 50, 100, 200, 251} and fs are {15.36 kHz, 50 kHz, 100 kHz, 200 kHz, 400 kHz, 600 kHz, 800 kHz,1 MHz}.

Firstly, it's possible to realize a relationship between the number os lobes in the frequency response and the NDS value, *i.e.*, the number of lobes is directly proportional to NDS. Also, trough Figures 3.10, 3.11, and 3.12, it is possible to understand that as the number of NDS coefficients are increased, the filter response relies in the lower part of the frequency band spectrum. Still, a relationship can be seen between f_s and the number of NDS, *i.e.*, for the

same value of NDS, as f_s is reduced, the smaller the range of the frequency spectrum to be analyzed. For example, as reported in (LOPES *et al.*, 2019), an IED that uses TW extraction techniques via DS filter performs the estimation using a number of coefficients equal to 21 for a sampling frequency of 1 MHz. In this aspect, via frequency response analysis, the filter extracts the TWs mainly located in the first 100 kHz of the frequency spectrum.

Finally, Table 3.1 presents the frequency values with greater lobes peaks, *i.e.*, greater gain of each NDS and f_s evaluated. Thus, it is possible to realize that the combination of the DS and Butterworth filters can be used in any f_s to focus the TW extraction in a particular range of the frequency spectrum.

Table 3.1: Frequency with greater gain obtained in DS·Butter frequency response for different NDS vs. f_s.

Frequency with greater gain (kHz)						
f_s \ NDS	10	21	50	100	200	251
15.36 kHz	1.149	0.5428	0.2280	0.114	0.057	0.0454
50 kHz	3.7407	1.7671	0.7423	0.3711	0.1855	0.1478
100 kHz	7.4814	3.5342	1.4845	0.7421	0.371	0.2956
200 kHz	14.9628	7.0684	2.969	1.4842	0.742	0.5912
400 kHz	29.9256	14.1368	5.938	2.9684	1.484	1.1824
600 kHz	44.8884	21.2052	8.907	4.4526	2.226	1.7736
800 kHz	59.8512	28.2736	11.876	5.9368	2.968	2.3648
1 MHz	74.814	35.342	14.845	7.421	3.71	2.956

Source: Own authorship.

Figure 3.10: DS filter sampling frequency variation for: (a) $NDS = 10$; and (b) $NDS = 21$.

(a)

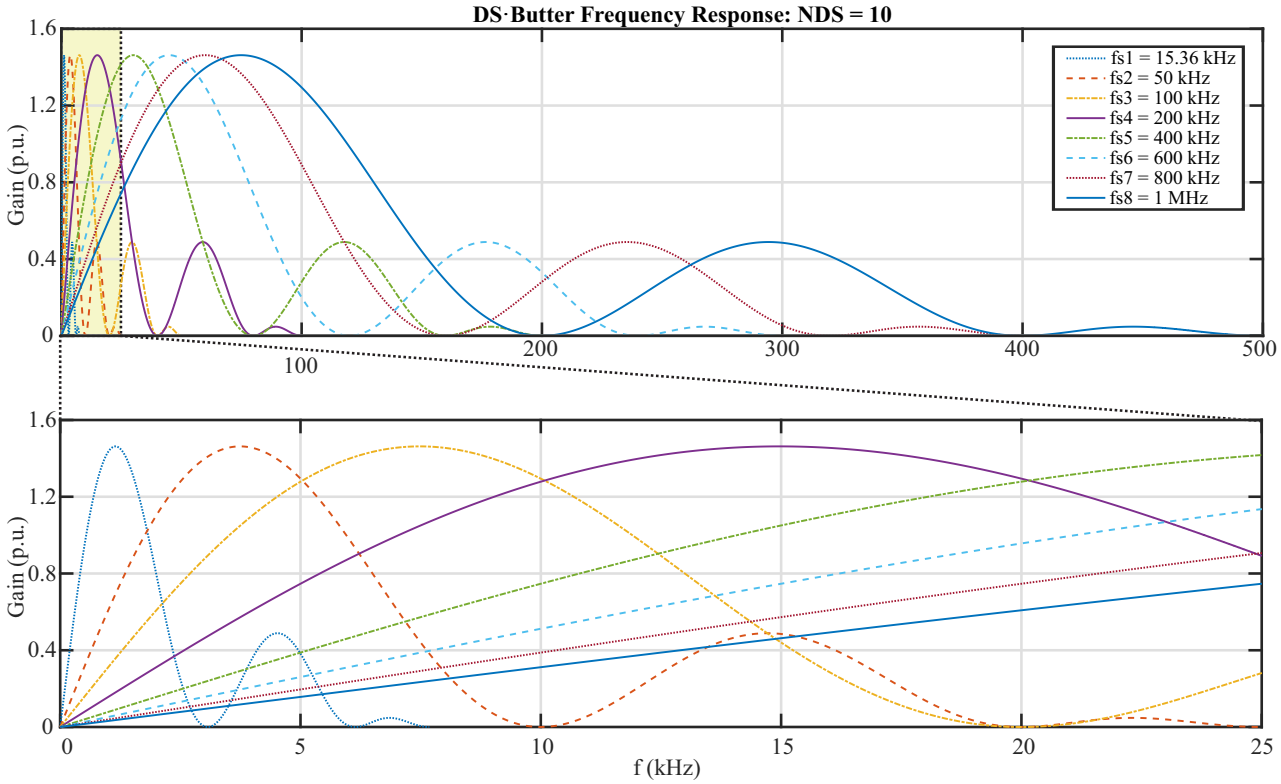

(b)

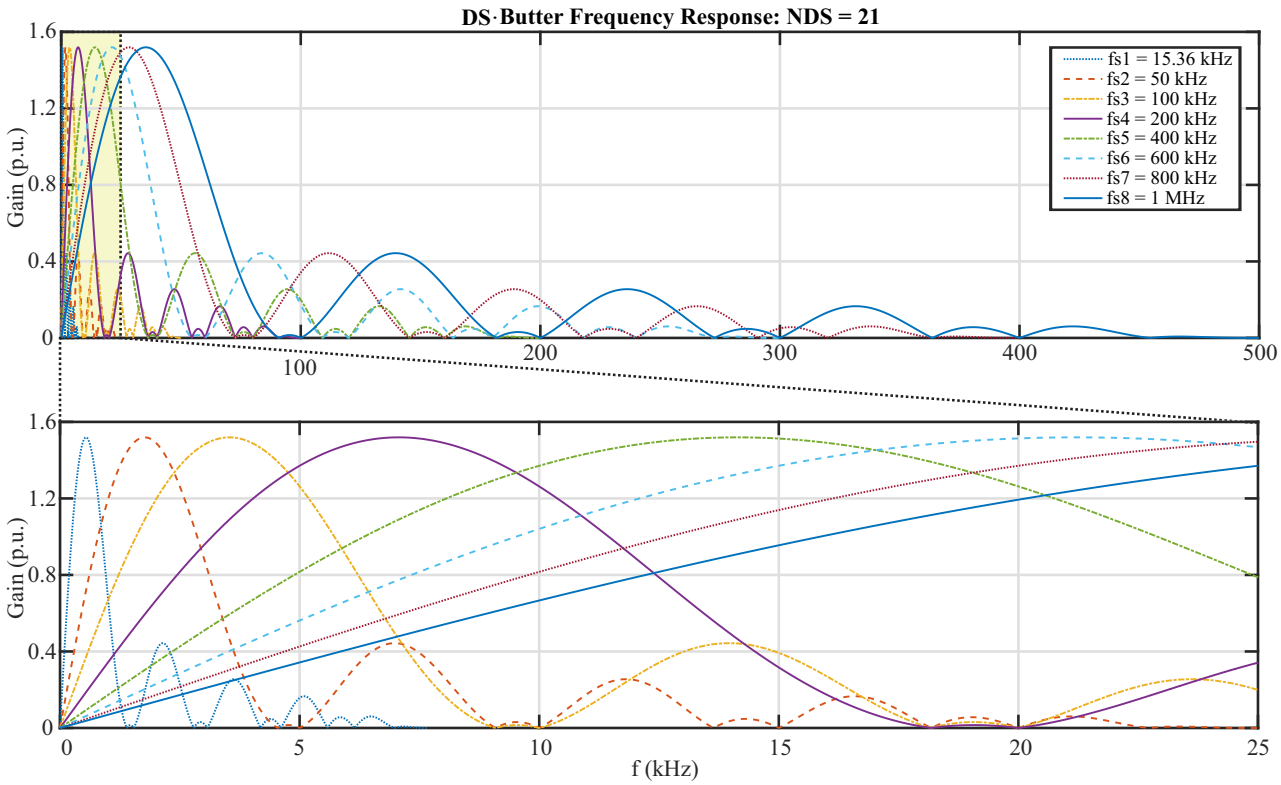

Source: Own authorship.

Figure 3.11: DS filter sampling frequency variation for: (a) $NDS = 50$; and (b) $NDS = 100$.

(a)

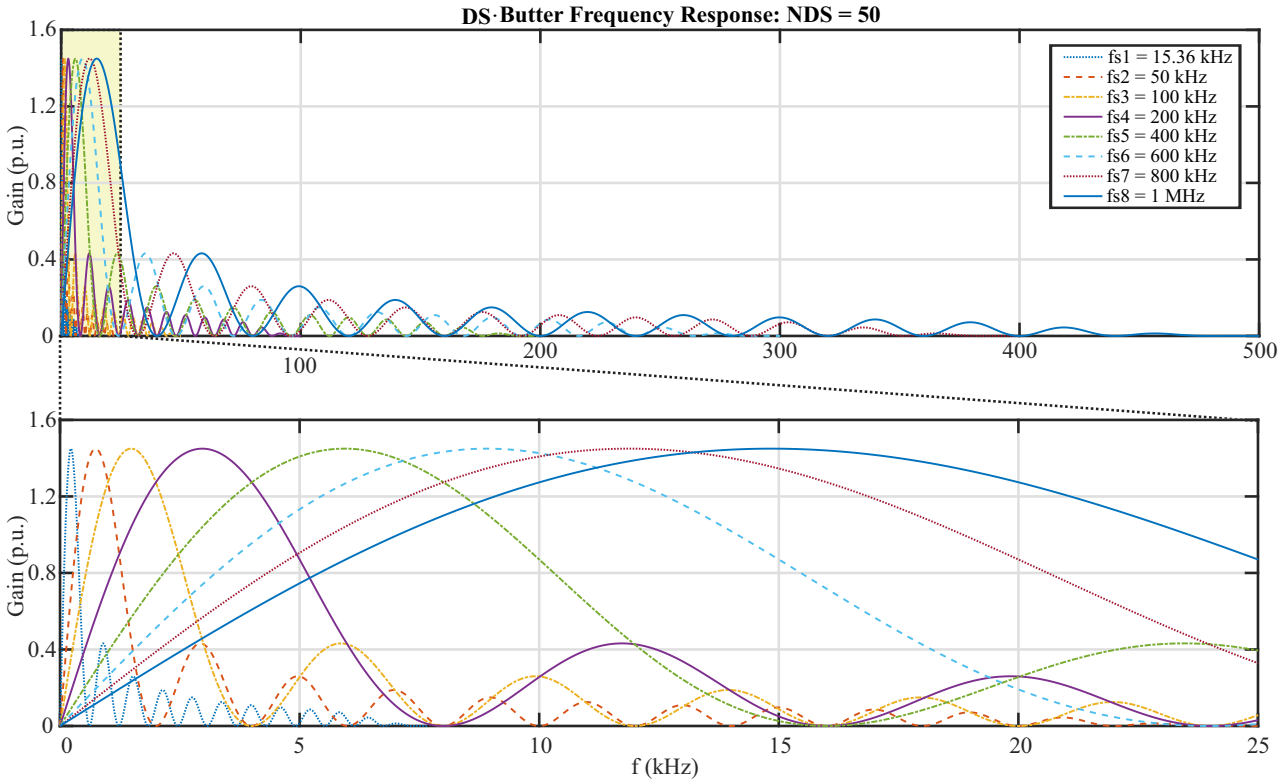

(b)

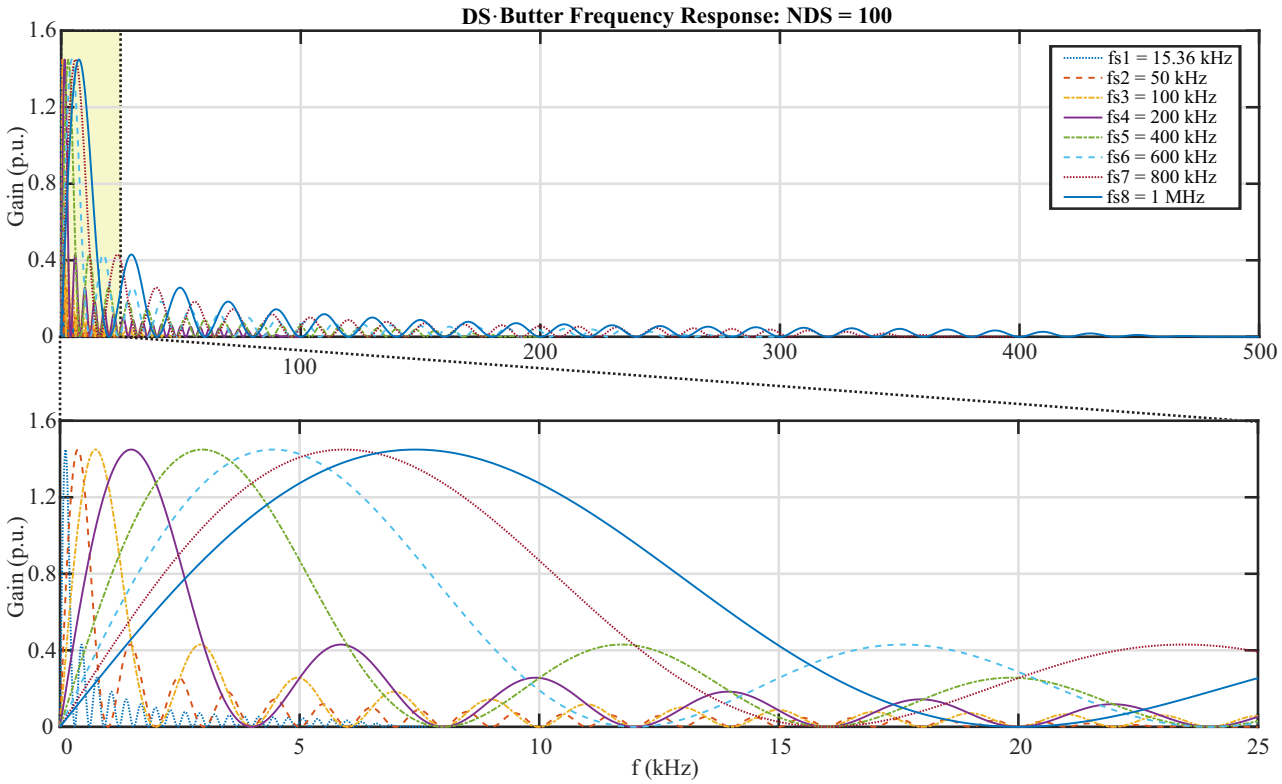

Source: Own authorship.

Figure 3.12: DS filter sampling frequency variation for: (a) $NDS = 200$; and (b) $NDS = 251$.

(a)

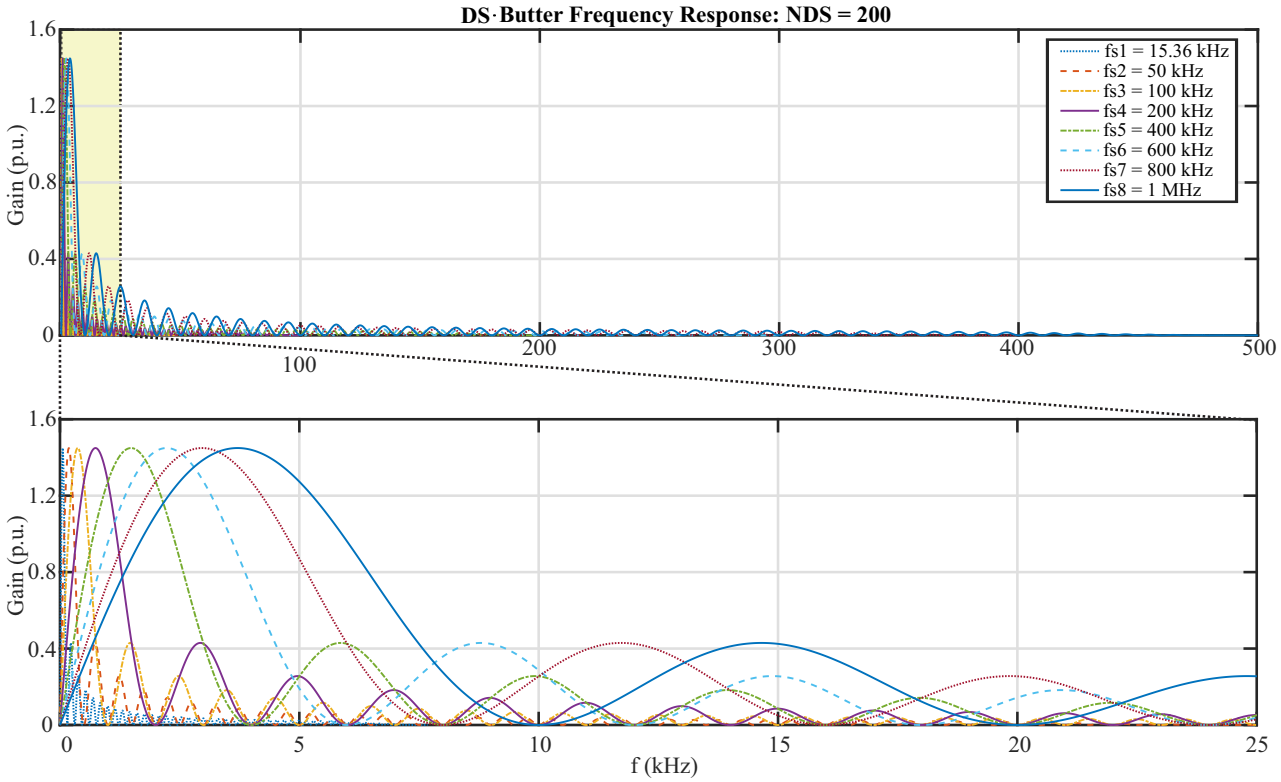

(b)

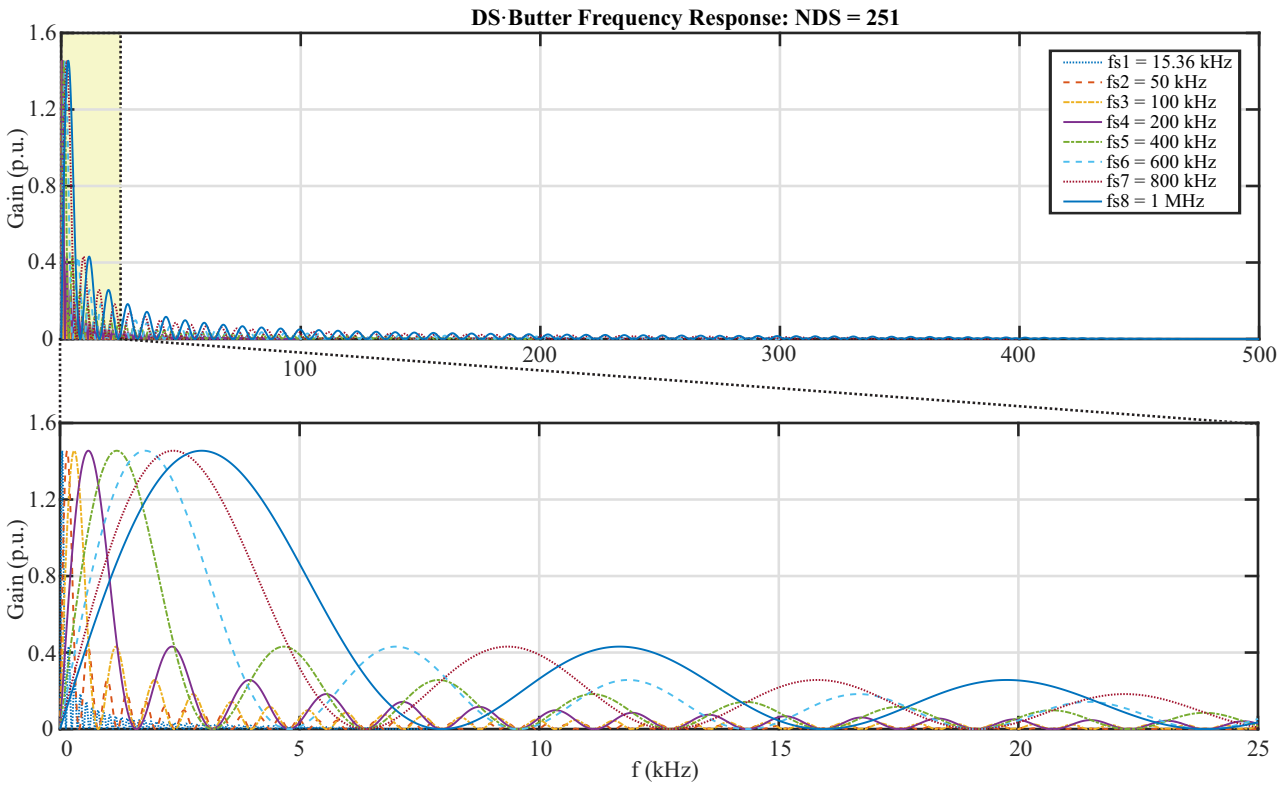

Source: Own authorship.

3.4.2 On Combining IF and Butterworth Filters Frequency Responses

The IF filter frequency response behavior is illustrated in Figures 3.13, 3.14, and 3.15. It is depicted that the higher the interpolation factor is, the smaller the final frequency spectrum to be explored by the technique will be. It can be seen that the IF filter has similar behavior to the Butterworth filter, but its cutoff frequency is a function of f_s, that is, the first time its frequency response reaches zero is equal to the input f_s of the IF filter. Therefore, the frequency spectrum range of interest must lie between zero and $f_s/2$, being the IF technique used before the application of the DS filter to extract TWs using the low-frequency spectrum content.

To facilitate the understanding of the Figures 3.13, 3.14, and 3.15, Table 3.2 presents what is called here as the "original frequency" needed to obtain the final f_s using the adopted L factor.

Table 3.2: Original frequency to obtain f_s using the factor L.

Original frequency (kHz)						
Final f_s \ L	10	20	30	40	50	65
15.36 kHz	1.536	0.768	0.512	0.384	0.3072	0.2363
50 kHz	5	2.5	1.6667	1.25	1	0.7692
100 kHz	10	5	3.3333	2.5	2	1.5385
200 kHz	20	10	6.6666	5	4	3.0769
400 kHz	40	20	13.3333	10	8	6.1538
600 kHz	60	30	20	15	12	9.2308
800 kHz	80	40	26.6667	20	16	12.3077
1 MHz	100	50	33.3333	25	20	15.3846

Source: Own authorship.

Finally, according to (LOPES *et al.*, 2022) it is essential to realize that the Butterworth filter limits the analysis spectrum to, typically, 40% of f_s to guarantee compliance with the Nyquist criteria and thus avoid the aliasing phenomenon. Therefore, it is essential to consider the presence of the Butterworth filter when choosing f_s, aiming to maintain the frequency spectrum of interest between 0 and 40% of f_s. Therefore, it is suggested to use the following boundary conditions

$$0 < \frac{f_i}{f_s} \leq 0.4 \ , \tag{3.34a}$$

$$0 < \frac{f_i}{f_c} \leq 1 \ , \tag{3.34b}$$

$$0 < \frac{f_c}{f_s} \leq 0.4 \ , \tag{3.34c}$$

in which f_i is the frequency of interest in the frequency spectrum.

This way, if the three conditions expressed by Equations (3.34a), (3.34b), and (3.34c) are met, it is guaranteed that the frequency spectrum of interest will not be affected by the filtering techniques of the Butterworth and IF filters. Lopes *et al.* (2022) suggest that, for transmission line faults, signals with frequencies in the order of 20 kHz represent significant results regarding to TW-based fault location. Therefore, for using the IF filter in relation to the extraction of TWs originated from transients in transmission lines, $f_s \geq 50$ kHz is suggested.

3.4.3 Strategy for IF and DS Filter Coefficients Choice

To correctly choose the number of coefficients of the DS and IF filter, it is necessary to evaluate the behavior of the convolution of the DS, IF, and Butterworth filters, aiming to identify which one has a higher gain for the used sampling frequency and, finally, check if the choices result in the desired behavior to the TW extraction from the original signal. As aforementioned, the Butterworth filter cutoff frequency is equal to 40% of the Nyquist frequency. Indeed, knowing the order and the cutoff frequency of the Butterworth filter is essential to correctly choosing the most suitable DS and IF filter. Therefore, as demonstrated in the previous subsection, the choice of f_s must be made based on f_i. Finally, when also considering the DS filter, it is important to ensure that the final form of the frequency response covers f_i.

Figure 3.13: IF filter sampling frequency variation for: (a) L = 10; and (b) L = 20.

(a)

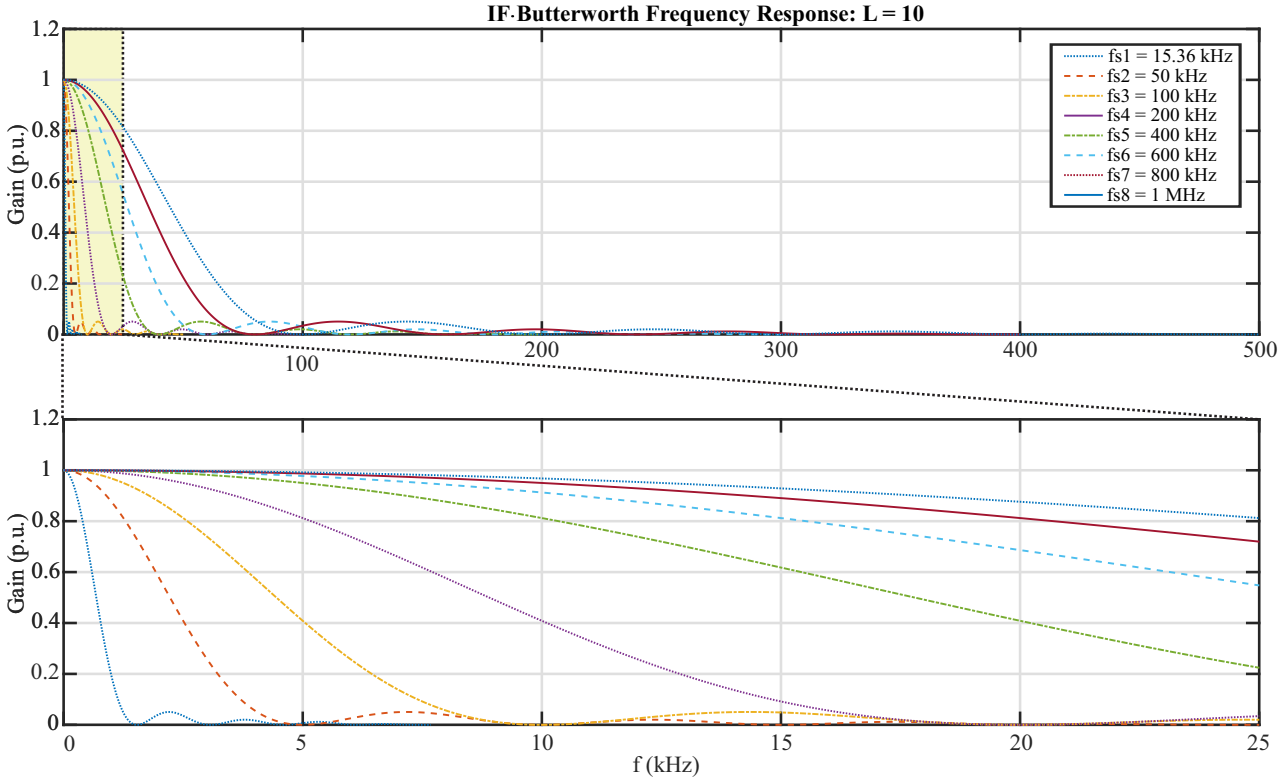

(b)

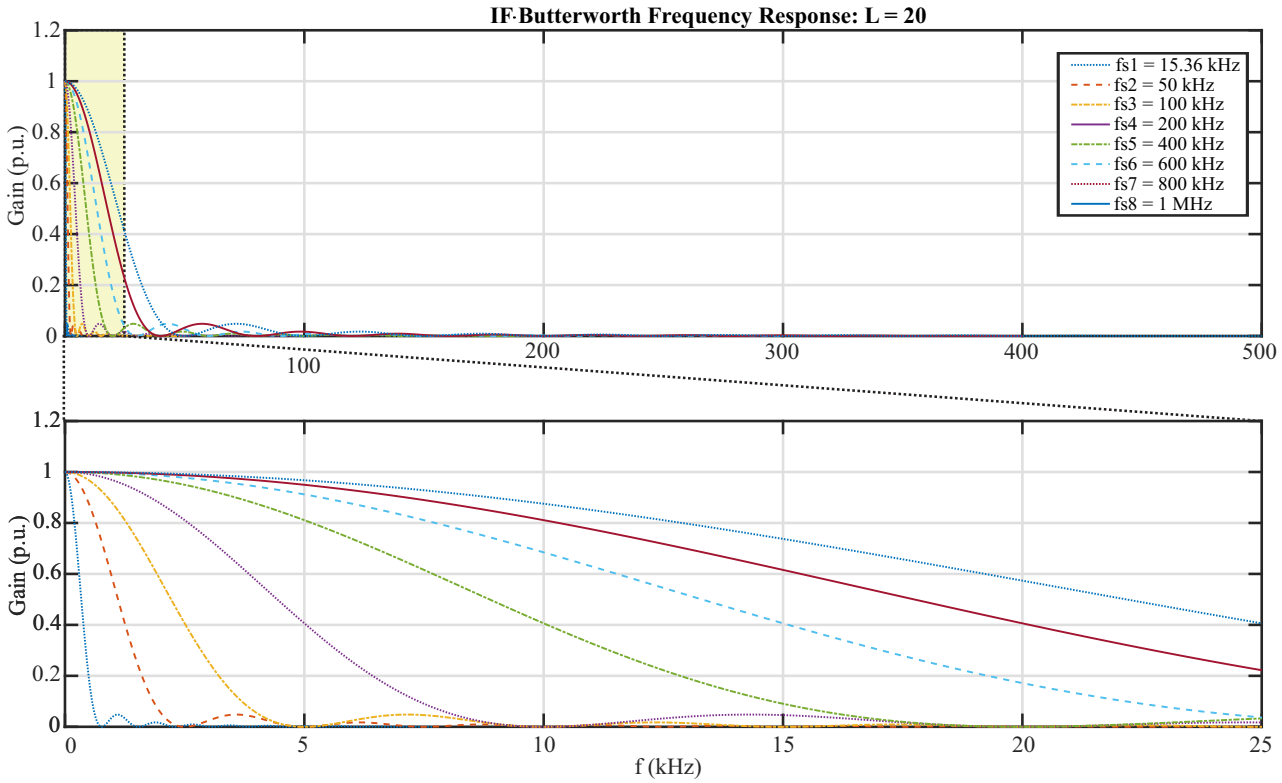

Source: Own authorship.

Figure 3.14: IF filter sampling frequency variation for: (a) L = 30; and (b) L = 40.

(a)

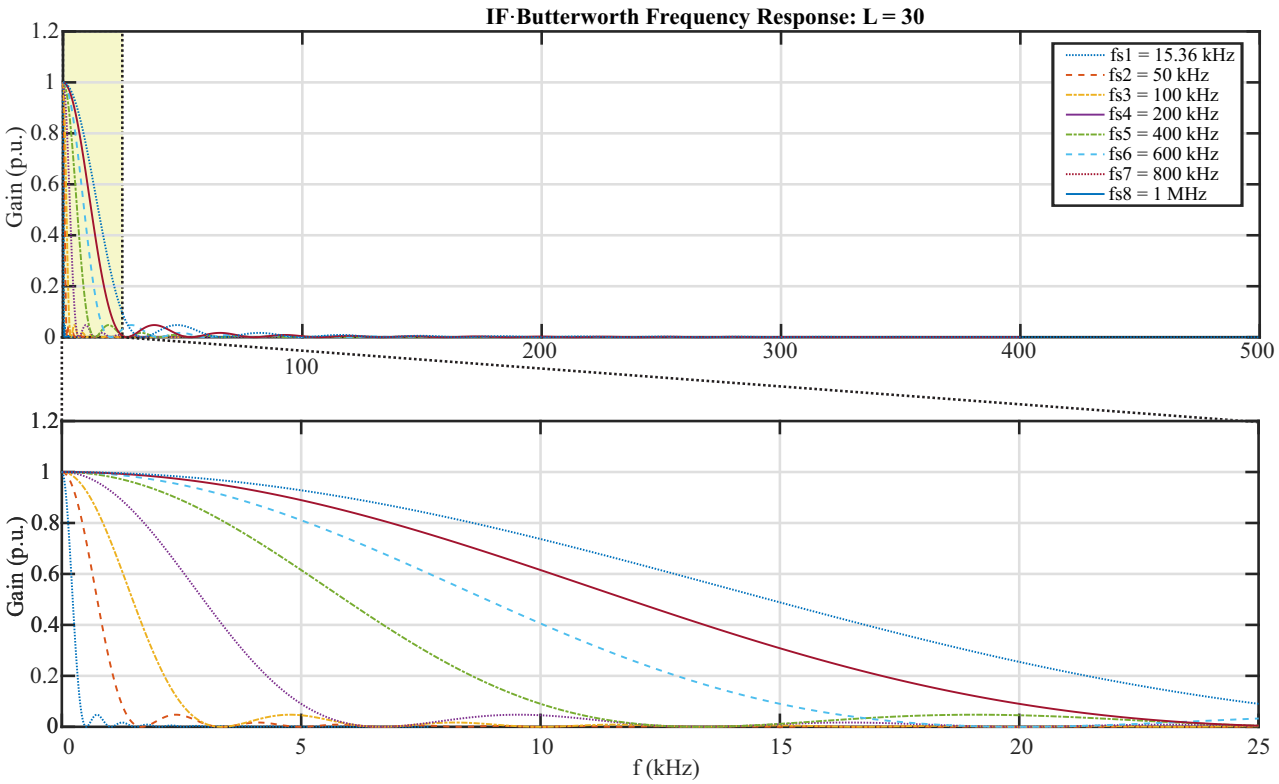

(b)

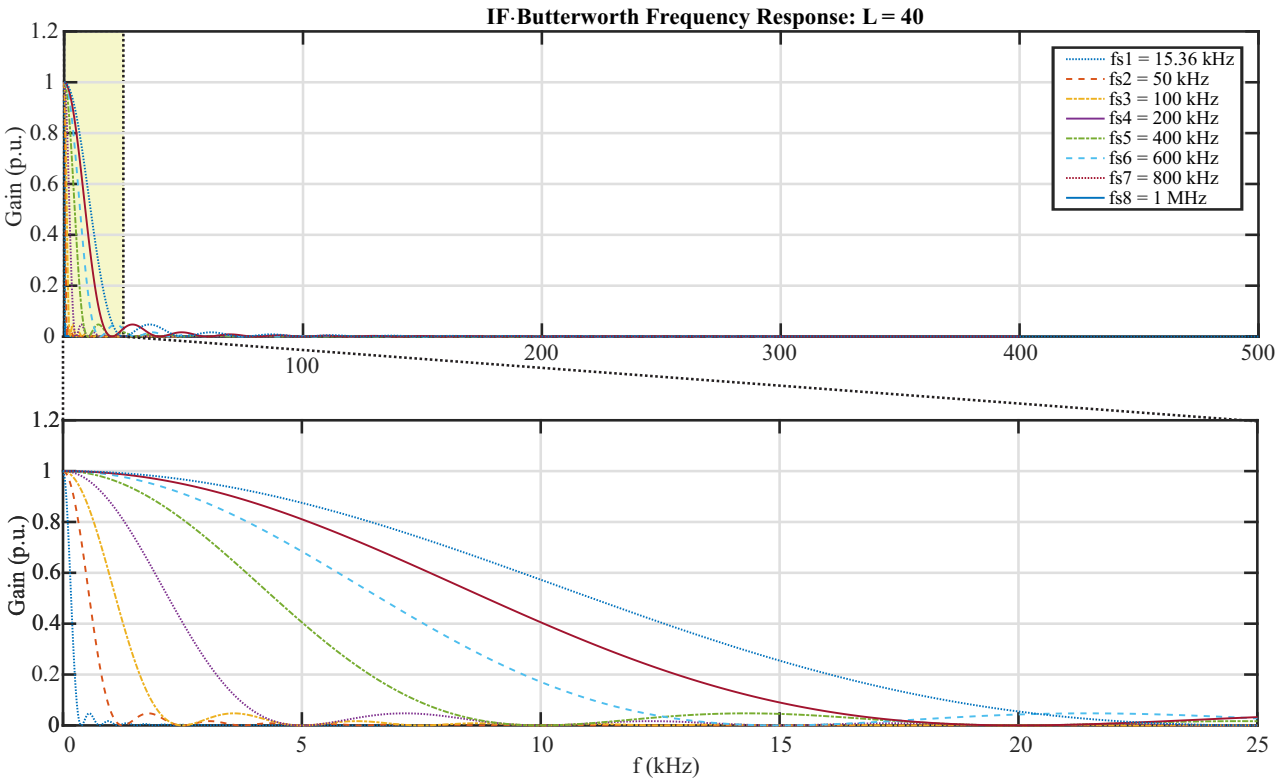

Source: Own authorship.

Figure 3.15: IF filter sampling frequency variation for: (a) L = 50; and (b) L = 65.

(a)

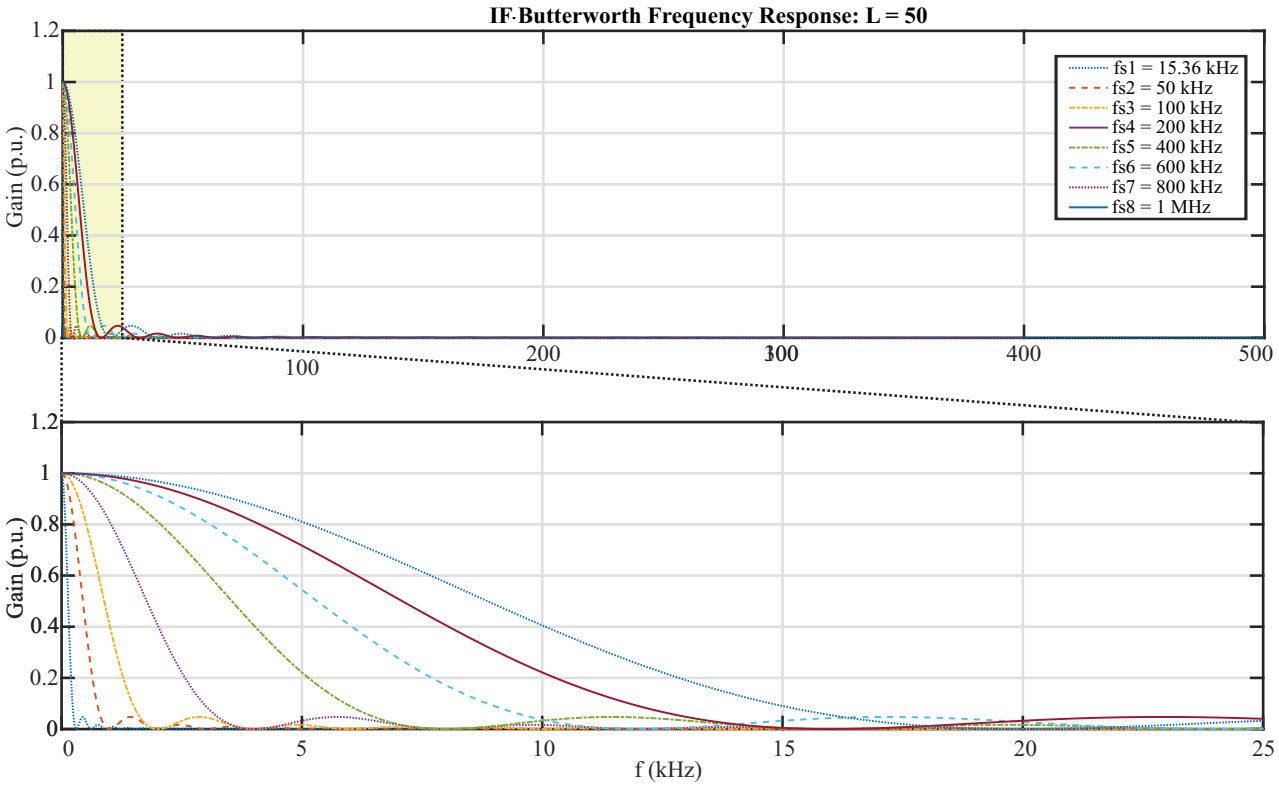

(b)

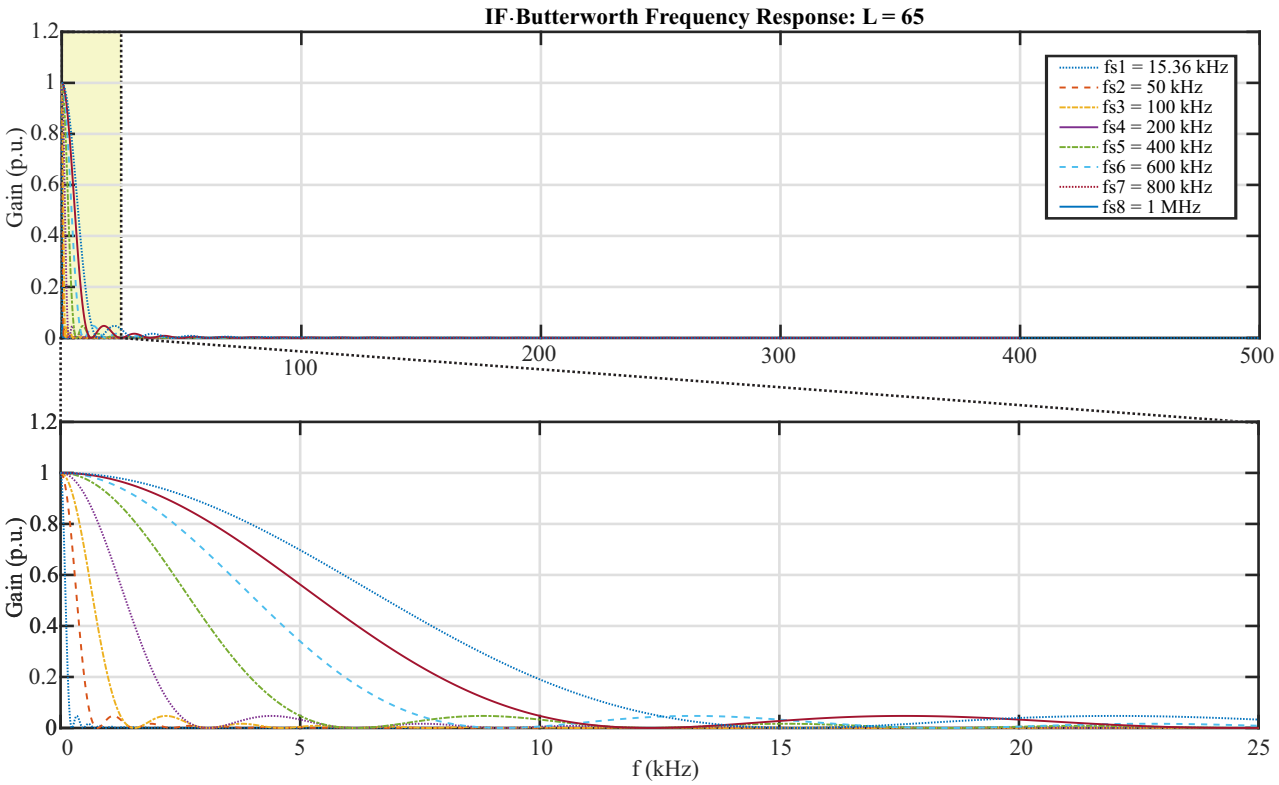

Source: Own authorship.

CHAPTER 4

METHODOLOGY AND TEST POWER SYSTEM

4.1 PROPOSED SCHEME

In this chapter, the linear interpolation technique is proposed for DFRs with relatively low sampling rates. Here, case studies are carried out considering DFRs which employ 1,024 samples/cycle. Thus, the number of samples in the records are increased to obtain the same number of samples found in traditional TW-based fault locators. By doing so, although only the inferior transient spectrum band is available, as reported in (LOPES *et al.*, 2022), TW filters can be adapted to properly analyze such a spectrum content, preserving accuracy in the TW arrival time stamping procedure.

4.1.1 Anti-Aliasing Filter

The parameters of the analog Butterworth filters used to assess the fault location solutions are presented in Table 4.1. Aiming to define the IF and DS filter settings, a series of studies were also performed.

Table 4.1: Analog Butterworth filter settings for the evaluated methods.

Method	Order	fc (Hz)
PH1	3	180
PH2	3	180
TW1	2	400 k
Proposed	2	24,576

Source: Own authorship.

4.1.2 Proposed Combination of IF and DS Filter

Combinations of different values of L and number of coefficients of the DS filter (NDS) were analyzed. Figures 4.1a and 4.1b present the frequency responses obtained from the convolution of implemented anti-aliasing Butterworth filters, DS filters, and IF filters, considering all the analyzed combinations between L and NDS. From the obtained results, $L = 16$ is chosen because the interpolated frequency of 983,040 Hz is the closest one to the 1 MHz sampling frequency used in the actual TW-based device taken as reference (SCHWEITZER *et al.*, 2015; GUZMÁN *et al.*, 2017; SHARMA; MYNAM, 2018).

Moreover, the original DS filter with NDS = 21 reported in (SCHWEITZER *et al.*, 2015; GUZMÁN *et al.*, 2017) results in step responses with unitary gains when applied to signals sampled directly on 1 MHz. However, here, NDS = 251 is chosen to provide a step response with gain close to the unit for the combination of DS, IF, and Butterworth filters when applied to the interpolated signal using $L = 16$ (see Figure 4.2). By doing so, the proper analysis of the lower frequency spectrum band, which concentrates most of line fault-induced transients energy, is guaranteed (LOPES *et al.*, 2022). It is noteworthy that the inherent delay on TW peak detection when using the DS Filter with NDS = 251 does not compromise the fault location procedure, since the same filter is applied to signals from both line terminals, thereby the time difference between incident local and remote TWs is preserved.

4.2 TEST POWER SYSTEM

The test power system used to validate the proposed interpolation-based solution was modeled in ATP/ATPDraw and it corresponds to part of the 500 kV/60 Hz Brazilian interconnected power system described in Figure 4.3. Through the 500 kV lines, two Brazilian states are interconnected to the rest of the Brazilian power grid. Between power stations Lechuga and Xingu there are 1,173 kilometers of 500 kV overhead transmission lines which cross the Amazon rainforest, as depicted in Figure 4.4, facing a high density of trees that achieve from 40 meters up to 110 meters in height. It highlights the importance of using an accurate fault location method for this kind of line.

Figure 4.1: Convolution of Butterworth, DS, and IF filters in function of: (a) L; (b) NDS.

(a)

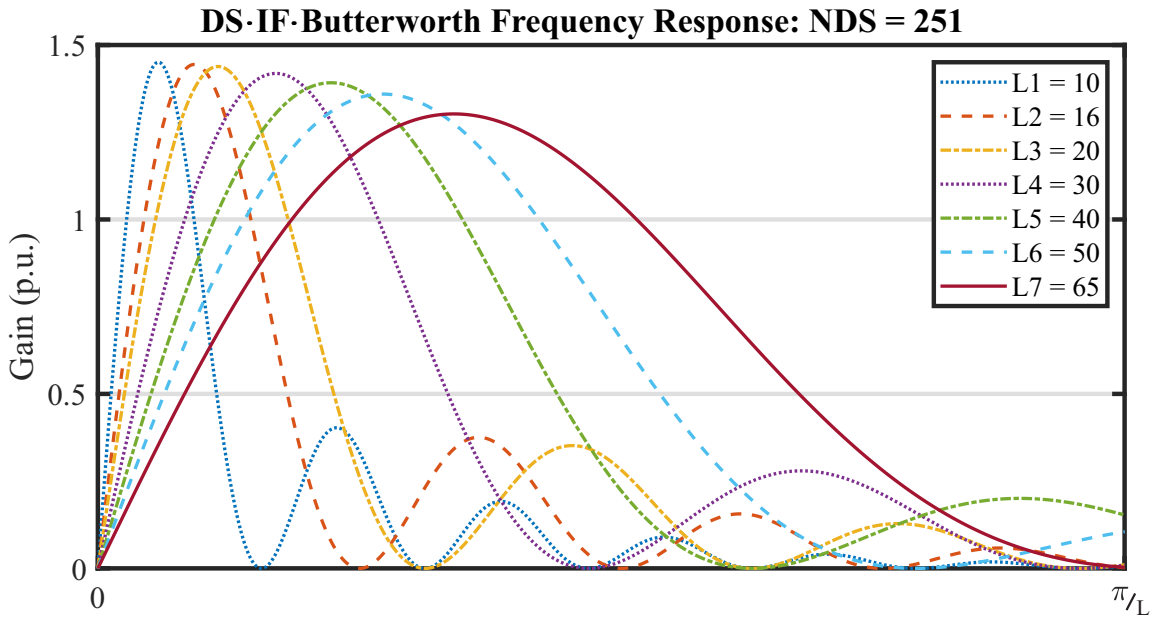

(b)

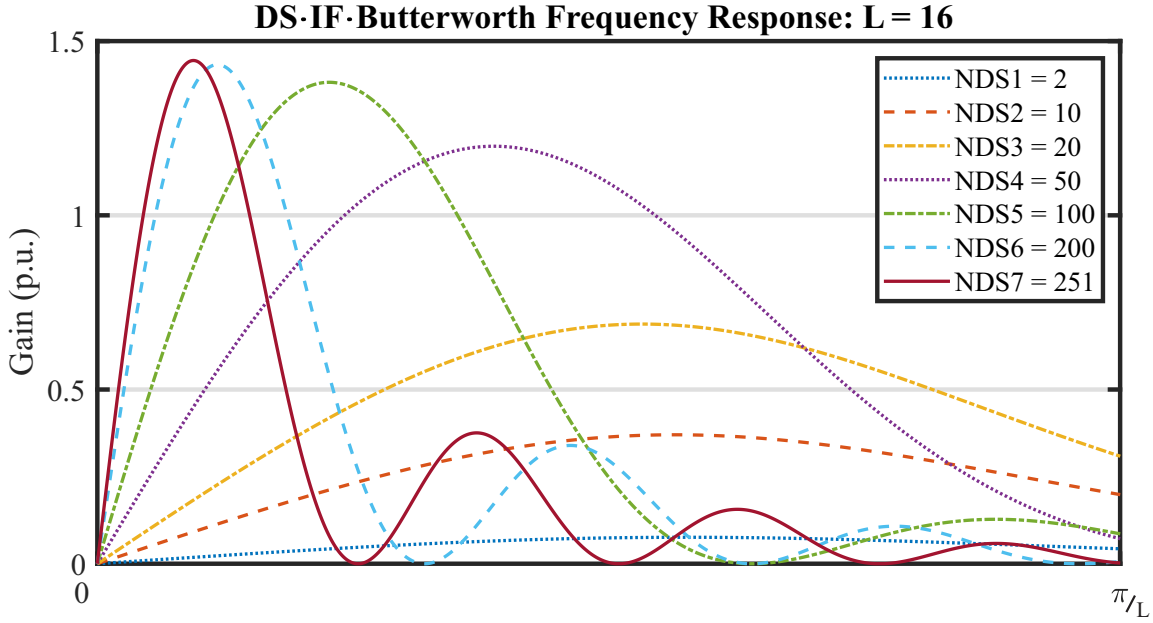

Source: Own authorship.

Besides the environmental challenging, the following equipment are installed nearby, revealing how much complex is to operate such a part of the Brazilian power grid:

(i) 800 kV bipole LCC-HVDC 2,084 km long between stations Xingu and Estreito;

(ii) 800 kV bipole LCC-HVDC 2,518 km long between stations Xingu and Terminal Rio;

Figure 4.2: Comparison between the DS filter step response using the signal sampled directly on 1 MHz and the interpolated one obtained from the signal sampled on 61.44 kHz.

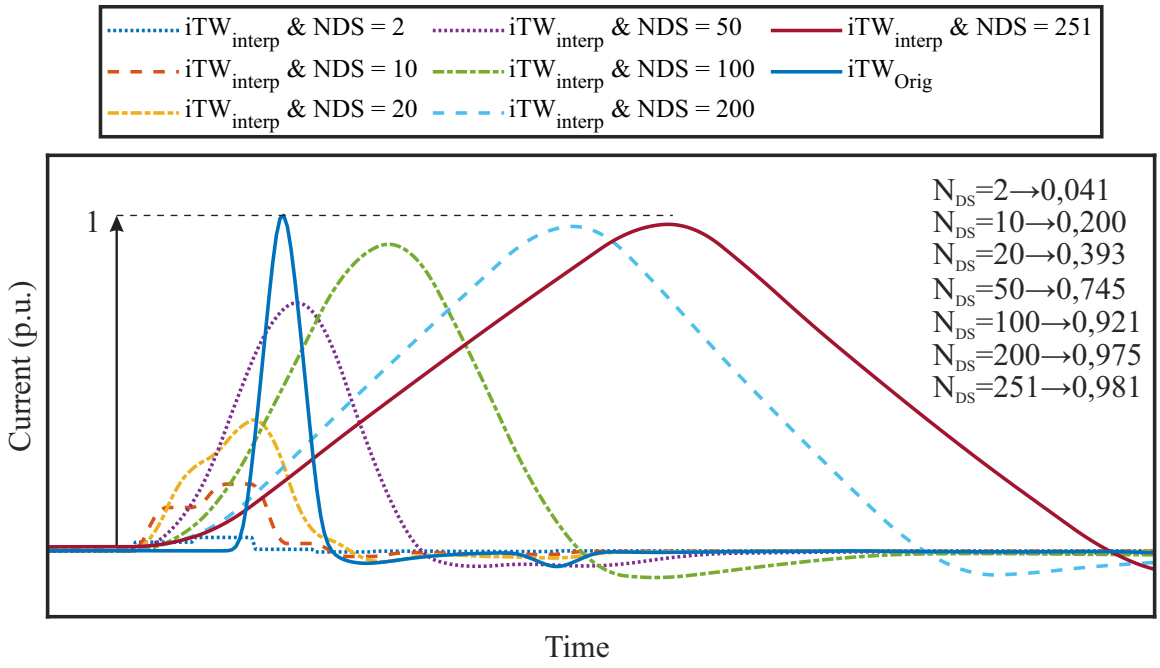

Source: Own authorship.

(iii) Three 500 kV SVCs installed on stations Silves, Oroximiná, and Jurupari;

(iv) FSCs on each terminal of the double-circuit line between stations Lechuga and Xingu, and on the terminal Xingu of the double-circuit line between Xingu and Tucuruí;

(v) Belo Monte hydroelectric power plant with 18 generator units whose capacity is 611 MW each;

(vi) Tucuruí hydroelectric power plant with 23 generator units, among which 12 have capacity of 350 MW each, whereas 11 have capacity of 390 MW each;

(vii) Thermal and hydroelectric power plants on the 230/138 kV subsystems connected to the Lechuga station.

Table 4.2 represent a description of simulations carried out to evaluate and validate the proposed solution, where 132 phase-A-to-ground (AG) and 132 phase-B-to-phase-C (BC) fault cases were simulated on the circuit 2 of the 500 kV double-circuit line between stations Silves and Oroximiná (with 333.5 km long and $\tau = 1.116$ ms), varying the fault distance from station Silves. Two loading scenarios were considered: 1) light load (with 360 A at steady-state);

Figure 4.3: Single-line diagram of the part of the Brazilian power grid modeled in ATP/ATPDraw.

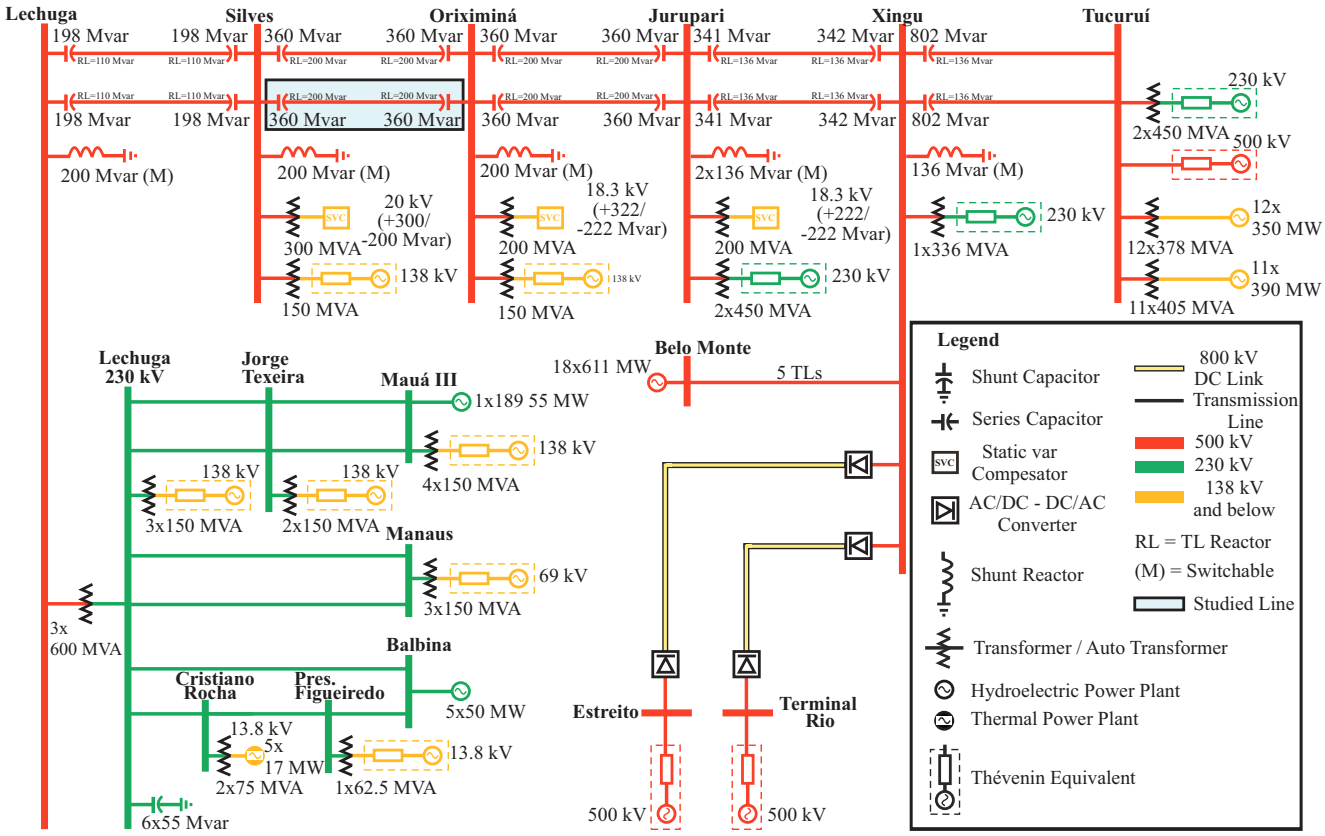

Source: Own authorship.

and 2) heavy load (with 805 A at steady-state). For each loading condition, 66 cases were simulated, resulting in the above-mentioned 132 cases per fault type, accounting for 264 case studies. Furthermore, all scenarios were simulated as solid faults, *i.e.*, fault resistance was set with values equal to 1E-5 Ω.

Table 4.2: Details of simulated cases.

Parameter	Value
Power system simulation frequency	1 MHz
Fault resistance	1E-5 Ω
Number of fault locations	66
Steady-state loading scenarios	2 (360 A and 805 A)
Fault types	2 (AG and BC)

Source: Own authorship.

It is important to emphasize that the studied double-circuit 500 kV transmission line between stations Lechuga and Oroximiná was modeled using J. Marti model, being the SVC

Figure 4.4: Photograph of the evaluated 500 kV double-circuit transmission line between stations Silves and Oriximiná.

Source: Own authorship.

models connected at the Lechuga, Silves and Oroximiná stations, such as indicated by the manufacturer. The FSCs were modeled to provide the expected behavior of the internal protections and phenomena associated to its triggering and, to represent the HVDC lines, the models of 800 kV Xingu / Estreito and Xingu / Terminal Rio links were also included in the ATP/ATPDraw simulation.

CHAPTER 5

RESULTS OVER ATP/ATPDRAW SIMULATIONS

This chapter describes the performance analysis of the assessed algorithms. Firstly, the issues of the PHFL-based algorithms are highlighted, and the differences between the TW waveforms obtained with the TW1 method and the proposed one are presented. Then, the comparison of PH1, PH2, TW1, and proposed methods is carried out over 264 simulated cases for a sampling rate of 1,024 samples/cycle; 264 cases for a sampling rate of 512 samples/cycle; 264 cases for a sampling rate of 256 samples/cycle; 2,640 cases to evaluate the influence of noise present in the electrical signals over the proposed algorithm; 264 cases to assess different TW extraction strategies; and 2,112 cases to clarify differences between interpolation methods.

5.1 WAVEFORMS ANALYSIS

In order to further explain the performance of each fault location method, consider Figures 5.1 and 5.2 which depicts the current signals measured at station Silves for an AG solid fault with inception angle equal to 90° simulated at 25 km (*i.e.*, 0.075 pu of the line length) from Silves in the circuit 2 of the 500 kV double-circuit line between stations Silves and Oriximiná. The fault location estimations, m, obtained from both PH1 and PH2, and the TW1 and proposed method were calculated from these waveforms.

From Figures 5.1a, during the pre-fault period, one can observe harmonic distortions even in the steady-state currents generated by the natural behavior of thyristors switching in SVCs and HVDCs. The pre-fault period ends with the arrival of the first incident TWs, followed by the phase-A amplitude-raising. The monitored line and the others in its vicinity are series compensated, so that subsynchronous oscillation may take place during faults (ANDERSON; FARMER, 1996). Thus, even when the FSC spark gap is triggered in the station Silves, the subsynchronous oscillation phenomena remains. The FSC bypass at Silves also induces

additional transients, which may affect fault location methods. Moreover, it can be noticed that the subsynchronous oscillation leads m estimation to present errors when PHFL-based methods are used. This effect is depicted in Figure 5.1b. Indeed, when fault transients reach Silves, the m values estimated by PH1 and PH2 methods oscillate around the actual fault location. It can be also observed that the PH2 presents a better performance than the PH1, but their performances are compromised by the subsynchronous oscillation.

Figures 5.2a and 5.2b depict the aerial mode current waveforms ($i\alpha TW$) computed for signals measured at stations Silves and Oriximiná, which are used by TW1 and proposed method. One can see that the subsynchronous oscillation phenomena and SVC and HVDC effects over steady-state do not affect TW-based solutions because the first incident TWs on both terminals can be easily identified from the analysis of the waveform.

Additionally, one can see that, despite the difference between the input sampling frequencies for TW1 and proposed method as presented in Table 4.2, the obtained result when subtracting NS by NR (0.95 ms and 0.947 ms) for both methods is quite accurate, leading to fault locations of 25.2516 km and 24.7863 km, respectively. Indeed, the use of a DS filter with NDS = 251 in the proposed method does not jeopardize the first incident TW detection, which can be observed by the amplitude and waveform of the first incident TWs. Also, a lower attenuation is observed in the $i\alpha TWR$ in the proposed technique in comparison to the TW1 method, which shall be better investigated in future works to investigate the feasibility of precise single-ended TWFL solutions using low sampling rate interpolated signals.

Figure 5.1: PHFL and TWFL-methods behavior: (a) Monitored current signals; and (b) PH1 and PH2-methods.

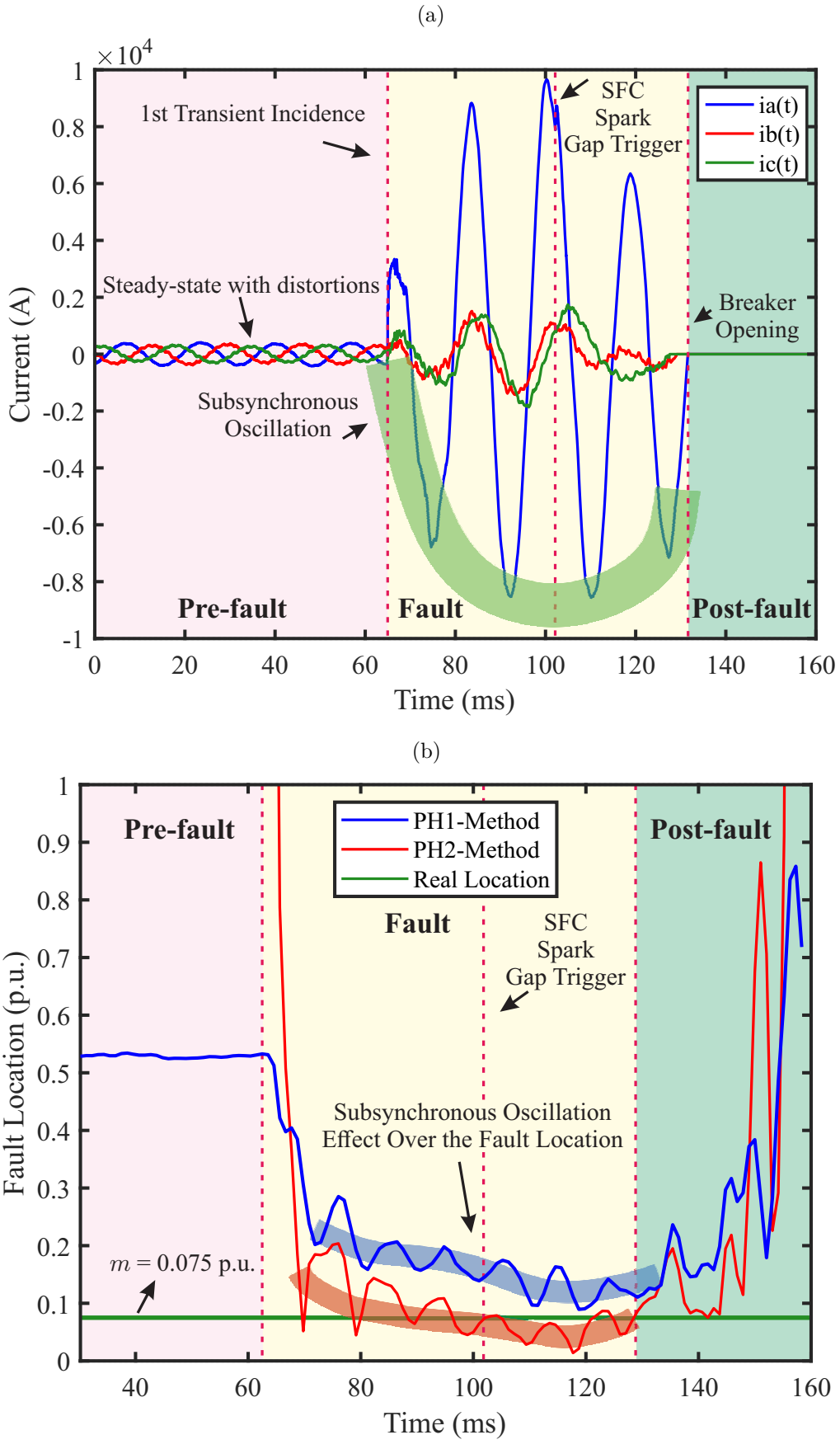

Source: Own authorship.

Figure 5.2: TWFL-methods behavior: (a) TW1 method; (b) Proposed method.

(a)

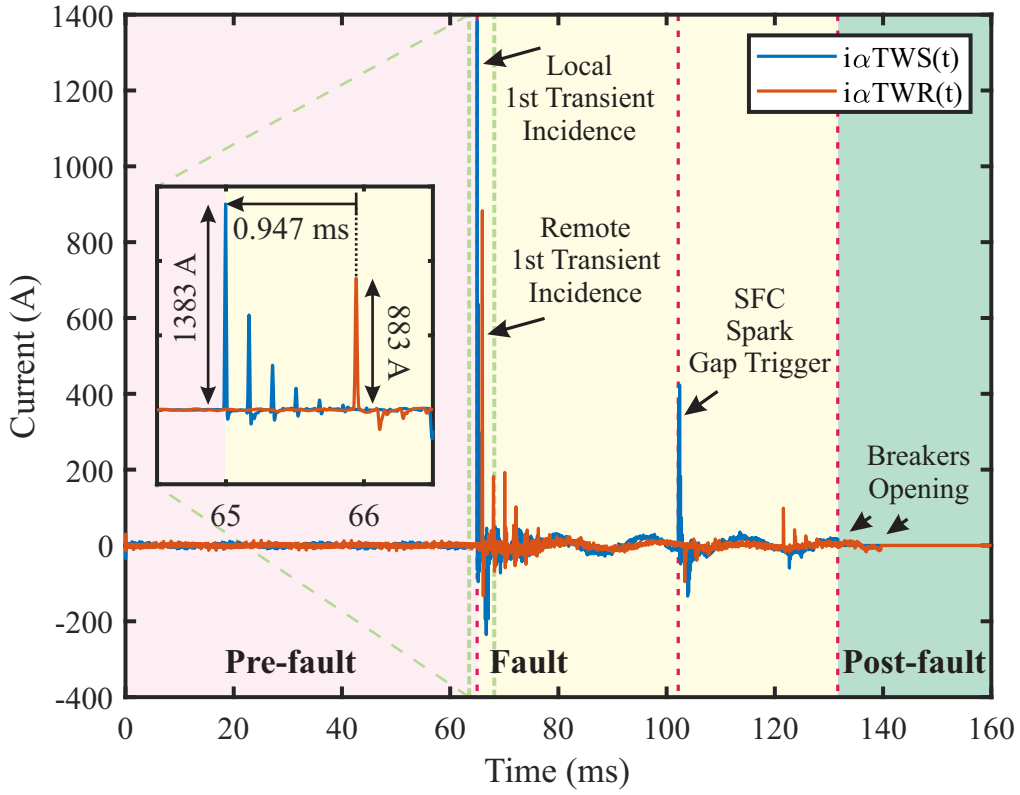

(b)

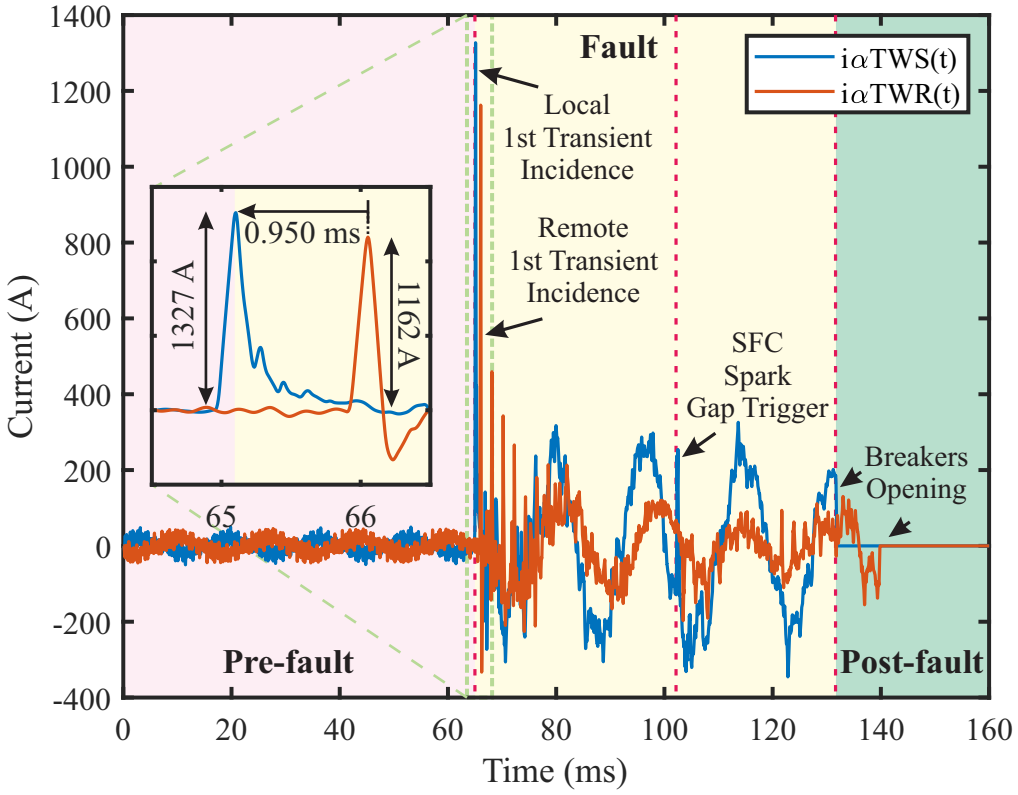

Source: Own authorship.

5.2 FAULT LOCATION ALGORITHMS COMPARISON

As the main result of this chapter, a comparison between the fault location errors for the evaluated algorithms in each fault scenario is depicted in Figures 5.3 and 5.4. It can be seen that for the assessed AG faults, the influence of SVCs, HVDCs, and subsynchronous oscillation caused by FSC jeopardizes PH1 and PH2-methods, resulting in errors about few tens of kilometers. Although the PH1 method also presents approximately the same error rates for BC fault cases, the PH2 method has an enhanced accuracy. Conversely, TW-based methods TW1 and the proposed one are not jeopardized by the fault type, load scenario, and different equipment installed on the system, because they do not influence the TWs generated at the fault point. As a result, high accuracy is guaranteed for both methods, highlighting the reliability and robustness of TWFL approaches.

Furthermore, although the proposed method results in average fault location error in the order of 500 meters (using low sampling rate interpolated signals), these errors are still about only 350 meters greater than those obtained via traditional TW1-method (using high sampling rate signals). Even so, these errors are considered quite close to each other, such that benefits of the proposed solution can be clearly identified, especially from a cost perspective, since it is much cheaper to develop a device with 61.44 kHz sampling frequency rather than with 1 MHz. Indeed, the obtained errors remain around 0.15% of the line length, and they are almost constant for faults at different locations. Therefore, the obtained results highlight the effectiveness of the proposed interpolation methodology for TW-based applications when DFRs with high sampling rates are unavailable.

Figure 5.3: Fault location algorithms comparison on light load scenario for sampling rate equal to 1.024 samples per cycle, *i.e.*, 61.440 kHz: (a) A-phase-to-ground; and (b) B-phase-to-C-phase.

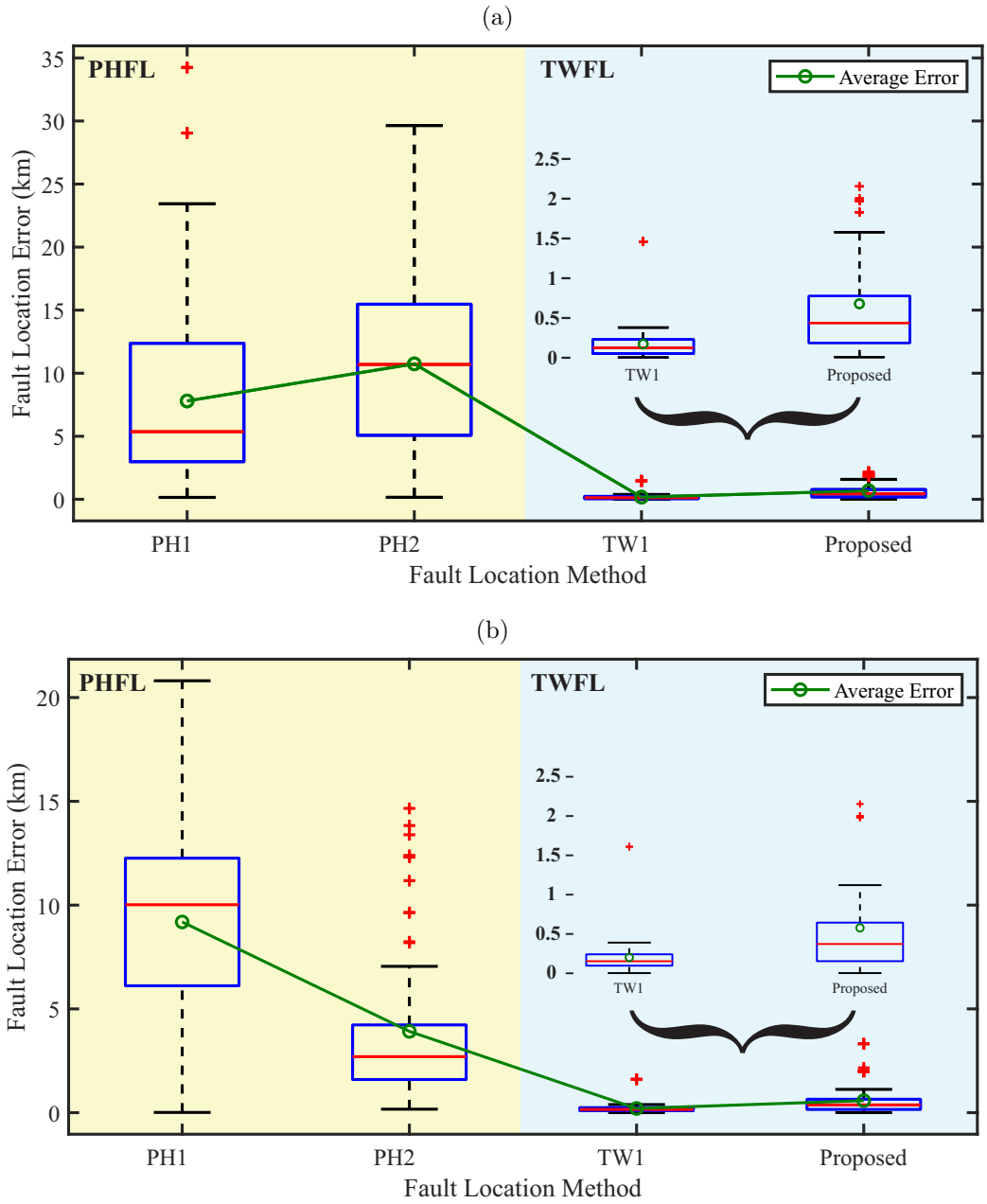

Source: Own authorship.

Figure 5.4: Fault location algorithms comparison on heavy load scenario for sampling rate equal to 1.024 samples per cycle, *i.e.*, 61.440 kHz: (a) A-phase-to-ground; and (b) B-phase-to-C-phase.

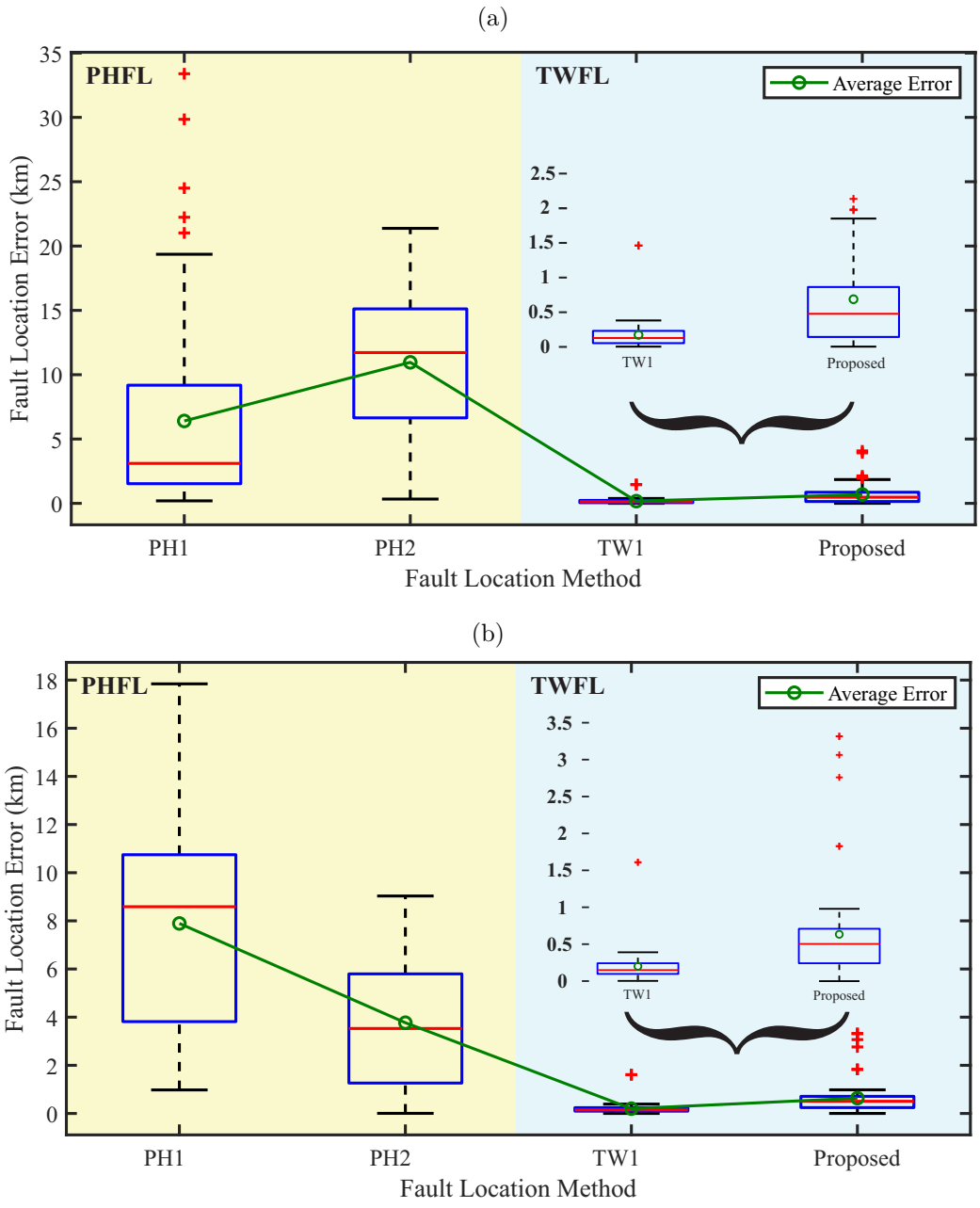

Source: Own authorship.

5.3 FAULT LOCATION ERRORS FOR LOWER SAMPLING RATES

In this section, an extension of the presented studies is provided. In order to analyze the errors obtained when considering records with lower initial sampling rates, *i.e.*, locating the faults using lower bands of the frequency spectrum. To do this kind of analysis, the number of samples/cycle equal to 256 and 512, traditionally used in commercially available DFRs, were chosen. Thus, the 264 simulated cases aforementioned and analyzed with a sampling frequency equal to 61.440 kHz were simulated considering the sampling frequencies of 30.720 kHz and 15.360 kHz. To do so, new L values were used for each sampling frequency, aiming to result in a final sampling frequency next to 1 MHz.

5.3.1 Sampling Rate Equal to 512 Samples per Cycle, *i.e.*, 30.720 kHz

Considering an initial sampling rate of 30.720 kHz, the interpolation factor, L, equal to 33 is used, which results in a final sampling frequency equal to 1.0138 MHz. In Figures 5.5 and 5.6 a boxplot of the errors obtained for each type of fault studied here is presented and compared with the errors obtained for the PH1 and PH2 algorithms and the TW1 method.

As a result, the errors obtained using the proposed method for an initial sampling frequency of 30.720 kHz remain in the order of 2 km. This result is superior to that obtained with 1,024 samples/cycle, but is still better when compared to the PH1 and PH2 methods errors, being a good choice when high frequency DFRs are not available.

Figure 5.5: Fault location algorithms comparison when using the IF filter over an original sampling rate of 512 samples per cycle, *i.e.*, 30.720 kHz on light load scenario: (a) A-phase-to-ground; and (b) B-phase-to-C-phase.

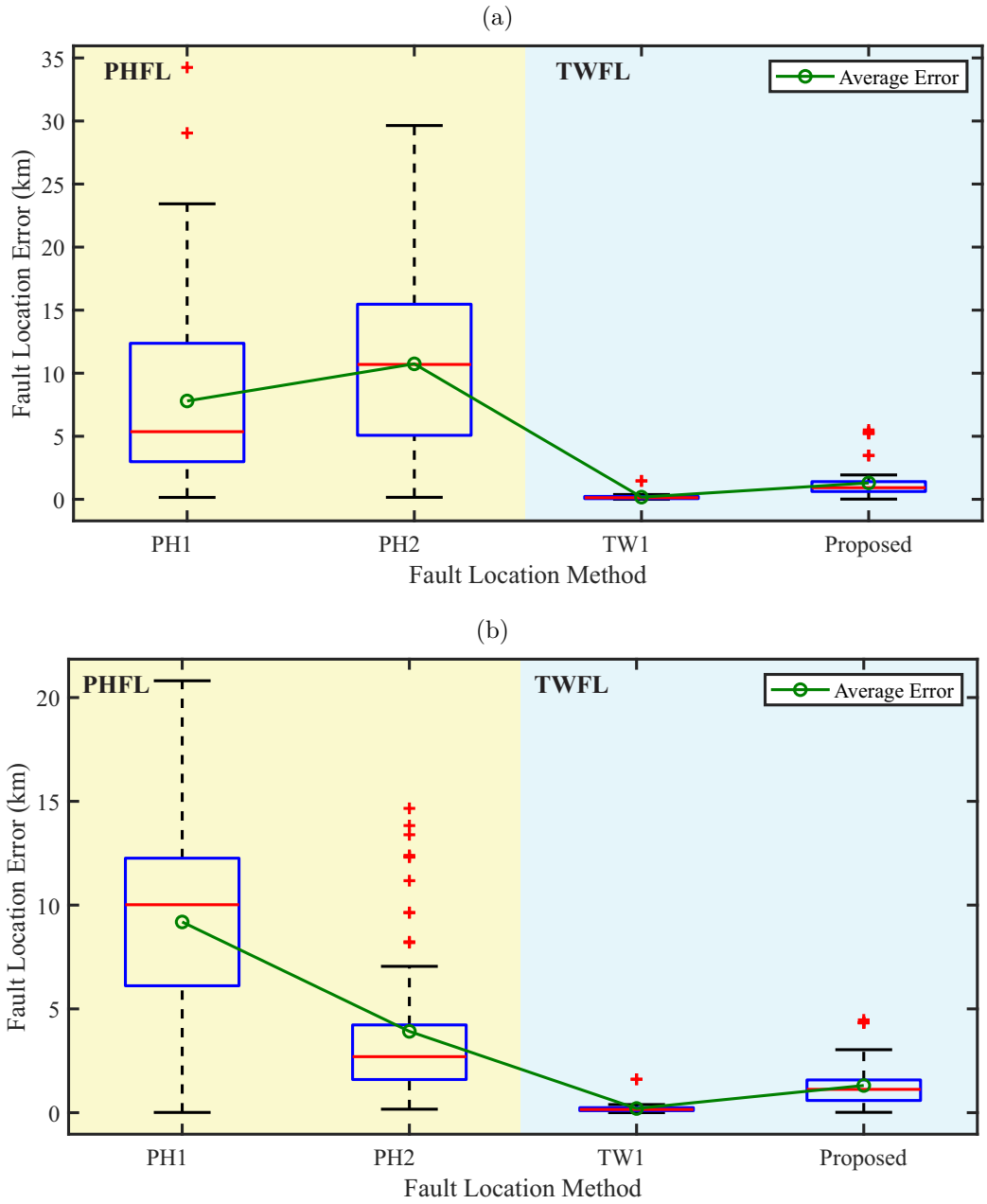

Source: Own authorship.

Figure 5.6: Fault location algorithms comparison when using the IF filter over an original sampling rate of 512 samples per cycle, *i.e.*, 30.720 kHz on heavy load scenario: (a) A-phase-to-ground; and (b) B-phase-to-C-phase.

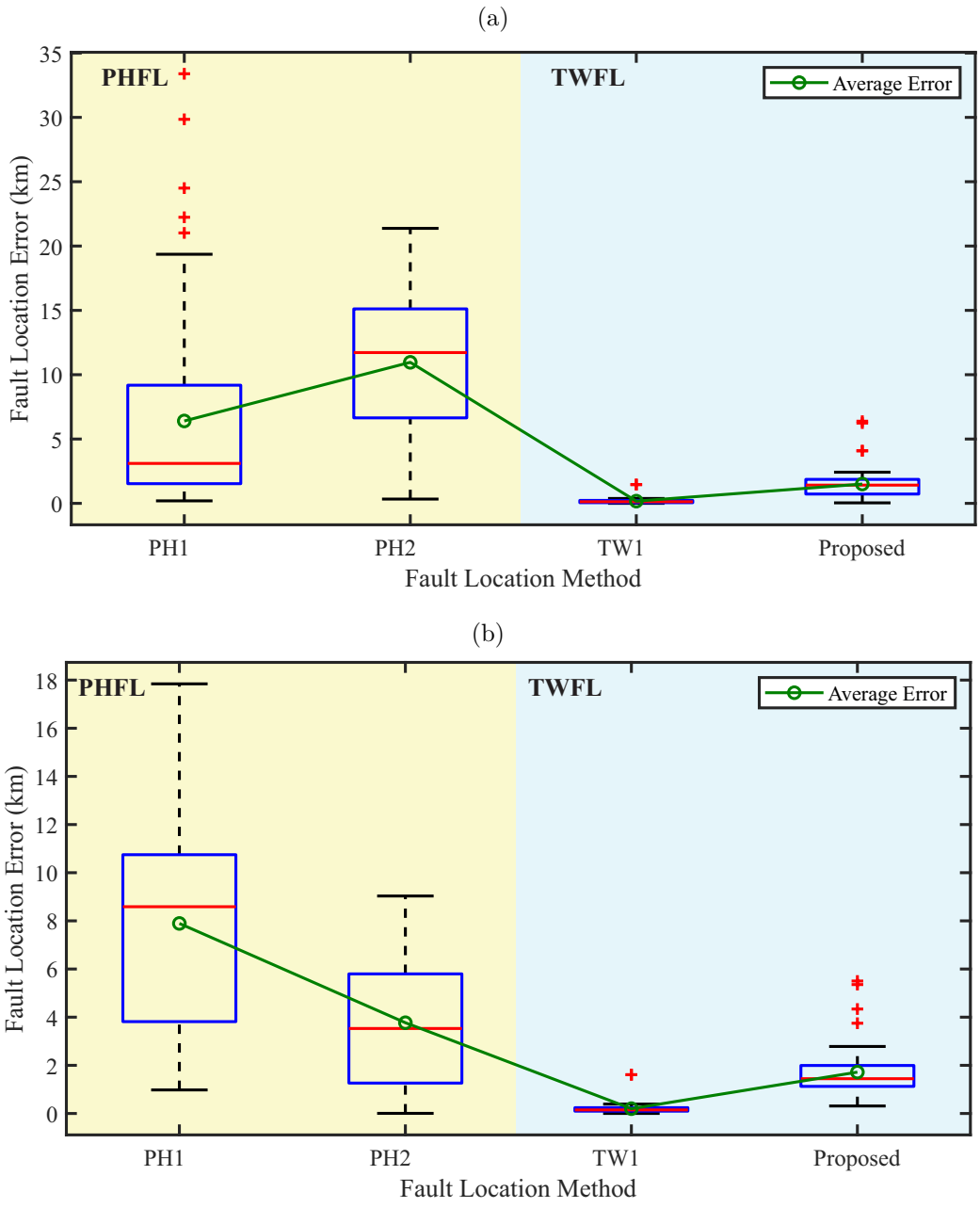

Source: Own authorship.

5.3.2 Sampling Rate Equal to 256 Samples per Cycle, *i.e.*, 15.360 kHz

Finally, considering an initial sampling rate of 15.360 kHz, the interpolation factor, L, equal to 65 is used, which results in a final sampling frequency equal to 0.9984 MHz. In Figures 5.7 and 5.8 a boxplot of the errors obtained for each type of fault studied here is presented with the errors obtained for the PH1 and PH2 algorithms and the TW1 method.

As a result, the errors obtained using the proposed method for an initial sampling frequency of 15.360 kHz remain in the order of 4 to 5 km. This result is worst than the one obtained using 512 and 1,024 samples/cycle, but is still lower than the results obtained using PH1 and PH2 methods, being a good alternative when high sampling frequencies DFRs aren't available.

Figure 5.7: Fault location algorithms comparison when using the IF filter over an original sampling rate of 256 samples per cycle, *i.e.*, 15.360 kHz on light load scenario: (a) A-phase-to-ground; and (b) B-phase-to-C-phase.

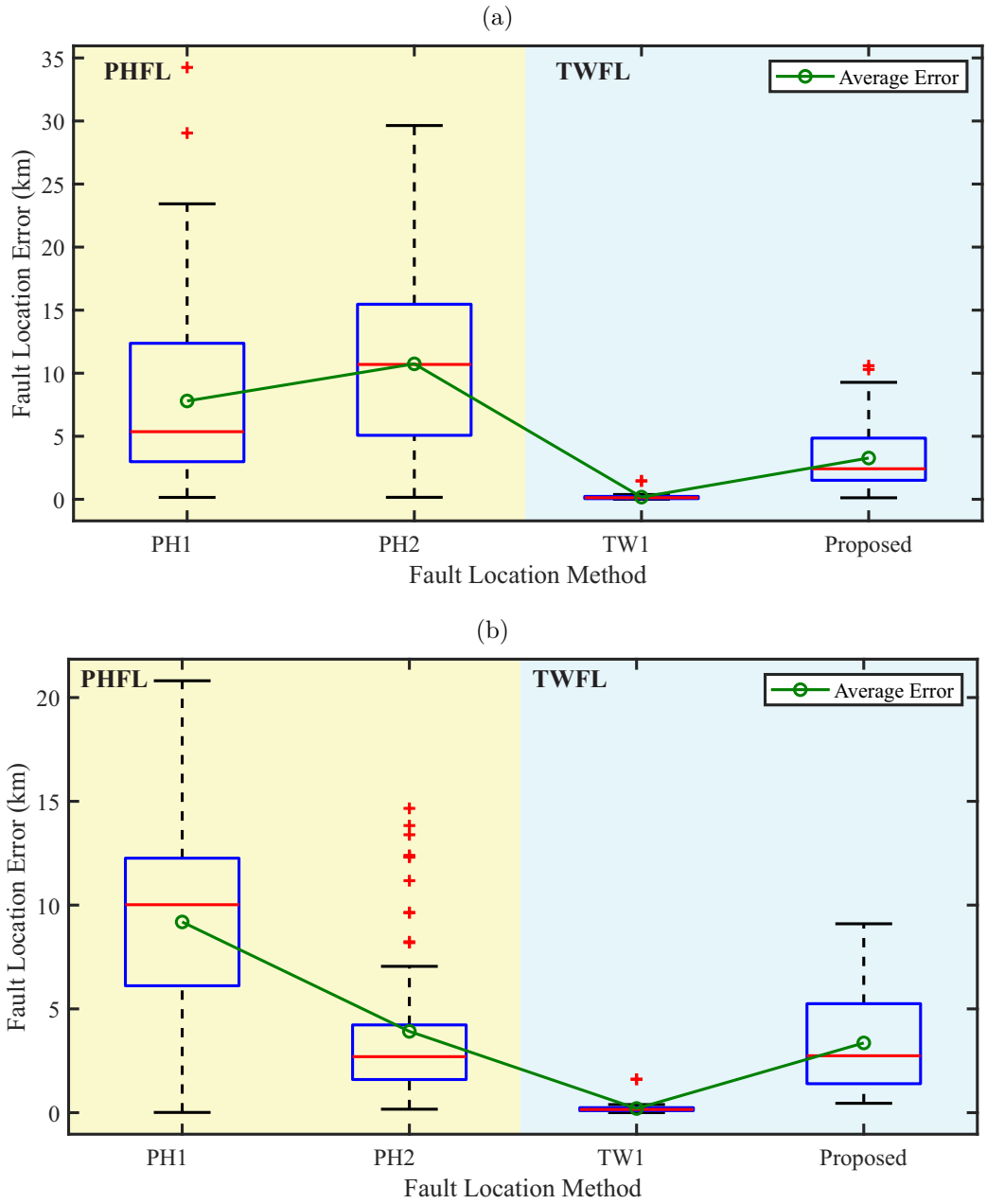

Source: Own authorship.

Figure 5.8: Fault location algorithms comparison when using the IF filter over an original sampling rate of 256 samples per cycle, *i.e.*, 15.360 kHz on heavy load scenario: (a) A-phase-to-ground; and (b) B-phase-to-C-phase.

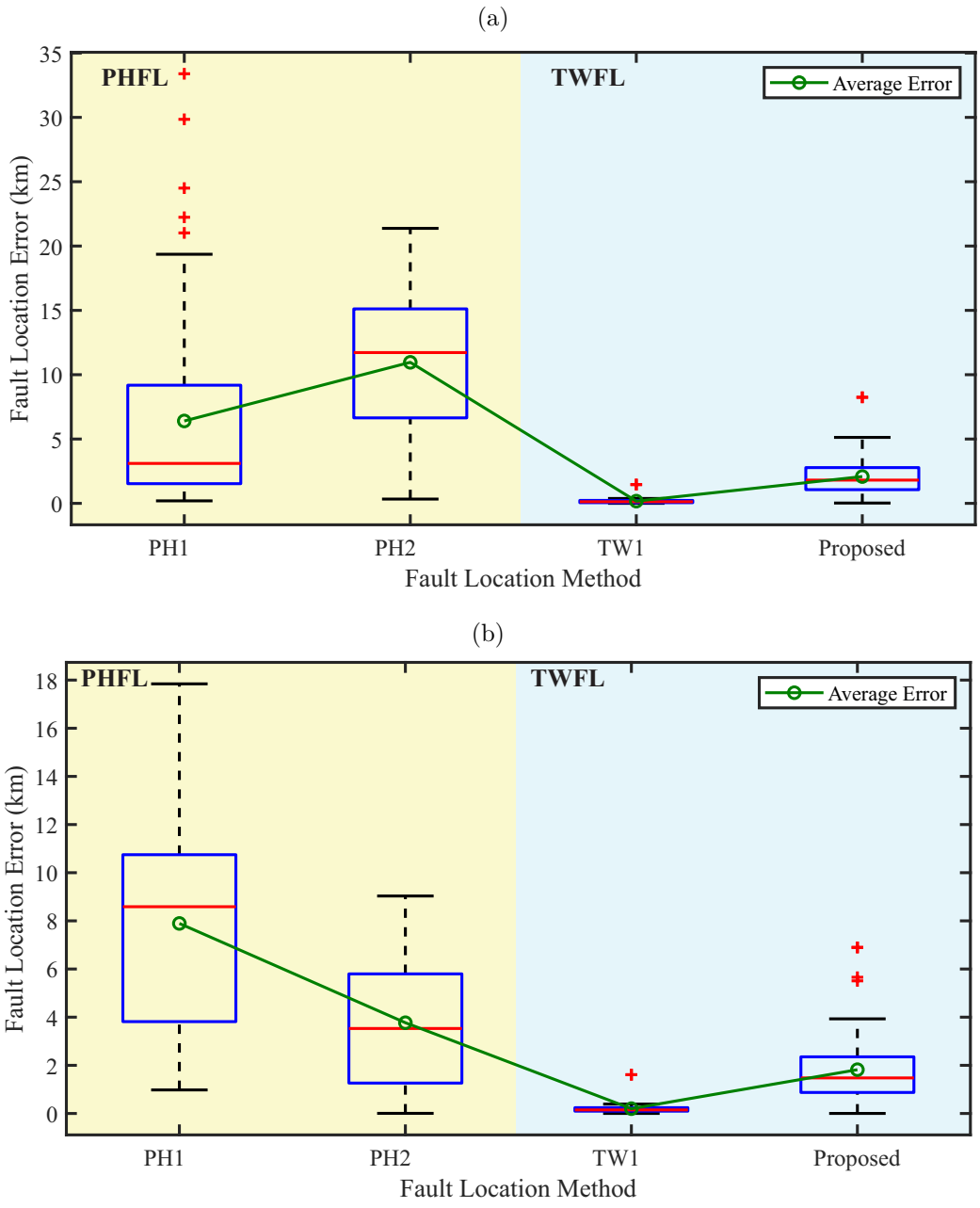

Source: Own authorship.

5.4 FAULT LOCATION ERRORS IN THE PRESENCE OF WHITE GAUSSIAN NOISE

In order to assess the influence of noise on the proposed algorithm, the 264 cases initially presented in Section 5.2, for the sampling rate of 1.024 samples/cycle, were evaluated under distortion scenarios caused by white Gaussian noise. In Figures 5.9 and 5.10, the results obtained are presented in the form of a boxplot of the fault location errors obtained by the TW1 and Proposed methods under conditions of signal-to-noise ratio (SNR) equal to 30 dB, 40 dB, 50 dB, and 60 dB, totaling 2,640 simulated fault cases.

To better detail the results, Figures 5.9 and 5.10 are divided into light load and heavy load scenarios of the power system under the occurrence of AG and BC fault types. For each scenario, 660 fault cases were simulated. For all scenarios, it is possible to state that the TW1 method wasn't affected by any order of SNR. Therefore, the proposed method is less sensitive to SNR, keeping accuracy even in scenarios with high distortion levels caused by noise in the grid.

Figure 5.9: Fault location errors in the presence of white gaussian noise in light load scenario: (a) A-phase-to-ground; and (b) B-phase-to-C-phase.

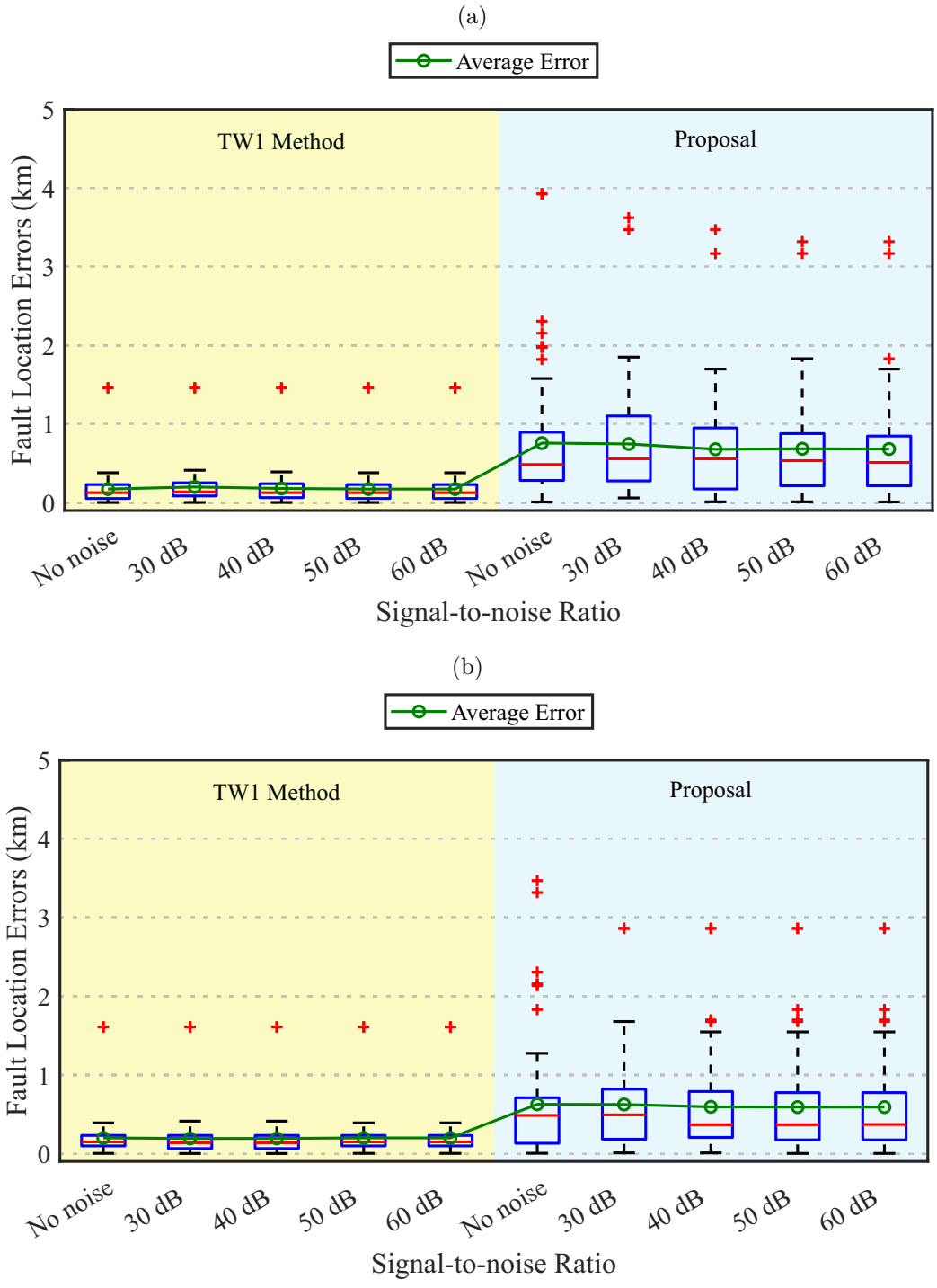

Source: Own authorship.

Figure 5.10: Fault location errors in the presence of white gaussian noise in heavy load scenario: (a) A-phase-to-ground; and (b) B-phase-to-C-phase.

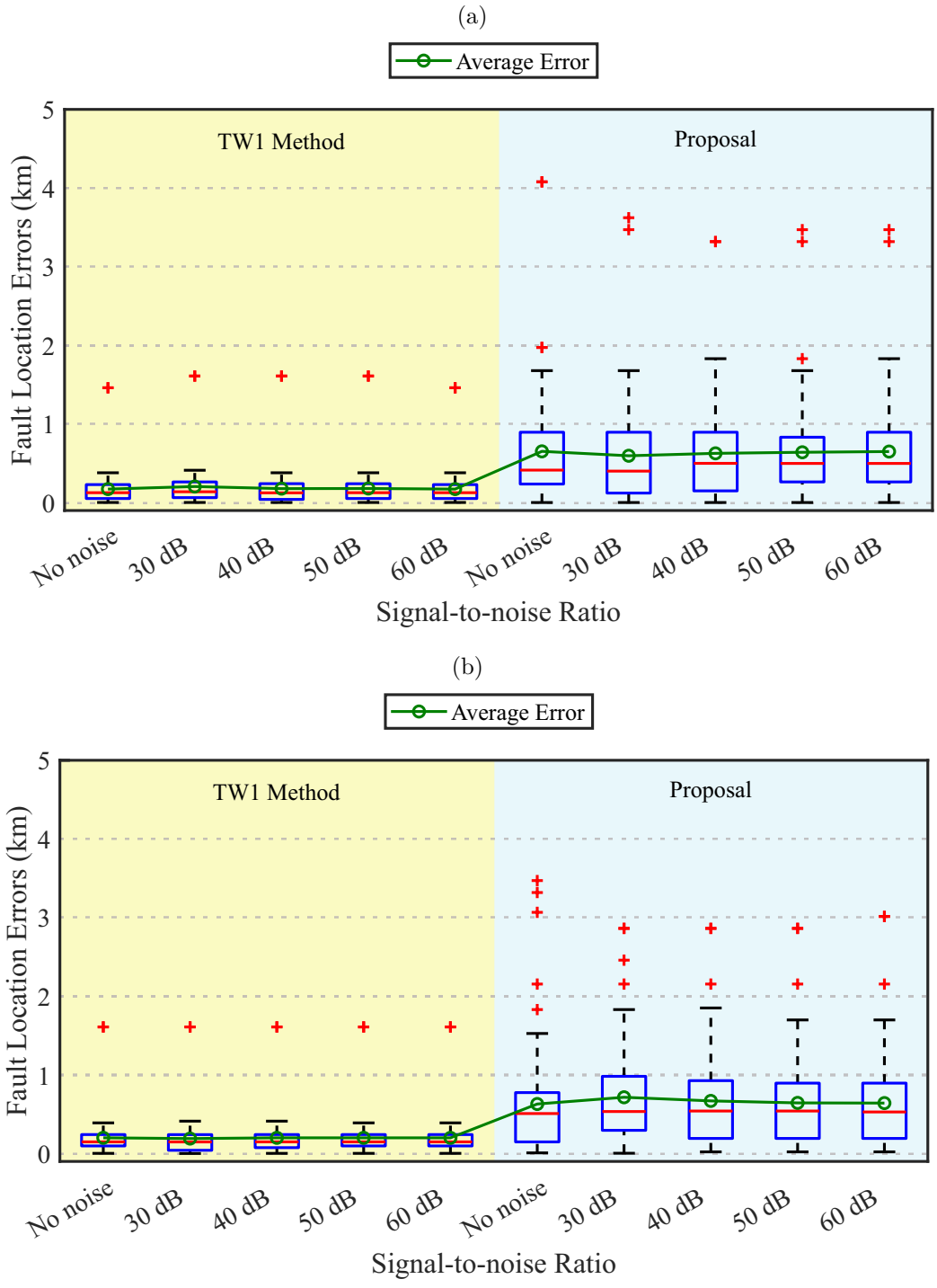

Source: Own authorship.

5.5 FAULT LOCATION COMPARISON WITH ANOTHER TW EXTRACTION STRATEGY

Aiming to verify the compatibility of the interpolation technique proposed in this thesis with another TW extraction strategy well accepted in the literature, this section details the comparison of the results obtained when using the DS filter, previously discussed, with the test strategy developed in Wang *et al.* (2020). In this strategy, the TW extraction is employed by an infinite impulse response (IIR) filter, described in Equation 5.1, and applied to a directional pilot protection scheme for hybrid LCC-modular multilevel converter (MMC)-HVDC transmission line. It is essential to highlight that in Wang *et al.* (2020), the sampling rate adopted in the proposed solution is not informed.

$$i^{1,TW}[n] = -0.9048 \cdot i^{1,TW}[n-1] + 0.9524 \cdot i^{1}[n] - 0.9524 \cdot i^{1}[n-1] \ , \tag{5.1}$$

where:

- $i^{1,TW}$ represents the filter output; and
- i^{1} represent the filter input.

Thus, in this context, it was evaluated and concluded that the proposal to use the interpolation technique is not limited to the DS filter application. To better detail this result, Figure 5.11 depicts a comparison for the 264 cases presented in Section 5.2.

In general, for both fault types and loading levels evaluated, the strategy proposed by Wang *et al.* (2020) has results as accurate as the ones obtained when using the DS filter. Nonetheless, it should be highlighted that this thesis' proposed TW extraction strategy presents better results for all evaluated scenarios.

On the other hand, the difference between the results obtained through the two mentioned strategies is negligible, meaning that the strategy by Wang *et al.* (2020) can be used also in the proposed method. Finally, it is important to mention that the strategy by Wang *et al.* (2020) does not present any outlier in all sets of calculated errors, being an advantage compared to this thesis' adopted strategy.

Figure 5.11: Fault location errors comparison when using another TW extraction strategy: (a) A-phase-to-ground in light load scenario; (b) A-phase-to-ground in heavy load scenario; and (c) B-phase-to-C-phase in light load scenario; and (d) B-phase-to-C-phase in heavy load scenario.

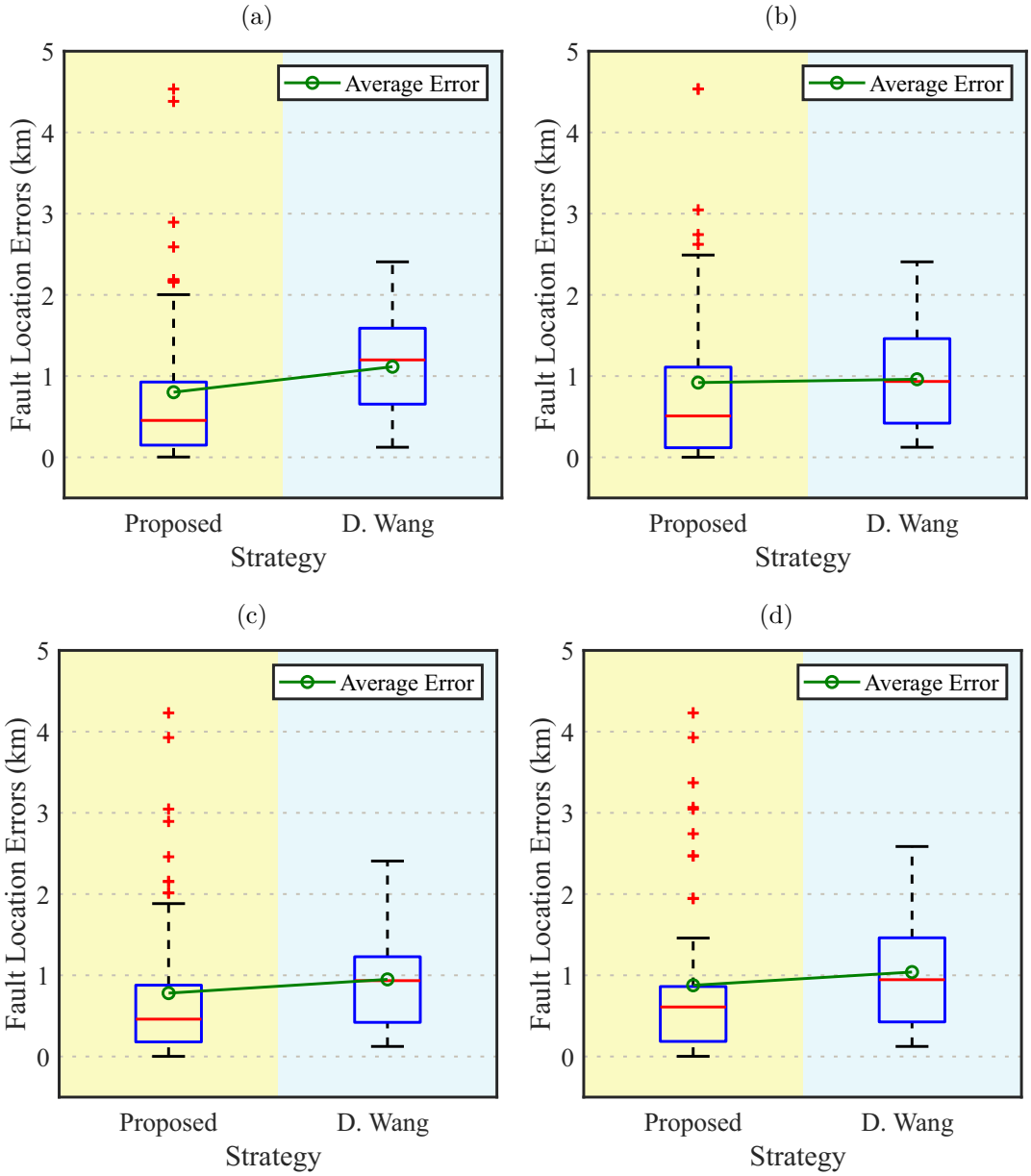

Source: Own authorship.

5.6 FAULT LOCATION COMPARISON BETWEEN INTERPOLATION METHODS

As the final result of this chapter, in this section, an assessment comparing the interpolation methods, described in Table 5.1, is detailed. The assessed methods are available in the MATLAB environment. The requirement of sample points to perform each interpolation method is also described, along with a relative comparison of computational cost.

Table 5.1: Description of the evaluated interpolation methods.

Method	Continuity	Comments
Linear	Based on linear interpolation of the values at neighboring grid points in each respective dimension.	Requires at least 2 points; and requires more memory and computation time than nearest neighbor.
Nearest	The interpolated value at a query point is the value at the nearest sample grid point.	Requires at least 2 points; modest memory requirements; and fastest computation time.
Next	The interpolated value at a query point is the value at the next sample grid point.	Requires at least 2 points; and same memory requirements and computation time as nearest.
Previous	The interpolated value at a query point is the value at the previous sample grid point.	Requires at least 2 points; and same memory requirements and computation time as nearest.
Pchip	The interpolated value at a query point is based on a shape-preserving piecewise cubic interpolation of the values at neighboring grid points.	Requires at least 4 points; and requires more memory and computation time than linear.
Cubic	Cubic convolution used in MATLAB® 5.	Requires at least 3 points; points must be uniformly spaced; falls back to spline for irregularly-spaced data; and similar memory requirements and computation time as pchip.
Makima	Modified Akima cubic Hermite interpolation. The interpolated value at a query point is based on a piecewise function of polynomials with degree at most three. The Akima formula is modified to avoid overshoots.	Requires at least 2 points; produces fewer undulations than spline, but does not flatten as aggressively as pchip; computation is more expensive than pchip, but typically less than spline; and memory requirements are similar to those of spline.
Spline	The interpolated value at a query point is based on a cubic interpolation of the values at neighboring grid points in each respective dimension.	Requires at least 4 points, falling back to linear or quadratic interpolation if 2 or 3 points are supplied, respectively; and requires more memory and computation time than pchip.

Source: Extracted from (MATLAB, 2024).

Thereby, to compare the methods mentioned above, a total of 2,112 fault cases were evaluated, *i.e.*, 264 cases for each interpolation method with the characteristics presented in section 5.2. Thus, comparing the fault location errors obtained when using each method makes it possible to justify which method fits better to this thesis proposal. Therefore, for all cases, the intrinsic differences of the interpolation methods are expressed in Figures 5.12 and 5.13 by means of fault location errors.

By the analysis of the fault location errors depicted in Figure 5.12, it is possible to itemize some clarifications for light load scenarios:

- Nearest, Next, and Previous methods have a poor performance when compared with the others assessed methods, but with a lower number of outliers;
- Linear, Pchip, Cubic, Makima, and Spline methods present a relatively similar performance; and
- Makima and Pchip methods present the lower obtained median of errors in the boxplot.

Finally, analyzing the fault location errors detailed in Figure 5.13, it is obtained that for heavy load scenarios:

- Nearest, Next, and Previous methods have the poorest performance observed when compared with the others assessed methods, but without outliers in A-phase-to-ground faults and fewer outliers in B-phase-to-C-phase fault;
- Linear, Pchip, Cubic, Makima, and Spline methods present a relatively similar performance;
- Makima and Pchip methods present the lower maximum values of errors in the boxplot; and
- Linear method presents fewer outliers than the Pchip, Cubic, Makima, and Spline methods.

According to the obtained results and considering that linear interpolation requires less computational cost than Makima and Pchip methods, it is justified why the linear interpolation was chosen in the proposed method. However, other interpolation methods can be chosen without losing reliability when employed in the proposed fault location application.

Figure 5.12: Fault location errors comparison when choosing another interpolation method in light load scenario: (a) A-phase-to-ground; and (b) B-phase-to-C-phase.

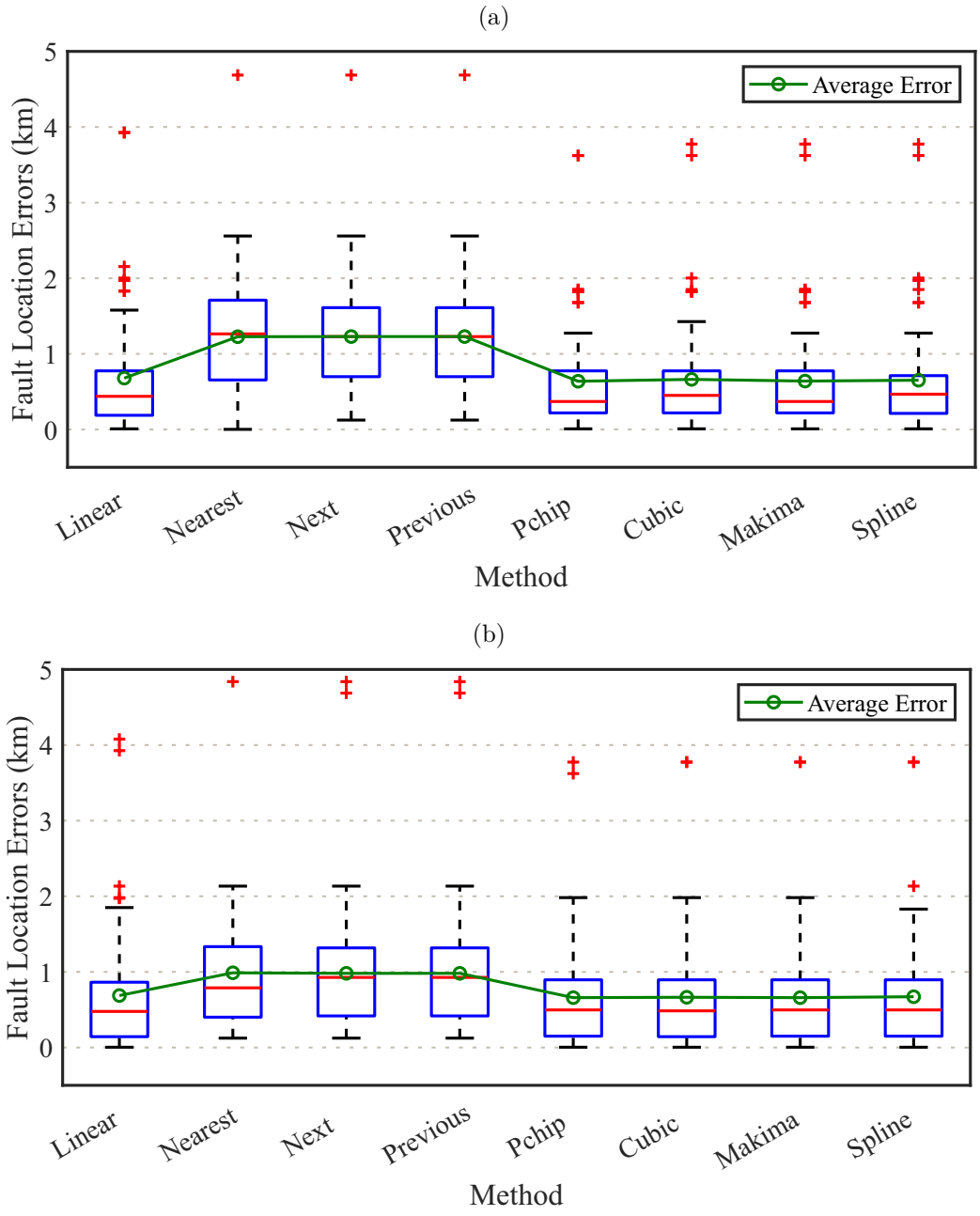

Source: Own authorship.

Figure 5.13: Fault location errors comparison when choosing another interpolation method in heavy load scenario: (a) A-phase-to-ground; and (b) B-phase-to-C-phase.

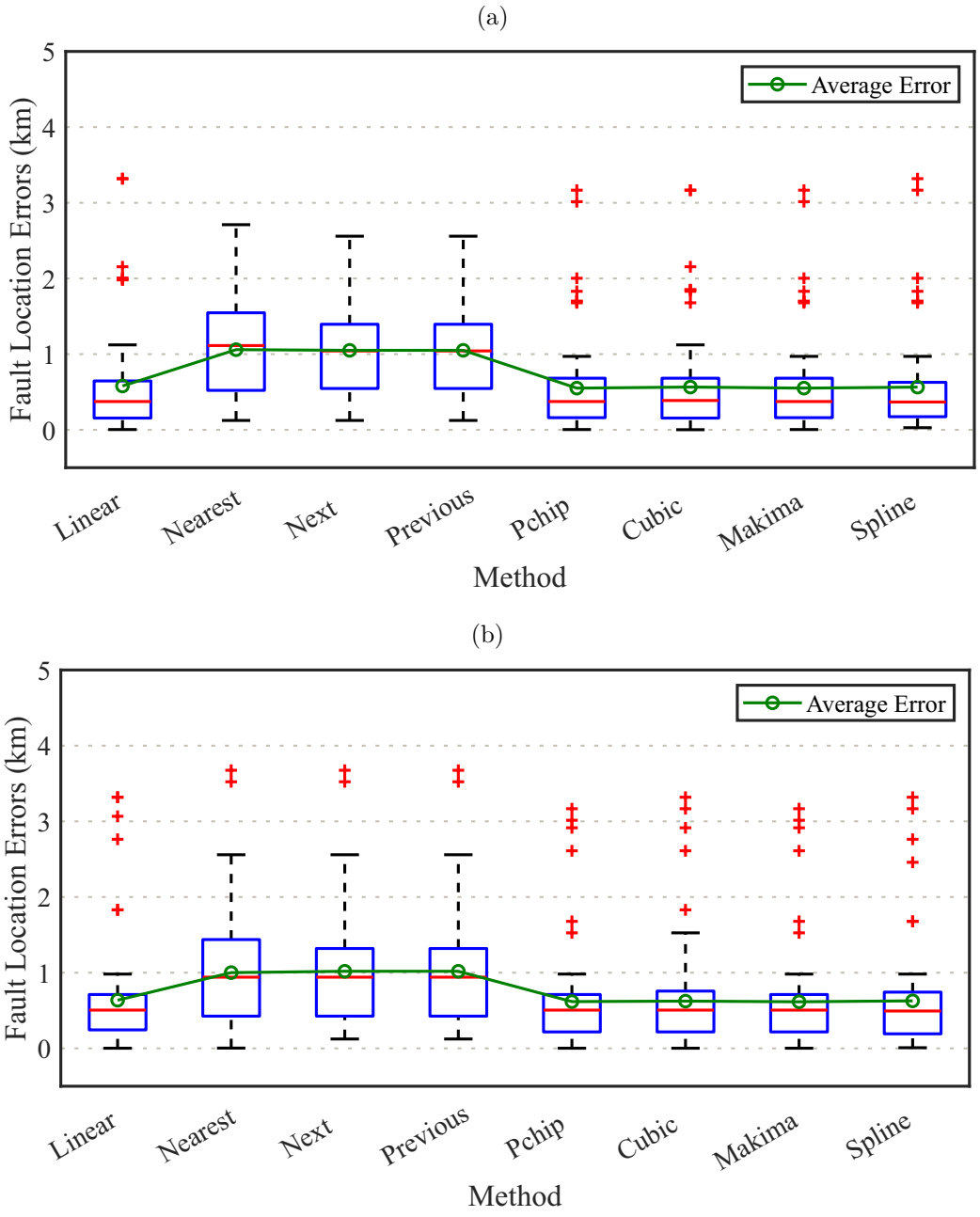

Source: Own authorship.

CHAPTER 6

RESULTS OVER REAL FAULT DATA

6.1 ACTUAL CASES

After theoretically proving the efficiency of the proposed algorithm and aiming to confirm its usefulness in real world applications, this Chapter describes results obtained from applying the proposed algorithm over real oscillographic data recorded in traditional DFRs. As is widely known, most faults in transmission lines are one phase-to-ground. So, to assess the proposed algorithm, the 500 kV double-circuit transmission line Silves / Oriximiná operator provided actual samples of oscillographic data in the sampling rate of 256 samples/cycle (*i.e.*, 15.360 kHz).

The following sections depict the assessment of one actual case of phase-to-phase-to-ground, one actual case of inter-citcuit single-line-to-ground, and one actual case of single-line-to-ground faults recorded in the referred transmission line, highlighting the proposed usefulness of the method from a practical point of view. Therefore, voltage and current oscillographic data recorded by field DFRs installed at Silves and Oriximiná substations are illustrated along with their respective TWs signals filtered using the proposed combination of IF and DS filters (detailed in Subsection 4.1.2) and their assessments through fault location methods studied in this thesis. Finally, it is important to inform that α-TW mode is used for single-line-to-ground faults, and β-TW mode is used for line-to-line faults, identified for a fault type selection algorithm applied before the fault location is performed (SCHWEITZER *et al.*, 2014).

6.2 ACTUAL CASE 01 — C-PHASE-TO-A-PHASE-TO-GROUND FAULT

The 1st actual case is of a CAG fault recorded in circuit number 2 of the 500 kV double-circuit transmission line Silves / Oriximiná. Figures 6.1a to 6.1d depicts the oscillographic data recorded by DFRs installed at Silves and Oriximiná stations. Figures 6.1e to 6.1h depict the β-TW signal extracted from the measured currents and the PH1, PH2, and proposed fault

location method performance in both transmission line terminals.

As a first important note, no field report is available for this case. Secondly, it is important to highlight that Figures 6.1g and 6.1h present behavior close to the one depicted in Figure 5.1. Furthermore, one can observe that throughout the fault location results in Table 6.1, PH1 and the Proposed methods have presented similar results for both Silves and Oriximiná. The PH2 method presented a difference larger than 100 km in comparison with the others methods.

Table 6.1: Fault location results for actual case 01 — C-phase-to-A-phase-to-ground fault.

	Fault Location	
Method	Silves	Oriximiná
PH1	76.4868 km	258.5132 km
PH2	194.9655 km	140.0345 km
Proposed	77.5528 km	257.4472 km

Source: Own authorship.

Figure 6.1: Actual case 01 — C-phase-to-A-phase-to-ground over the 500 kV double-circuit transmission line Silves / Oriximiná circuit number 2: (a) voltages measured at Silves terminal; (b) voltages measured at Oriximiná terminal; (c) currents measured at Silves terminal; (d) currents measured at Oriximiná terminal; (e) β-mode measured at Silves terminal; (f) β-mode measured at Oriximiná terminal; (g) fault location comparison at Silves terminal; and (h) fault location comparison at Oriximiná terminal.

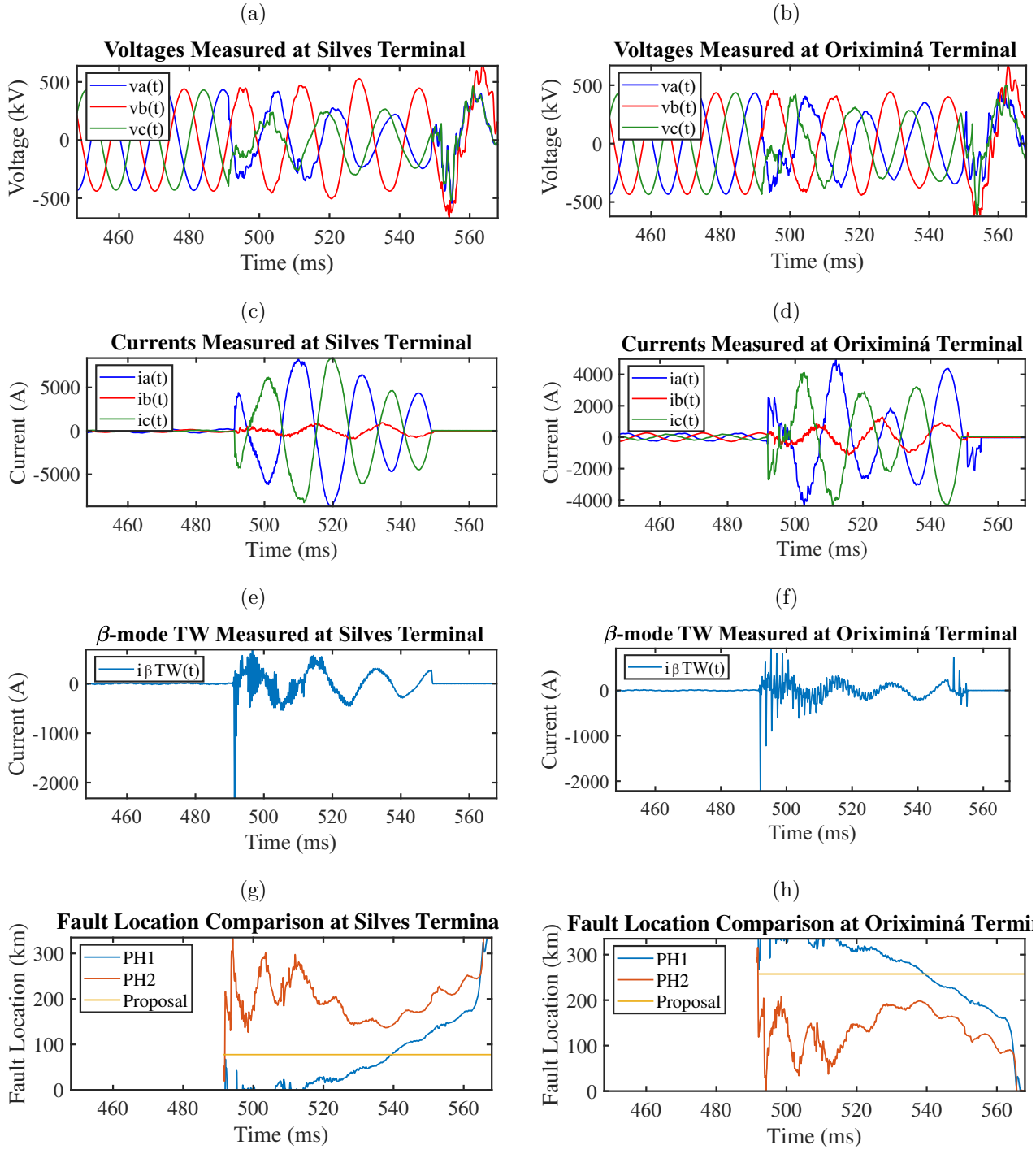

Source: Own authorship.

6.3 ACTUAL CASE 02 — INTER-CIRCUIT SINGLE-LINE-TO-GROUND FAULT

The 2nd actual case is an inter-circuit AG fault recorded in both circuits of the 500 kV double-circuit transmission line Silves / Oriximiná. Figure 6.2 and 6.3 depicts the oscillograph data recorded by field DFRs installed at Silves and Oriximiná substations from Figures 6.2a to 6.2d and Figures 6.3a to 6.3d. Figures 6.2e to 6.2h and Figures 6.3e to 6.3h depict the α-TW signal extracted from the measured currents and the PH1, PH2, and proposed fault location method behavior in both transmission line terminals.

For this actual case, no field report is available either, and it is possible to ascertain that a monopolar circuit breaker opening was performed in circuit number 2 in order to eliminate the fault. Furthermore, the behavior observed in Figure 5.1 is also presented in Figures 6.2g and 6.2h and Figures 6.3g and 6.3h.

Regarding fault location, assessing the results reported in Table 6.2, one can observe that, due to the FSC bypass at circuit number 2, PH1 and PH2 methods results were affected by the subsynchronous oscillation. Although, throughout circuit number 1 results, in which the transmission line's series capacitor wasn't bypassed due to a fault resistance-associated (lower current levels in circuit 2), the algorithms presented similar results, stating the accuracy of the Proposed method estimation, which has proven itself immune to FSC switching effects.

Table 6.2: Fault location results for actual case 02 — inter-circuit single-line-to-ground fault.

Fault location report					
	Circuit 01			Circuit 02	
Method	Silves	Oriximiná	Method	Silves	Oriximiná
PH1	192.4943 km	142.5057 km	PH1	13.0339 km	321.9661 km
PH2	195.0984 km	139.9016 km	PH2	208.7864 km	126.2136 km
Proposed	186.8335 km	148.1665 km	Proposed	186.8335 km	148.1665 km

Source: Own authorship.

Figure 6.2: Actual case 02 — Part 01 — inter-circuit A-phase-to-ground over the 500 kV double-circuit transmission line Silves / Oriximiná circuit number 1: (a) voltages measured at Silves terminal; (b) voltages measured at Oriximiná terminal; (c) currents measured at Silves terminal; (d) currents measured at Oriximiná terminal; (e) α-mode measured at Silves terminal; (f) α-mode measured at Oriximiná terminal; (g) fault location comparison at Silves terminal; and (h) fault location comparison at Oriximiná terminal.

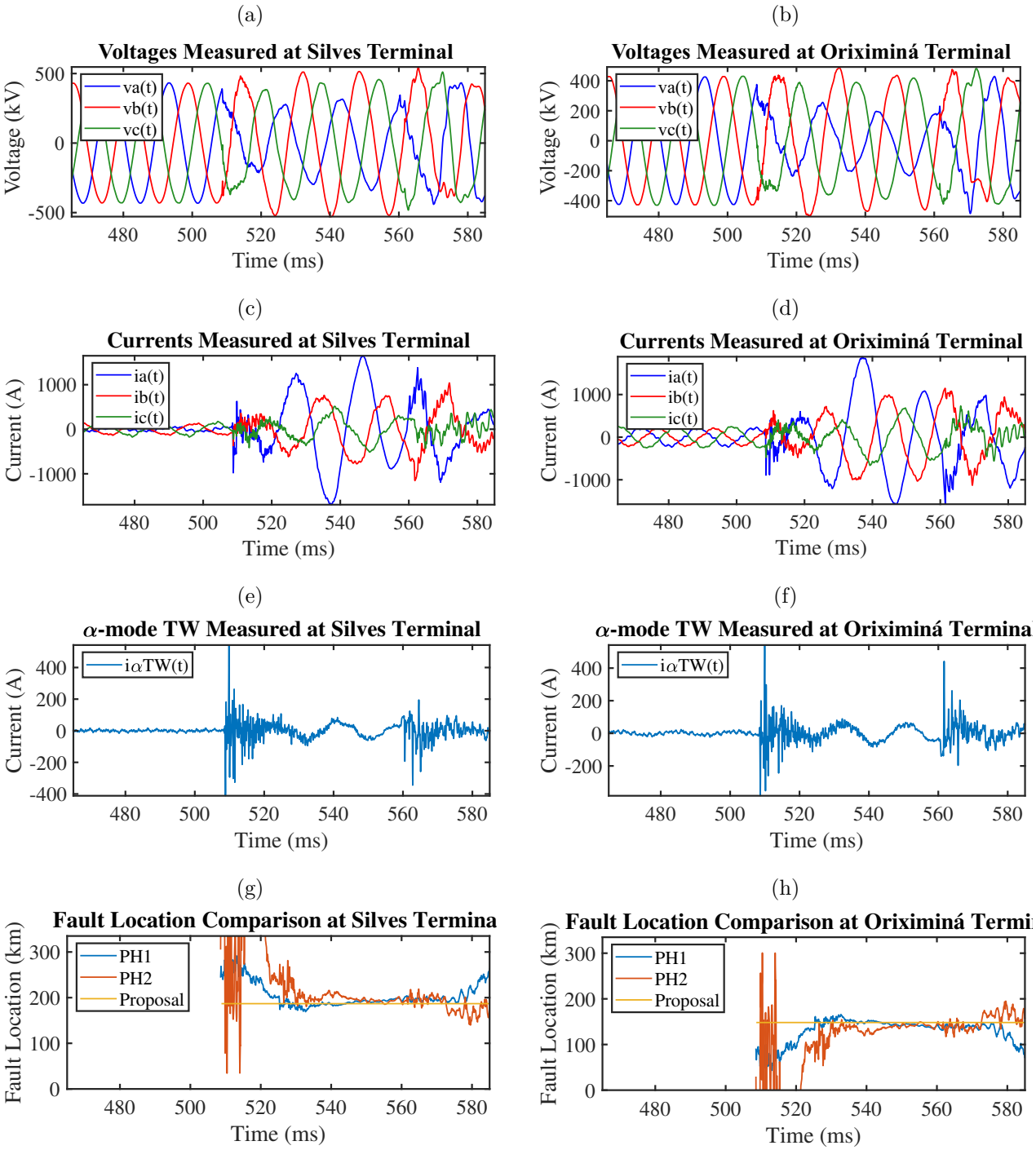

Source: Own authorship.

Figure 6.3: Actual case 02 — Part 02 — inter-circuit A-phase-to-ground over the 500 kV double-circuit transmission line Silves / Oriximiná circuit number 2: (a) voltages measured at Silves terminal; (b) voltages measured at Oriximiná terminal; (c) currents measured at Silves terminal; (d) currents measured at Oriximiná terminal; (e) α-mode measured at Silves terminal; (f) α-mode measured at Oriximiná terminal; (g) fault location comparison at Silves terminal; and (h) fault location comparison at Oriximiná terminal.

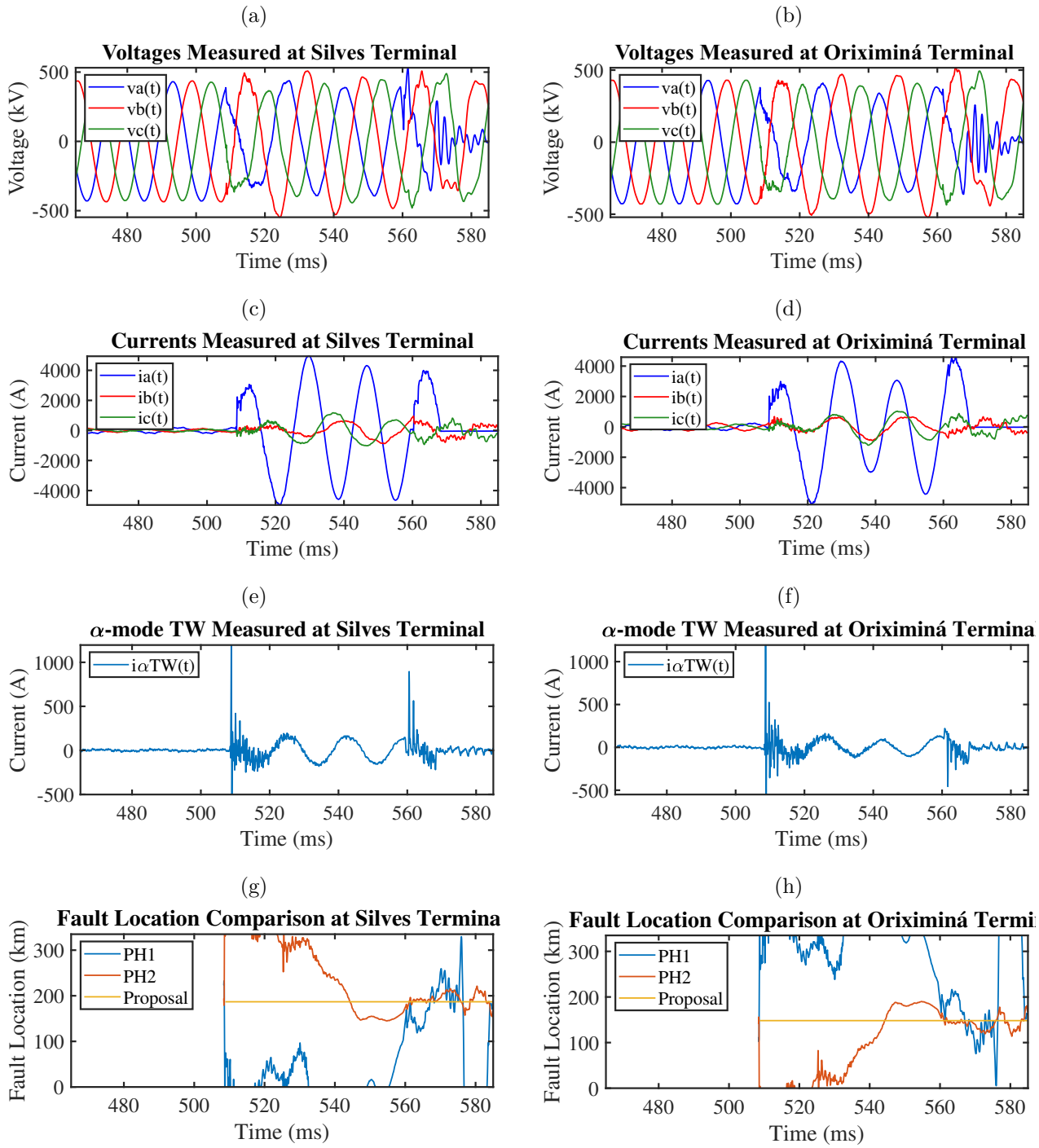

Source: Own authorship.

6.4 ACTUAL CASE 03 — A-PHASE-TO-GROUND FAULT

The 3rd actual case is an AG fault recorded in circuit number 2 of the 500 kV double-circuit transmission line Silves / Oriximiná. Figure 6.4 depicts the oscillographic data recorded by field DFRs installed at Silves and Oriximiná substations from Figures 6.4a to 6.4d. Figures 6.4e to 6.4h depict the α-TW signal extracted from the measured currents and the PH1, PH2, and proposed fault location method behavior in both transmission line terminals.

For this case, a monopolar circuit braker oppening can be observed in Figures 6.4c and 6.4d. As in the previous actual cases, the behavior illustrated in Figure 5.1 for the subsynchronous oscillation is verified over fault location results depicted in Figures 6.4g and 6.4h.

As an essential factor for comparisons, a field report is available for this current case, which indicates a fault location 26 km distant from Silves terminal. Results printed in Table 6.3 highlight the accuracy of the Proposed method, presenting fault location with approximately 3 km difference from the value detailed in the field report, while PH1 and PH2 methods oscillate over the actual fault location due to the subsynchronous oscillation, without accommodating, causing error in the final fault location.

Table 6.3: Fault location results for actual case 03 — A-phase-to-ground fault.

	Fault Location	
Method	Silves	Oriximiná
PH1	55.1144 km	279.8856 km
PH2	102.4940 km	232.5060 km
Proposed	29.3845 km	305.6155 km

Source: Own authorship.

Figure 6.4: Actual case 03 — A-phase-to-ground over the 500 kV double-circuit transmission line Silves / Oriximiná circuit number 2: (a) voltages measured at Silves terminal; (b) voltages measured at Oriximiná terminal; (c) currents measured at Silves terminal; (d) currents measured at Oriximiná terminal; (e) α-mode measured at Silves terminal; (f) α-mode measured at Oriximiná terminal; (g) fault location comparison at Silves terminal; and (h) fault location comparison at Oriximiná terminal.

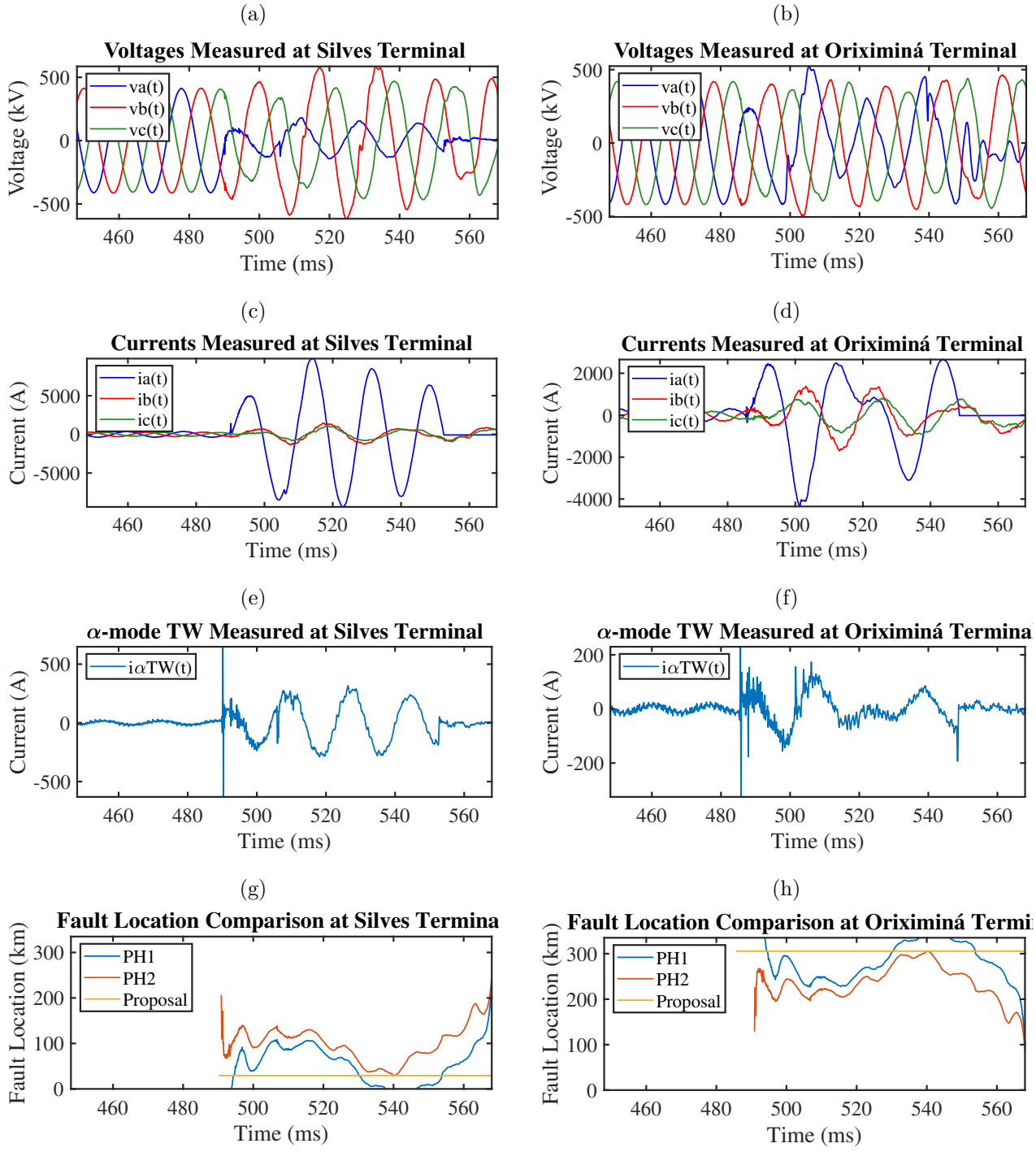

Source: Own authorship.

CHAPTER 7

CONCLUSIONS

This thesis proposes the use of an interpolation technique in conjunction with DS filter and TW-based fault location approaches, when DFRs with high sampling rates are unavailable. As a result, relatively low sampling rates can be used. Moreover, the proposed method presents an almost unitary step response, providing good representation of arriving TWs at line terminals. A total of 264 case studies for three commercially available and applied sampling rates in the field were carried out, totaling 792 case studies. This allows the proposed methodology to be compared with other phasor-based techniques and the traditional TW-based double-ended solution. To do so, ATP/ATPDraw simulations of faults on a 500 kV/60 Hz Brazilian transmission system were performed.

In the simulations, PHFL-based and TWFL-based methods are described and assessed through waveforms. The obtained results show that the proposed solution is effective, being capable of estimating faults with an accuracy comparable to those obtained via traditional TW-based fault location methods but using a much smaller sampling rate, which is attractive from a cost perspective. Furthermore, the fault location estimative is not affected by elevated SNR scenarios, attesting to the validity of the proposed solution. Indeed, the errors presented averages of 500 m, 1 km, and 2 km for the sampling frequencies of 61,440 Hz, 30,720 Hz, and 15,360 Hz, respectively, attesting to the validity of the proposed solution. Additionally, the proposed solution is not limited to one specific TW extraction strategy, *i.e.*, other techniques can be used without losing accuracy. Furthermore, among the interpolation methods available in the literature, linear interpolation stand out for presenting results with the same quality as those more robust interpolation methods but with lower computational memory and time.

To confirm the applicability of the proposed solution in the field, oscillographic of real fault cases on the studied transmission line were collected and used to evaluate the performance of the algorithm. As result, it was possible to prove the immunity of the proposed solution to

subsynchronous oscillation, while PHFL-based methods are affected by the phenomenon. Not least, the proposed solution presented an accurate and reliable fault location based on the real cases analyzed, achieving an accurate fault location that matches the values described in the field report. Therefore, the results show that the proposed solution accuracy is comparable to classical TW-based fault location solutions, revealing its usefulness for practical application when only traditional DFRs are available.

Regarding future work, after proving the efficiency of the TW extraction from low sampling rate record data, some topics gain prominence:

- Development of a TW-based protection schemes using low sampling rate record data;
- Evaluate the technical applicability of one-terminal fault location methods using low sampling rate data;
- Investigation of the applicability of other TW extraction strategies, such as boundary wavelet; and
- Use of the proposed method over HVDC fault location.

REFERENCES

ABBOUD, R.; DOLEZILEK, D. Time-domain technology–benefits to protection, control, and monitoring of power systems. In: *INTERNATIONAL CONFERENCE AND EXIBITION-RELAY PROTECTION AND AUTOMATION FOR ELECTRIC POWER SYSTEMS*. [S.l.: s.n.], 2017. p. 16. Cited in page 3.

ABUR, A.; MAGNAGO, F. Use of time delays between modal components in wavelet based fault location. *International Journal of Electrical Power & Energy Systems*, Elsevier, v. 22, n. 6, p. 397–403, 2000. Cited 2 times in pages 11 and 15.

ANDERSON, P. M.; FARMER, R. G. *Series compensation of power systems*. [S.l.: s.n.], 1996. Cited in page 45.

ANDERSON, P. M.; FOUAD, A. A. *Power system control and stability*. [S.l.]: John Wiley & Sons, 2008. Cited in page 1.

BUCELLI, M.; REGAZZONI, F.; QUARTERONI, A. *et al.* Preserving the positivity of the deformation gradient determinant in intergrid interpolation by combining rbfs and svd: application to cardiac electromechanics. *Computer Methods in Applied Mechanics and Engineering*, Elsevier, p. 116292, 2023. Cited in page 10.

CLARKE, E. *Circuit analysis of AC power systems: symmetrical and related components*. [S.l.]: Wiley, 1943. v. 1. Cited in page 20.

COMMITTEE, P. S. R. *et al.* Guide for determining fault location on ac transmission and distribution lines. *IEEE C37*, v. 114, p. 1–36, 2005. Cited in page 25.

COSTA, F.; SOUZA, B.; BRITO, N. A wavelet-based algorithm to analyze oscillographic data with single and multiple disturbances. In: IEEE. *2008 IEEE Power and Energy Society General Meeting-Conversion and Delivery of Electrical Energy in the 21st Century*. [S.l.], 2008. p. 1–8. No citation in text.

COSTA, F. B. Boundary wavelet coefficients for real-time detection of transients induced by faults and power-quality disturbances. *IEEE Transactions on Power Delivery*, IEEE, v. 29, n. 6, p. 2674–2687, 2014. Cited in page 21.

COSTA, F. B.; LOPES, F.; SILVA, K.; DANTAS, K. M. C.; FRANÇA, R.; LEAL, M. M.; RIBEIRO, R. Mathematical development of the sampling frequency effects for improving the two-terminal traveling wave-based fault location. *International Journal of Electrical Power & Energy Systems*, Elsevier, v. 115, p. 105502, 2020. Cited 2 times in pages 13 and 15.

COSTA, F. B.; SOUZA, B.; BRITO, N. S. D. Real-time detection of fault-induced transients in transmission lines. The Institution of Engineering and Technology, 2010. Cited 2 times in pages 20 and 21.

CROCHIERE, R. E.; RABINER, L. R. *Multirate digital signal processing: Prentice-Hall, Inc. Englewood Cliffs, New Jersey 07362, 1983, 411 pp., ISBN 0-13-605162-6*. [S.l.]: Elsevier, 1983. Cited in page 27.

DAI, Q.; KATSAGGELOS, A. K.; YU, S.; KANG, W.; JEON, J.; PAIK, J. Directionally adaptive cubic-spline interpolation using optimized interpolation kernel and edge orientation for mobile digital zoom system. In: IEEE. *The 18th IEEE international symposium on consumer electronics (ISCE 2014)*. [S.l.], 2014. p. 1–2. Cited in page 10.

DONG, X. *The Theory of Fault Travel Waves and Its Application*. [S.l.]: Springer, 2022. Cited in page 3.

ELETROBRAS. *Evolution of the Brazilian transmission system, horizon of 2027*. 2018. Available in <https://eletrobras.com/pt/AreasdeAtuacao>. Accessed in July 2023. Cited in page 2.

GALE, P.; CROSSLEY, P.; BINGYIN, X.; YAOZHONG, G.; CORY, B.; BARKER, J. Fault location based on travelling waves. In: IET. *1993 Fifth International Conference on Developments in Power System Protection*. [S.l.], 1993. p. 54–59. Cited 7 times in pages 9, 11, 14, 15, 24, 26, and 27.

GLOVER, J. D.; SARMA, M. S.; OVERBYE, T. *Power system analysis & design, SI version*. [S.l.]: Cengage Learning, 2012. Cited 2 times in pages 18 and 19.

GRAINGER, J. J.; STEVENSON, W. D.; STEVENSON, W. D. *et al. Power system analysis*. [S.l.: s.n.], 2003. Cited in page 1.

GREENWOOD, A. Electrical transients in power systems. New York, NY (USA); John Wiley and Sons Inc., 1991. Cited in page 20.

GUZMÁN, A.; MYNAM, M. V.; SKENDZIC, V.; ETERNOD, J. L.; MORALES, R. M. Directional elements - how fast can they be. In: *proceedings of the 44th Annual Western Protective Relay Conference*. [S.l.: s.n.], 2017. p. 1–16. Cited 3 times in pages 22, 24, and 40.

JIA, H. An improved traveling-wave-based fault location method with compensating the dispersion effect of traveling wave in wavelet domain. *Mathematical Problems in Engineering*, Hindawi, v. 2017, 2017. Cited 2 times in pages 12 and 15.

JOHNS, A.; JAMALI, S. Accurate fault location technique for power transmission lines. In: IET. *IEE Proceedings C (Generation, Transmission and Distribution)*. [S.l.], 1990. v. 137, n. 6, p. 395–402. Cited in page 25.

LIN, S.; HE, Z.; LI, X.; QIAN, Q. Travelling wave time–frequency characteristic-based fault location method for transmission lines. *IET generation, transmission & distribution*, IET, v. 6, n. 8, p. 764–772, 2012. Cited 3 times in pages 11, 12, and 15.

LOPES, F. *Localização de Faltas em Tempo Real Baseada na Teoria de Ondas Viajantes Usando Dados Não Sincronizados de Dois Terminais. Campina Grande, PB, 2014*. Tese (Doutorado) — Tese (Doutorado), 2014. Cited in page 17.

LOPES, F.; FERNANDES, D.; NEVES, W. A traveling-wave detection method based on park's transformation for fault locators. *IEEE Transactions on Power Delivery*, IEEE, v. 28, n. 3, p. 1626–1634, 2013. Cited in page 21.

LOPES, F.; LEITE, E.; RIBEIRO, J. P.; LOPES, L.; PIARDI, A.; OTTO, R. *et al.* Using the differentiator-smoother filter to analyze traveling waves on transmission lines: Fundamentals settings and implementation. In: *Intern. Conf. on Power Systems Transientes*. [S.l.: s.n.], 2019. p. 1–6. Cited 5 times in pages 20, 21, 22, 26, and 30.

LOPES, F. V.; REIS, R.; FACINA, D.; MELO, K.; DANTAS, K.; COSTA, F. How much "villain"is the anti-aliasing filter for traveling wave-based fault location methods? *Electric Power Systems Research*, Elsevier, v. 212, p. 108369, 2022. Cited 6 times in pages 14, 15, 34, 35, 39, and 40.

LOPES, F. V.; REIS, R. L.; SILVA, K. M.; MARTINS-BRITTO, A.; RIBEIRO, E. P.; MORAES, C. M.; RODRIGUES, M. A. M. Past, present, and future trends of traveling wave-based fault location solutions. In: IEEE. *2021 Workshop on Communication Networks and Power Systems (WCNPS)*. [S.l.], 2021. p. 1–6. Cited 3 times in pages 3, 9, and 14.

LUO, W.; LIU, J.; LI, Z.; SONG, J. High order interpolation error analysis based on triangular interpolations. In: IEEE. *2020 IEEE International Conference on Computational Electromagnetics (ICCEM)*. [S.l.], 2020. p. 79–80. Cited in page 10.

MARIHART, D.; HAAGENSON, N. Automatic fault locator for bonneville power administration. In: *proceedings of the 1972 IEEE Power and Energy Society Summer Meeting, San Francisco, CA*. [S.l.: s.n.], 1972. Cited in page 9.

MATLAB. *MATLAB: The Language of Technical Computing*. 2024. Available in <https://www.mathworks.com/help/matlab/ref/double.interp1.html?searchHighlight=interp1&s_tid=srchtitle_support_results_1_interp1/>. Accessed in October 2024. Cited in page 63.

METZGER, N.; CARSTENS, B.; HELENIAK, F. Practical experience with ultra-high-speed line protective relays". In: *22nd Annual Georgia Tech Fault and Disturbance Analysis Conference*. [S.l.: s.n.], 2018. Cited in page 22.

MITRA, B.; DEBNATH, S.; CHOWDHURY, B. Fault location using the natural frequency of oscillation of current discharge in mtdc networks. *IEEE Access*, IEEE, v. 9, p. 49415–49423, 2021. Cited 3 times in pages 13, 14, and 15.

NA, J.; KIM, H.; ZHAO, H.; GOLE, A.; HUR, K. An improved high-accuracy interpolation method for switching devices in emt simulation programs. *Electric Power Systems Research*, Elsevier, v. 223, p. 109630, 2023. Cited in page 10.

NAIDU, S. Electromagnetic transients in power systems. *GRAFSET Publisher, Campina Grande, Brazil*, 1985. Cited in page 17.

ONS, B. T. P. S. O. *Equipment shutdowns in the Brazilian national interconnected system*. 2023. Available in <https://www.ons.org.br/>. Accessed in July 2023. Cited in page 1.

ONS, B. T. P. S. O. *Extension of the Brazillian Basic Transmission Network*. 2023. Available in <https://www.ons.org.br/paginas/sobre-o-sin/o-sistema-em-numeros/>. Accessed in July 2023. Cited in page 1.

OPPENHEIM, A. V. *Discrete-time signal processing*. [S.l.]: Pearson Education India, 1999. Cited 2 times in pages 27 and 28.

PHADKE, A. G.; THORP, J. S. *Computer relaying for power systems*. [S.l.]: John Wiley & Sons, 2009. Cited in page 21.

REPORT, A. C. Bibliography and summary of fault location methods [includes discussion]. *Transactions of the American Institute of Electrical Engineers. Part III: Power Apparatus and Systems*, IEEE, v. 74, n. 3, p. 1423–1428, 1955. Cited in page 9.

RIBEIRO, E.; LOPES, F.; SILVA, K.; MARTINS-BRITTO, A.; REIS, R. L.; MORAES, C. M.; AGOSTINHO, R. L.; RODRIGUES, M. A. An interpolation-based solution to use low sampling rate records in traveling wave-based fault location methods. *Electric Power Systems Research*, Elsevier, v. 224, p. 109605, 2023. Cited 4 times in pages 3, 4, 14, and 15.

RIBEIRO, E. P. A.; LOPES, F. V.; RIBEIRO, J. P. G.; LEITE, E. J. Atp/models differentiator-smoother filter model validated using actual time-domain relay. In: IEEE. *2018 Workshop on Communication Networks and Power Systems (WCNPS)*. [S.l.], 2018. p. 1–4. Cited 3 times in pages 20, 22, and 24.

RIBEIRO, L.; CUNHA, G.; MARTINS-BRITTO, A.; RIBEIRO, E.; LOPES, F. Impact of transmission line modeling aspects on tw-based fault location studies. *Electric Power Systems Research*, Elsevier, v. 196, p. 107204, 2021. Cited in page 20.

SAHA, M. M.; IZYKOWSKI, J.; ROSOLOWSKI, E. *Fault location on power networks*. [S.l.]: Springer, 2010. v. 2. Cited 4 times in pages 3, 9, 16, and 21.

SCHWEITZER, E. O.; GUZMÁN, A.; MYNAM, M. V.; SKENDZIC, V.; KASZTENNY, B.; MARX, S. Locating faults by the traveling waves they launch. In: IEEE. *2014 67th annual conference for protective relay engineers*. [S.l.], 2014. p. 95–110. Cited 5 times in pages 21, 23, 26, 27, and 67.

SCHWEITZER, E. O.; KASZTENNY, B.; GUZMÁN, A.; SKENDZIC, V.; MYNAM, M. V. Speed of line protection-can we break free of phasor limitations? In: IEEE. *2015 68th Annual Conference for Protective Relay Engineers*. [S.l.], 2015. p. 448–461. Cited 3 times in pages 22, 24, and 40.

SCHWEITZER, E. O.; KASZTENNY, B.; MYNAM, M. V. Performance of time-domain line protection elements on real-world faults. In: IEEE. *2016 69th Annual Conference for Protective Relay Engineers (CPRE)*. [S.l.], 2016. p. 1–17. Cited in page 21.

SCHWEITZER, E. O. I.; SKENDZIC, V.; GUZMÁN, A.; MYNAM, M. V.; ETERNOD, J. L.; GONG, Y. Mystery solved: Five surprises discovered with megahertz sampling and traveling-wave data analysis. In: *proceedings of the 72nd Annual Conference for Protective Relay Engineers, College Station, TX*. [S.l.: s.n.], 2019. Cited 2 times in pages 13 and 15.

SHARMA, S.; MYNAM, M. V. Field experience with an ultra-high-speed line relay and traveling-wave fault locator. In: *45th Annual Western Protective Relay Conference*. [S.l.: s.n.], 2018. v. 10. Cited 3 times in pages 22, 24, and 40.

SHRESTHA, A.; MUTHA, S. Accurate multi-ended fault locating algorithm using incremental sequence quantities. *Protection, Automation and Control World Conference*, 2023. Cited in page 25.

TAN, G.; FENG, Y.; SHEN, H. A combined interpolation method for waveform reconstruction in beacon transmitter detector. IET, 2011. Cited in page 9.

TZIOUVARAS, D. A.; ROBERTS, J. B.; BENMOUYAL, G. New multi-ended fault location design for two-or three-terminal lines. IET, 2001. Cited in page 25.

WANG, D.; HOU, M.; GAO, M.; QIAO, F. Travelling wave directional pilot protection for hybrid lcc-mmc-hvdc transmission line. *International Journal of Electrical Power & Energy Systems*, Elsevier, v. 115, p. 105431, 2020. Cited in page 61.

WEDEPOHL, L.; WILCOX, D. Transient analysis of underground power-transmission systems. system-model and wave-propagation characteristics. In: IET. *Proceedings of the institution of electrical engineers*. [S.l.], 1973. v. 120, n. 2, p. 253–260. Cited in page 20.

ZHAO, L.; WANG, Z.; CHEN, T.; LV, S.; YUAN, C.; SHEN, X.; LIU, Y. Missing interpolation model for wind power data based on the improved ceemdan method and generative adversarial interpolation network. *Global Energy Interconnection*, Elsevier, v. 6, n. 5, p. 517–529, 2023. Cited in page 10.

ZIMATH, S.; RAMOS, M. *et al.* Comparison of impedance and travelling wave fault location using real faults. In: IEEE. *IEEE PES T&D 2010*. [S.l.], 2010. p. 1–5. No citation in text.